Institut für Geodäsie und Geoinformation der Universität Bonn

The application of impact factors to scheduling VLBI Intensive sessions with twin telescopes

Inaugural–Dissertation zur
Erlangung des akademischen Grades
Doktor–Ingenieur (Dr.–Ing.)
der Landwirtschaftlichen Fakultät
der Rheinischen Friedrich–Wilhelms–Universität
zu Bonn

vorgelegt am 14. Oktober 2014 von

Dipl.–Ing. Judith Leek
aus Remagen

Referent:	Priv.-Doz. Dr.-Ing. Axel Nothnagel
Korreferenten:	Univ.-Prof. Dr.-Ing. Heiner Kuhlmann
	Univ.-Prof. Dr.-Ing. Dr. h.c. Harald Schuh
Tag der mündlichen Prüfung:	23. Januar 2015
Publikation:	Diese Dissertation ist auf dem Hochschulschriftenserver der ULB Bonn `http://hss.ulb.uni-bonn.de/diss_online` elektronisch publiziert.
Erscheinungsjahr:	2015

Summary

This thesis deals with the scheduling of special purpose, 1h-long VLBI sessions, so-called *Intensives*, and its further extension by twin radio telescopes. The daily VLBI Intensive measurements make an important contribution to the regular monitoring of Earth rotation variations. Since these variations are quite rapid their knowledge is important for navigation with GNSS and for investigations in Earth sciences. Unfortunately, the precision of VLBI Intensive observations is 2 – 3 times worse than the precision of regular 24h-VLBI measurements with networks of 5 – 10 radio telescopes. For economical and logistical reasons, these are performed only twice a week and have the disadvantage of a latency of the results of about ten days. However, for reliable predictions of the Earth's rotation, the results have to be available as rapidly as possible.

For these reasons, the International VLBI Service for Geodesy and Astrometry (IVS) carries short duration ($\sim$ 1 h) sessions on a daily basis. The major task of research in this thesis is the improvement of VLBI Intensive results by using twin radio telescopes instead of single radio telescopes. Therefore, a new scheduling method for creating Intensive observing plans has been developed. With the aim of finding an appropriate method to schedule VLBI observations, preparatory investigations of Intensive sessions have been done using a regression diagnostics tool which is based on singular value decomposition of the design matrix and cluster analysis methods. These investigations suggest that the impact factors of the observations are well suited for the identification of the most influential observations which are needed for the determination of certain parameters within the entire design of a VLBI session. Thus, by using the impact factors of the observations as selection criteria, the developed scheduling method is designed for optimizing the observations' geometry for a given network of radio telescopes and a predefined set of parameters to be estimated. The configuration of at least two twin telescopes, or one twin and two single telescopes, offers the possibility of building pairwise sub-nets that observe two different radio sources simultaneously. As a consequence, the number of viable observations within a session duration increased. In addition to an optimized observing plan, a special parametrization for twin telescopes leads to an improved determination of the Earth rotation variations, as it is shown by simulated observations in this thesis. In general, an improvement of about 50 % in the formal errors can be realized by using twin radio telescopes.

Zusammenfassung

Die vorliegende Arbeit beschäftigt sich mit der Erstellung von Beobachtungsplänen für VLBI Intensives und deren Erweiterung durch Zwillings-Radioteleskope. Täglich durchgeführte VLBI Intensive Messungen leisten einen wichtigen Beitrag zur regelmäßigen Überwachung von Erdrotationsvariationen. Da diese Variationen von relativ schneller Natur sind, ist deren Kenntnis wichtig für die Navigation mit GNSS und für Forschungen auf dem Gebiet der Erdwissenschaften. Leider ist die Genauigkeit von VLBI Intensives $2-3$ mal schlechter als die der regulären 24-Stunden VLBI Messungen mit einem Netzwerk bestehend aus $5-10$ Radioteleskopen. Diese werden allerdings aus wirtschaftlichen und logistischen Gründen nur zweimal in der Woche durchgeführt und haben den Nachteil, dass die Ergebnisse erst etwa zehn Tage später zu Verfügung stehen. Für zuverlässige Prädiktionen der Erdrotationsgeschwindigkeit sind allerdings schnell verfügbare Daten erforderlich.

Aus diesem Grund betreibt der International VLBI Service for Geodesy and Astrometry (IVS) tägliche Kurzzeitbeobachtungen ($\sim 1\,\mathrm{h}$). Das Hauptforschungsthema dieser Arbeit stellt die Verbesserung von VLBI Intensive Ergebnissen durch den Einsatz von Zwillings-Radioteleskopen anstelle von Einzel-Radioteleskopen dar. Zu diesem Zwecke wurde eine neue Planungsstrategie entwickelt um Intensive-Beobachtungspläne zu erstellen. Um eine geeignete Methode zur Erstellung von Beobachtungsplänen zu entwickeln, wurden vorbereitende Untersuchungen von Intensive-Beobachtungsplänen mittles Regressionsanalyse durchgeführt. Die angewandte Regressionsanalyse basiert auf der Singulärwertzerlegung der Designmatrix eines Ausgleichungsproblems und Clusteranalyse-Verfahren. Diese Untersuchungen weisen darauf hin, dass die Einflussfaktoren der Beobachtungen gut geeignet sind, um einflussreiche Beobachtungen zur Bestimmung gewisser Parameter unter Berücksichtigung des gesamten Designs eines VLBI-Experiments zu detektieren. Durch die Nutzung von Einflussfaktoren der Beobachtungen als Auswahlkriterium ist die entwickelte Methode zur Beobachtungsplanerstellung darauf ausgelegt die Beobachtungsgeometrie für ein bestehendes Stationsnetzwerk von Radioteleskopen und einen vordefinierten Satz an zu schätzenden Parametern zu optimieren. Die Konfiguration von mindestens zwei Zwillings-Radioteleskopen, oder einem Zwillings-Radioteleskop und zwei Einzel-Radioteleskopen bietet die Möglichkeit der Paarbildung zwischen den Teleskopen und somit das zeitgleiche Beobachten von zwei unterschiedlichen Radioquellen. Eine Konsequenz daraus ist eine erhöhte Beobachtungsanzahl innerhalb der Dauer eines Experiments. Neben einem optimierten Beobachtungsplan führt auch die spezielle Parametrisierung aufgrund der räumlichen Nähe der Zwillings-Radioteleskope zueinander zu einer verbesserten Bestimmung der Erdrotationsvariationen, wie es in dieser Arbeit mit Hilfe simulierter Beobachtungen gezeigt wird. Im Allgemeinen kann eine Verbesserung des formalen Fehlers um 50% und mehr durch die Verwendung von Zwillings-Radioteleskopen für tägliche Intensive Messungen realisiert werden.

Contents

List of Figures

List of Tables

1. Introduction

Geodetic Very Long Baseline Interferometry (VLBI) is one of the most important techniques for the determination of Earth rotation parameters and the only one which is able to measure UT1, the natural time scale derived from the Earth's rotation, directly. Due to the variability of UT1 and its importance for various applications, a regular monitoring of UT1 is preferable. For this reason, daily short term single baseline VLBI sessions, so-called Intensives, were designed by the International VLBI Service for Geodesy and Astrometry (IVS, Schlüter and Behrend 2007) to determine UT1 with minimum latency. Unfortunately, the precision of VLBI Intensive observations is 2 – 3 times worse than the precision of regular VLBI measurements with a network of 5 – 10 radio telescopes and a duration of 24 hours which are performed only twice a week. For a reliable prediction of the UT1 series, both rapidly available and precise data is necessary. Overcoming this problem is the major field of research concerning VLBI Intensives.

The Wettzell Geodetic Observatory in the Bavarian Forest is the most important site in the world for UT1 observations since it has taken over a considerable share of the operational burden. Now, a further extension of the capabilities was realized by the construction of the Twin Telescope Wettzell (TTW) that is expected to become operational in late 2014. TTW is an installation of two identical radio telescopes of 13.2 m diameter at a distance of about 50 m.

Following future VLBI requirements, the construction of more and more twin radio telescopes all over the world is intended. Thus, it is easily conceivable that twin radio telescopes were also to be built at other important sites for VLBI Intensives in future. Indeed, it is envisaged to extend the existing geodetic radio telescope in Kokee Park (Hawaii, USA), which is one of those important sites, by a second radio telescope to obtain a further twin radio telescope. Also the Japanese uttered the desire for building a twin radio telescope in Tsukuba, the third of the main important sites of VLBI Intensives.

Due to the small network and the short duration of standard Intensive sessions, only a few observations can be performed, i.e. about 20 to 40 observations per single baseline session. Replacing the single radio telescopes by respective twin radio telescopes for Intensive sessions leads to a significantly increased number of observations within one hour. Furthermore, twin radio telescopes enable various observing constellations, as all radio telescopes might observe one source simultaneously or small sub-nets of the radio telescopes observe different sources at the same time.

A further advantage of twin radio telescopes is the spatial proximity of two independent operational VLBI antennas. Sharing the same frequency standard and sampling the same atmosphere leads to a reduced set of parameters that have to be estimated in the VLBI analysis. This is expected to help reducing systematic atmospheric effects, may reduce clock stability requirements as well as correlations between atmosphere, clocks and the Earth rotation what would strengthen the parameters estimated from the observations.

Because of the great east-west extent of Intensive baselines, which are most sensitive for UT1, the common visibility of the radio telescopes is very limited. Thus, only a small extract of radio sources is observable during an Intensive session. The scheduling of Intensive observing plans is a crucial point for achieving the highest possible quality of the estimated parameters, especially UT1. Due to the spatial and temporal restrictions of Intensive sessions, the observations of those sessions have to be selected with great care. Furthermore, supposed good observations might be very sensitive to outer influences that might worsen the UT1 determination. Because of several contradictory requirements to Intensive observing plans, finding the best compromise that produces the best possible results represents a special challenge. Using twin radio telescopes instead of single telescopes with their possibilities to form different observing constellations leads to further challenges concerning the scheduling of the observations.

Several studies were done to improve the scheduling of VLBI Intensive sessions (e.g., Baver et al. 2012, or Uunila et al. 2012). However, there is no clear strategy for the scheduling of VLBI Intensive sessions for the purpose of UT1 determination except of trying to spread the observations as evenly as possible over the sky at each telescope. In this thesis a completely new approach is developed for scheduling VLBI Intensive

sessions. This approach differs from all other scheduling procedures that have been investigated for VLBI experiments in general.

As a basis of this work serves the investigation of Vennebusch et al. (2009), who show that the singular value decomposition (SVD) is suitable as part of regression diagnostics for any geodetic adjustment problem and, therefore, for geodetic VLBI as well. The SVD can be used to derive indicators which contain information on the geometry of the design with respect to the influence of observational errors. Therefore, it can be used for planning the design of the measuring process (Förstner 1987). Further studies have been done to find out most convenient indicators and how they can be used for improving VLBI observing plans.

The developed scheduling procedure creates Intensive observing plans automatically by choosing the observations one after the other in a successive sequence. For the choice of the respective observations, the design matrix of the associated adjustment problem is investigated in terms of the SVD. Thus, the decision for the selection of the next observations depends only on the actual geometry of the previously scheduled observations in each step of the scheduling process.

First, the new scheduling method has been developed to create observing plans for standard VLBI Intensive sessions with single radio telescopes. That ensures its suitability for creating reasonable Intensive observing plans, leading to best possible results for the target parameter UT1. After that, the written program has been adjusted to deal with twin radio telescopes. On that account, the different parametrization of twin radio telescopes and the possibility of forming special observing constellations was implemented, while the optimization criterion remains the same. Thus, the developed scheduling procedure produces appropriate observing plans for any network of stations in terms of the predefined target parameters. In this respect, this thesis lay the groundwork for a qualified contribution of twin telescopes to IVS Intensive observations by developing state of the art observing schedules. The general structure of this thesis is as follows:

- Chapter 2 describes the necessary basic knowledge of VLBI focusing on the special requests of VLBI Intensives and future VLBI requirements.
- Chapter 3 is related to the scheduling of VLBI Intensive sessions, containing the current state of research as well as further investigations of VLBI observing plans via SVD and cluster analysis.
- On the basis of the previous studies a new scheduling method is developed in Ch. 4.
- In Ch. 5 the developed scheduling method is comprehensively and accurately tested for its capability to design standard Intensive sessions.
- The scheduling method will be extended for twin telescope observations in Ch. 6 and its results will be examined.
- Chapter 7 rates the developed scheduling method with respect to its advantages for scheduling VLBI observing plans by comparing it with other scheduling methods.
- The conclusions of all investigations are given in Ch. 8 together with an outlook for further examinations.

2. Very Long Baseline Interferometry

2.1 Introduction of geodetic VLBI

Since the end of the 1970s, Very Long Baseline Interferometry (VLBI) is used for geodetic purposes (e.g., Shapiro et al. 1974, Ma 1978 or Campbell and Witte 1978). The principle of VLBI is based on a classical interferometer which has been invented as early as 1890 by Michelson (1890). As distinguished from a classical radio interferometer, the two receiving devices are not connected for a very long baseline interferometer.

The measuring principle of geodetic VLBI is based on simultaneous observations of an extragalactic radio source by two or more radio telescopes, which can be as far apart as an Earth diameter. Ideal candidates of these radio sources are point-like and show no proper motions on decadal time scales (Charlot 1990, Zeppenfeld 1993, Feissel-Vernier 2003, Engelhardt and Thorandt 2006). The great distances between two VLBI antennas requires a very precise method of timing the receiving signals, which is realized by highly precise atomic clocks, usually hydrogen masers (Vanier 1982, Thompson et al. 1986). The time-marked signal is stored digitally and sent to so-called correlators, specially designed computers, which bring the signal to coherency and determine the difference of the arrival times of the signal at both VLBI antennas, the primary geodetic observable (see, e.g., Alef 1989, Whitney 2000 or Deller et al. 2007).

Interferometric measurements permit resolution on the order of the wavelength of the radiation. Since the radio waves are effected by the ionosphere, VLBI observations are recorded with a dual frequency of 8.4 GHz (X-band) and 2.3 GHz (S-band) to calibrate the dispersive ionospheric refraction (e.g. Lohmar 1985). The measurement precision of group delay achieved in VLBI observations depends strongly on the bandwidth of the observation (Schuh and Campbell 1994). Thus, the widest possible bandpass should be used. To overcome the limitations of recording equipment in terms of recordable bandwidth, the bandwidth synthesis technique is used (Rogers 1970). In principle, a large effective bandwidth is synthesized from a set of much narrower frequency channels (2 MHz each) that are spread out across the band. In fact, 8 channels represent the sky frequencies of 8210 – 8950 MHz in case of the X-band and 6 channels of the S-band covers 2225 – 2385 MHz.

By performing VLBI observing sessions with three to 15 globally distributed radio telescopes that observe several radio sources successively, global observing networks can be formed. The International VLBI Service for Geodesy and Astrometry (IVS, Schlüter and Behrend 2007), an international collaboration of organizations which operate or support VLBI components, provide such VLBI observing sessions regularly. A map of actual IVS network stations is depicted in Fig. 2.1.

The main objectives of the IVS is to provide terrestrial and celestial reference frames (TRF and CRF) and Earth orientation parameters (EOP). The CRF is a quasi-inertial reference frame that is defined by extragalactic sources, which are so far away that any angular motion is essentially zero. The TRF is an earth-fixed reference frame that is defined by a set of station positions and their velocities. The International Service for Earth Rotation and Reference Systems (IERS) regularly issues conventions to define standard reference systems to be used (Petit and Luzum 2010) and publishes the International Celestial Reference Frame (ICRF, Arias et al. 1995, Ma et al. 1998) and the International Terrestrial Reference Frame (ITRF, Altamimi et al. 2007, Altamimi et al. 2011).

The link between the ICRF and the ITRF is realized through the EOP. VLBI is the only geodetic observing technique that provides a direct link between the ICRF and the ITRF. Especially the Earth rotation phase angle UT1 is measurable by VLBI only. Satellite techniques like Global Navigation Satellite Systems (GNSS) or Satellite Laser Ranging (SLR) are not sensitive to the phase angle itself but only to its time derivative that is called Length of Day (LOD, see, e.g., Artz et al. 2012 or Schnell 2006). Therefore, geodetic VLBI provides an important contribution to a combined solution of the different space geodetic techniques.

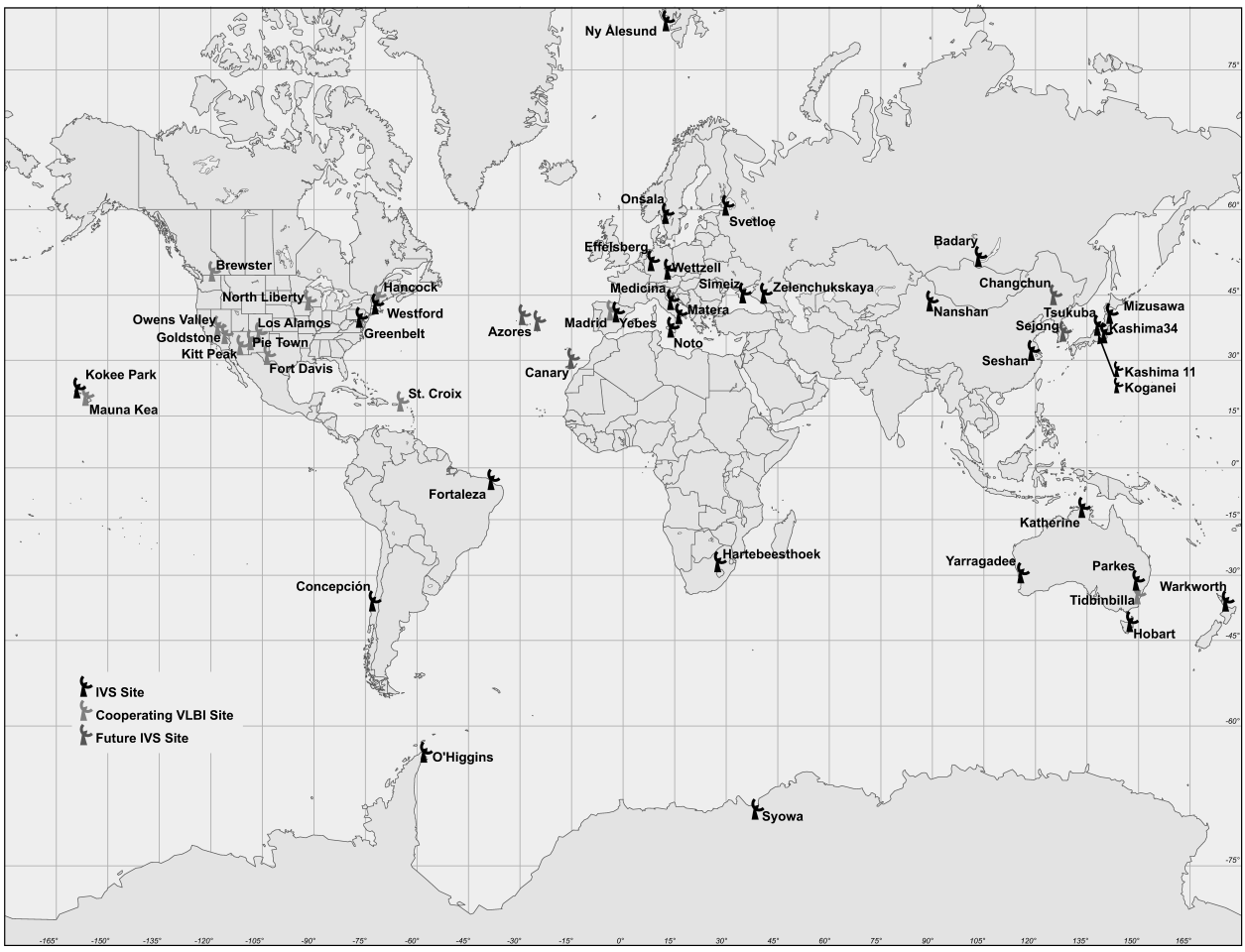

Figure 2.1: Globally distributed IVS network stations (http://ivscc.gsfc.nasa.gov/stations/ns-map.html).

2.2 Basic principle

In principle, two or more radio telescopes observe the same radio source simultaneously. Due to the great distance of the radio sources (several billion light-years), the signals arrive as plain wavefronts on Earth and cause different arrival times at the two radio telescopes forming a baseline $\mathbf{b}$ (Fig. 2.2).

As seen in Fig. 2.2, the geometric delay τ_{geom} can be described in a right-angled triangle by

$$\tau_{geom} = t_2 - t_1 = -\frac{1}{c} \cdot \mathbf{b} \cdot \mathbf{k} \tag{2.1}$$

with the baseline vector $\mathbf{b} = \mathbf{r}_2 - \mathbf{r}_1$ computed by the geocentric position vectors of the observing sites $\mathbf{r}_i$ and the unit vector in the direction of the radio source $\mathbf{k}$ (e.g., TAKAHASHI et al. 2000). t_1 and t_2 denote the arrival times of the signal at the two observing sites. The velocity of light c is needed to convert the delay to the unit of time. The unit vector in the direction of the radio source $\mathbf{k}$ can be computed from the right ascension α and declination δ of the source given in the CRF

$$\mathbf{k} = \begin{pmatrix} \cos\alpha \cdot \cos\delta \\ \sin\alpha \cdot \cos\delta \\ \sin\delta \end{pmatrix}. \tag{2.2}$$

Usually, the baseline vector $\mathbf{b}$ is given in an earth-fixed reference frame, a TRF, and the source position, thus, the vector $\mathbf{k}$, in a sky-bound reference frame, a CRF. As a consequence, a transformation between these two

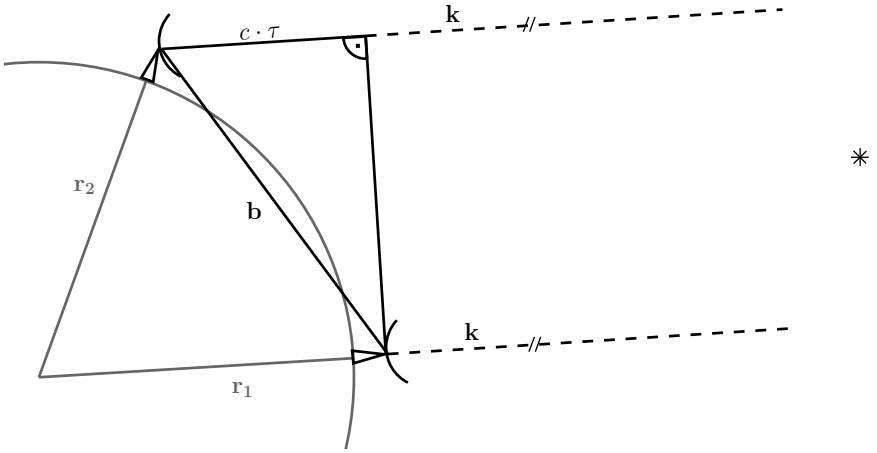

Figure 2.2: Basic principle of geodetic VLBI.

reference frames is necessary. This transformation can be performed by the description of the Earth motion, expressed as EOP. In detail, the transformation is represented by three time-dependent rotation matrices, so that Eq. 2.1 becomes

$$\tau_{geom} = -\frac{1}{c} \cdot \mathbf{b} \cdot \mathbf{W}(t) \cdot \mathbf{R}(t) \cdot \mathbf{Q}(t) \cdot \mathbf{k} \tag{2.3}$$

where $\mathbf{W}(t)$, $\mathbf{R}(t)$ and $\mathbf{Q}(t)$ are the transformation matrices arising from polar motion, from the rotation of the Earth around the axis associated with the pole, and from the motion of the celestial pole in the celestial reference system, respectively (Petit and Luzum 2010).

Since VLBI observations are affected by various effects on their way through interstellar space, the Solar System and the Earth's atmosphere, further terms have to be added to the geometrical delay in order to formulate the complete observation equation for high accuracy VLBI measurements. The observed time delay is thus described by

$$\begin{aligned} \tau_{obs} = \tau_{geom} + \tau_{j-aber} + \tau_{t-aber} + \tau_{rel} + \tau_{load} + \tau_{tid} \\ + \tau_{instr} + \tau_{clock} + \tau_{tropo} + \tau_{ionos} + \dots \end{aligned} \tag{2.4}$$

with

τ_{j-aber}	annual aberration because of the motion of the Earth around the Solar System barycenter,
τ_{t-aber}	diurnal aberration because of the rotation of the Earth,
τ_{rel}	relativistic corrections to the geometric delay τ_{geom},
τ_{load}	deformation of the Earth's surface because of loading effects (e.g. due to ocean tides and atmospheric pressure changes),
τ_{tid}	deformation of the Earth because of tides and changes of the angular momentum due to ocean tides,
τ_{instr}	propagation delays through on-site cable runs and other instruments,
τ_{clock}	mis-synchronization of the reference clocks at each observing site,
τ_{tropo}	propagation delays through the non-ionized portions of the Earth's atmosphere,
τ_{ionos}	propagation delays through the ionized portions of the Earth's atmosphere.

The general principle of VLBI has been described by many authors. Detailed descriptions of the general principles and the various effects are given, e.g., in Thomas (1972), Campbell (1987), Schuh (1987), Sovers et al. (1998), Ma and MacMillan (2000), Takahashi et al. (2000) or Tesmer (2004).

2.3 Intensive sessions

For the last 30 years, VLBI has been the principal method to determine the Earth's rotation angle, expressed by UT1. The definition of UT1 corresponding to the International Astronomical Union (IAU) 2000 resolutions is given in Capitaine et al. (2003). Most accurate UT1 estimates can be obtained from VLBI measurements with other EOP simultaneously. For this reason standard 24h VLBI sessions are carried out employing global networks of several, usually 6 – 10, stations. In addition to EOP, the station coordinates as well as the source positions can be determined from these network observations. However, results of these observations are only available within 8 – 15 days after the observations. Such a delay in disseminating the results is problematic for real-time applications and influences UT1 prediction accuracy (Luzum and Nothnagel 2010).

For continued inexpensive UT1 determinations, special observing programs are conducted in the framework of the IVS activity, which has been first studied by Robertson et al. (1985). These sessions, called Intensives, are short duration VLBI experiments of usually one hour duration. They are performed almost daily for a regular determination of UT1 on networks with two or three stations only. The small amount of data of these sessions permits a very quick data transport and postprocessing, and therefore it enables to provide UT1 results with a minimized time delay after the observations. According to Luzum and Nothnagel (2010), employing electronic data transfer (e-VLBI), the latency usually amounts to only 0.5 – 2 days.

2.3.1 Current Intensive sessions

Most sensitive for UT1 determinations are baselines with long east-west extensions. Currently, three different Intensive session types exist. INT1 and INT2 sessions consist of a long single baseline with an east-west alignment. INT1s are measured on the baseline Kokee Park (Hawaii, USA) – Wettzell (Germany) on Monday to Friday, and INT2s on the baseline Tsukuba (Japan) – Wettzell on Saturday and Sunday (Fischer et al. 2003). INT3 is an Intensive session type where observations are performed with three radio telescopes for redundancy purposes every Monday. The participating stations are Ny-Ålesund (Svalbard, Norway), Tsukuba and Wettzell. Figure 2.3 shows the geometry of the Intensive session types, and Tab. 2.1 gives an overview of the current organization.

	INT1	**INT2**	**INT3**
Stations	Kokee Park (Hawaii, USA) Wettzell (Germany)	Tsukuba (Japan) Wettzell (Germany)	Ny-Ålesund (Svalbard, Norway) Tsukuba (Japan) Wettzell (Germany)
Station-IDs	Kk, Wz	Ts, Wz	Ny, Ts, Wz
Length of baseline	10 357.4 km	8445.0 km	6498.0 km (Ny–Ts) 3283.0 km (Ny–Wz) 8445.0 km (Ts–Wz)
Observing days	Monday to Friday	Saturday and Sunday	Monday
Time frame	18.30 – 19.30 UT	07.30 – 08.30 UT	07.00 – 08.00 UT
Scheduler	GSFC Washington D.C.	BKG Leipzig	IGG Bonn
Correlator	USNO	GSI	IGG
Average number of scans per session[1]	21.2	42.2	34.2

Table 2.1: Current Intensive observing routines of the IVS.

[1] Evaluated for the time period of January 2009 to June 2013.

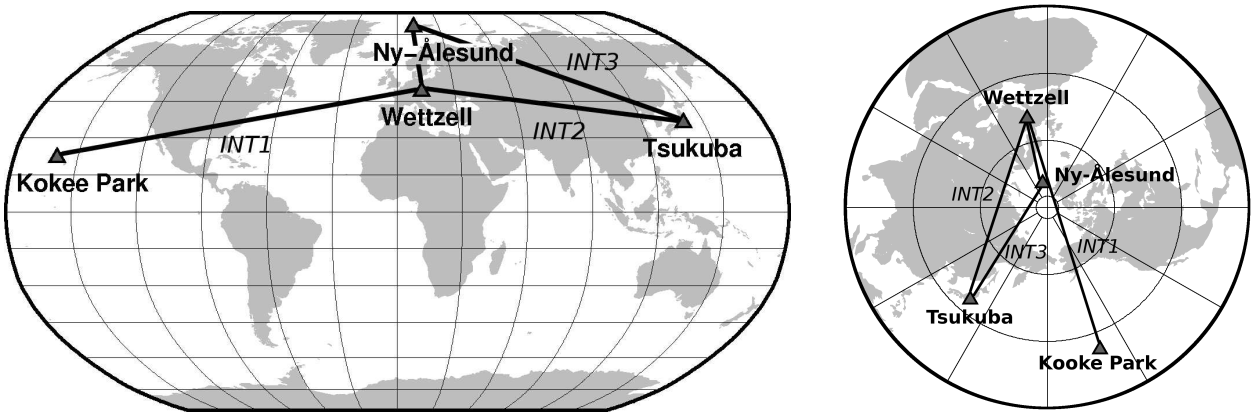

Figure 2.3: Baseline geometry of current Intensive observations.

2.3.2 Earths rotation parameter

In fact, the Earths rotation parameter, measured by VLBI is $\Delta UT1$ = UT1 − UTC. The Coordinated Universal Time (UTC) is a constant synthetic time scale, which is based on the International Atomic Time (TAI) provided by the Bureau International des Poids et Mesures (BIPM, Bureau International des Poids et Mesures 2006), while the Universal Time UT1 is a natural time scale directly derived from the Earth's rotation (Aoki et al. 1982). Therefore, the difference $\Delta UT1$ reflects all variations and irregularities of the Earth's rotation about its z-axis, like variations due to the zonal tides, to oceanic tides, to atmospheric circulation, to internal effects and to transfer of angular momentum to the Moon's orbital motion (Schuh et al. 2003). Due to tidal friction, the Earth slowly loses rotational energy and, thus, the duration of a day gradually becomes longer. As a consequence, UT1 and TAI diverge over the years. In order to avoid the atomic time scale diverging indefinitely from that of the Earth's rotation, a leap second is introduced whenever the difference becomes larger than 0.9 seconds averaged over one year. The resulting atomic time scale UTC runs parallel to TAI but follows UT1 in discrete steps of leap seconds. Thus, UTC is a compromise between the highly stable atomic time and the irregular Earth rotation. The decision to introduce a leap second in UTC is the responsibility of the IERS. The differences of UTC and UT1 to TAI are depicted in Fig. 2.5, while the VLBI target parameter $\Delta UT1$ is shown in Fig. 2.4.

2.3.3 Parameter Estimation

Analyzing INT sessions, only a minimal number of parameters can be estimated, due to low number of observations in comparison to 24 h sessions. The primary objective of INTs is the Earth rotation parameter $\Delta UT1$.

Since the synchronization of the station frequency standards is insufficient for determining the delay τ with satisfactory accuracy, this discrepancy has to be compensated for by the estimation of auxiliary parameters. As the clock behavior of all participating radio telescopes differs, an arbitrary clock has to be chosen as reference clock for the entire observing network. The remaining clocks show both a constant difference and a linear or an even higher order of change relative to the reference clock. According to, e.g., Sovers et al. (1998), a simple polynomial approach is used to describe the clock offsets, rates and second order terms mathematically

$$\tau_{clock} = cl_0 + cl_1 \cdot (t - t_0) + cl_2 \cdot (t - t_0)^2 \,. \tag{2.5}$$

In practice, this implies the estimation of three clock parameters per station, excluding the station being the reference clock. For higher variations of the frequency standards, further parameters of piecewise linear functions can be estimated, but that is not the case for Intensive sessions.

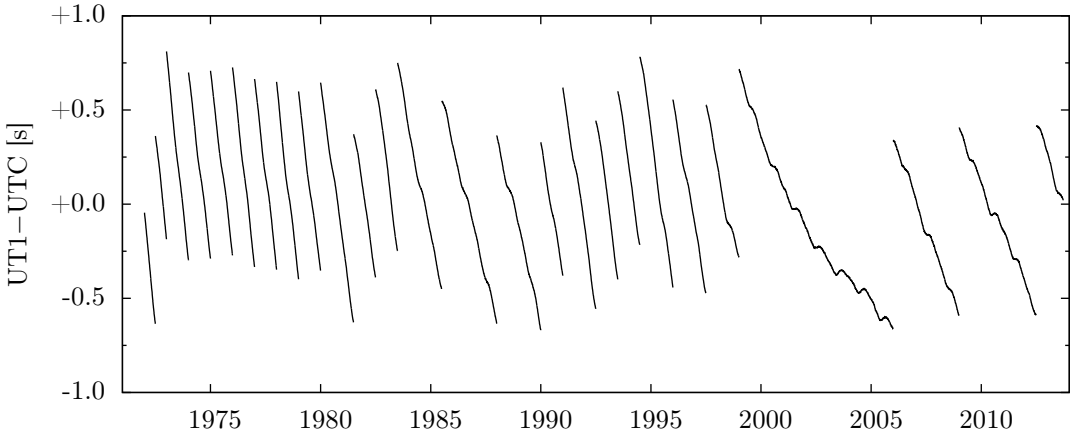

Figure 2.4: Earth rotation variations expressed in UT1−UTC (EOP 08 C04 / IAU2000A). The jumps are due to leap seconds.

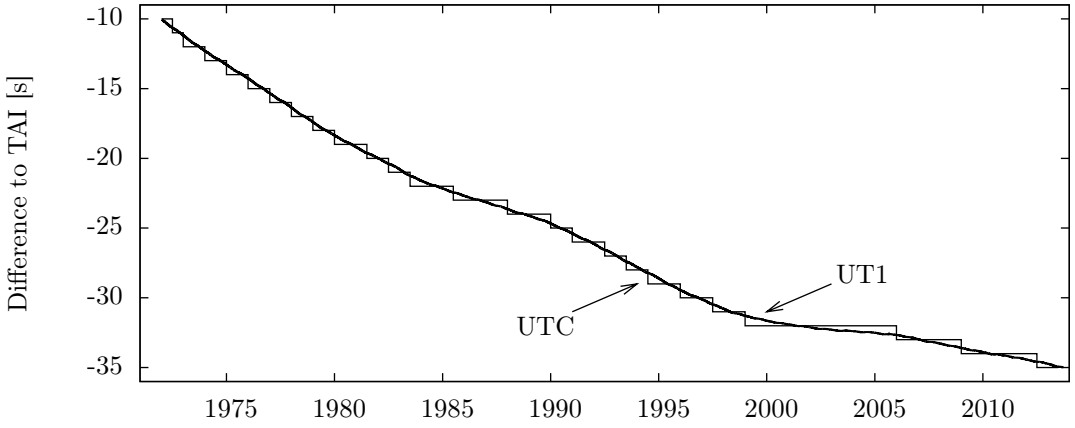

Figure 2.5: UTC following UT1 in integral steps.

Further attention has to be paid to propagation delays through the non-ionized portions of the Earth's atmosphere, the troposphere. Radio signals passing through the troposphere experience delay, bending and attenuation relative to an equivalent path through a vacuum (Davis et al. 1985). In fact, mis-modeling of the troposphere remains the dominant error source of VLBI observations (Sovers et al. 1998). Depending on varying temperature, atmospheric pressure and humidity, the signal is refracted differently along the signal's path through the troposphere (Wheelon 2001). The tropospheric delay can be determined by the integration of the index of refraction n along the signal's path S

$$\tau_{tropo} = \int_S (n-1)\, dS. \tag{2.6}$$

The index of refraction $n(\mathbf{r}(z), t)$ depends also on the observing time t and on the direction of the signal $\mathbf{r}(z)$ and, thus, on the elevation ε of the observed radio source. Commonly, the signal path delay is given in zenith direction ('zenith delay', $\varepsilon = 90°$). The ratio between the delay of an arbitrary elevation and the zenith delay is defined as mapping function $m(\varepsilon)$. Hence, the signal path delay in source direction can be determined by

$$\tau_{tropo}(\varepsilon) = m(\varepsilon) \cdot \tau_{tropo}(90°) \tag{2.7}$$

The most simple form of such a mapping function reads

$$m(\varepsilon) = \frac{1}{\sin(\varepsilon)} \tag{2.8}$$

(Sovers et al. 1998). Therefore, observations with low elevations are more sensitive to tropospheric influences because of their longer way through the atmosphere. Since the simple mapping function is inadequate for geodetic purposes, several refinements have been done by various authors. Accounting for the Earth's curvature, Marini (1972) has developed a mapping function in form of a continued fraction

$$m(\varepsilon) = \cfrac{1}{\sin(\varepsilon) + \cfrac{a}{\sin(\varepsilon) + \cfrac{b}{\sin(\varepsilon) + c}}} \tag{2.9}$$

with a, b and c being coefficients derived from actual atmospheric conditions. During the last decades numerous improved mapping functions have been developed, as e.g. the CfA by Davis et al. (1985), the mapping function by Chao (1972), the mapping function by Herring (1992), the Niell mapping function (NMF, Niell 1996), the Vienna mapping function (VMF, Böhm and Schuh 2004, Böhm et al. 2006b) or the Global mapping function (GMF, Böhm et al. 2006a). Most of them contain constants derived from analytic fits to ray-tracing results either for standard atmospheres or for observed atmospheric profiles based on numerical weather models. Detail descriptions of mapping functions can be found, e.g., in Nothnagel (2000) or Böhm (2004) and theirs influence on the VLBI estimates in Tesmer et al. (2007).

The behavior of temperature and atmospheric pressure can be well modeled. On the contrary, the atmospheric humidity can hardly be modeled because of the non-uniform and highly variable distribution of water vapor that cannot be determined by ground measurements (Sovers et al. 1998, Schwegmann 2004). Due to this fact, the description of the tropospheric effect on the signal path will be divided in a hydrostatic part zhd (zenith hydrostatic delay) and a wet part zwd (zenith wet delay)

$$\tau_{tropo}(\varepsilon) = m_h(\varepsilon) \cdot zhd + m_w(\varepsilon) \cdot zwd. \tag{2.10}$$

Because of differences in the effective height, mapping functions also have to be distinguished between hydrostatic mapping functions $m_h(\varepsilon)$ and wet mapping functions $m_w(\varepsilon)$. According to Saastamoinen (1972), the zenith hydrostatic delay can be modeled with sufficient accuracy and integrated in the VLBI analysis directly (Tesmer 2004). Since the zenith wet delay is hard to model, it is commonly introduced as unknown parameter in the VLBI analysis. For this purpose, piecewise linear functions as the parametrization of the clock behavior are used. The validity of mapping functions is limited by the assumption of azimuthal symmetry (Sovers et al. 1998). But in fact, there are North-South gradients in temperature, pressure and humidity as well as East-West gradients caused by motion of weather systems passing over a site. For these reasons, additional troposphere gradients will be estimated in typical VLBI analysis. However, it is assumed that atmospheric conditions vary hardly during brief Intensive sessions and furthermore just a small set of parameters can be estimated from such a minor data set. Thus, only one parameter per station describing the wet part of the tropospheric path delay will be estimated for Intensive sessions (see, e.g., Robertson et al. 1985). Böhm et al. (2010) and Nafisi et al. (2012) achieved slightly improved UT1 estimates from Intensive sessions by using external information about the azimuthal asymmetry of tropospheric delays around the stations from direct ray-tracing. This improvement has been validated by comparing length-of-day (LOD) estimates with those from Global Positioning System (GPS). The approach shows potential to improve UT1 estimates from Intensives, however, it has to be developed further.

Summarizing, the parametrization of Intensive sessions includes a clock polynomial per station except for the reference clock, an atmospheric offset per station, and the ΔUT1 parameter as the main objective. Necessarily, all other parameters have to be fixed to known values in advance from other observing series or from physical models for the parameter estimation. The non-linear equation of τ_{obs} (Eq. 2.4) has to be linearized in order to estimate the unknown parameters by a classical least-squares adjustment (e.g., Koch 1999)

$$\mathbf{A}^T \boldsymbol{\Sigma}_{\mathbf{yy}}^{-1} \mathbf{A} \boldsymbol{\Delta}\mathbf{x} = \mathbf{A}^T \boldsymbol{\Sigma}_{\mathbf{yy}}^{-1} \left(\mathbf{y} - \mathbf{y_0}\right), \tag{2.11}$$

where $\mathbf{\Delta x}$ denotes a specific set of parameters, $\mathbf{y - y_0}$ the vector of observed delays minus the vector of theoretical delays that is derived by inserting a priori values and model values into Eq. 2.4, $\mathbf{A}$ denotes the Jacobian matrix and $\mathbf{\Sigma_{yy}}$ the variance-covariance matrix of the observations. For this purpose, partial derivatives for the unknown parameters are needed, which are contained in the Jacobian matrix $\mathbf{A}$. For a baseline with the stations A and B the partial derivatives are

$$\frac{\partial \tau_{obs}}{\partial cl_{0_A}} = 1 \tag{2.12}$$

$$\frac{\partial \tau_{obs}}{\partial cl_{1_A}} = t - t_0 \tag{2.13}$$

$$\frac{\partial \tau_{obs}}{\partial cl_{2_A}} = (t - t_0)^2 \tag{2.14}$$

$$\frac{\partial \tau_{obs}}{\partial cl_{0_B}} = -1 \tag{2.15}$$

$$\frac{\partial \tau_{obs}}{\partial cl_{1_B}} = -(t - t_0) \tag{2.16}$$

$$\frac{\partial \tau_{obs}}{\partial cl_{2_B}} = -(t - t_0)^2 \tag{2.17}$$

$$\frac{\partial \tau_{obs}}{\partial at_A} = \frac{1}{c} \cdot m_w(\varepsilon) \tag{2.18}$$

$$\frac{\partial \tau_{obs}}{\partial at_B} = -\frac{1}{c} \cdot m_w(\varepsilon) \tag{2.19}$$

$$\frac{\partial \tau_{obs}}{\partial \Delta UT1} = \frac{1}{c} \cdot \Omega \cdot \cos\delta \cdot (b_x \sin(h(t)) - b_y \cos(h(t))) \tag{2.20}$$

with

$t - t_0$	time passed since the beginning of the session,
c	velocity of light,
$m_w(\varepsilon)$	atmospheric wet mapping function,
ε	elevation of the radio telescope,
Ω	conversion factor from universal time to sidereal time ($\approx$1),
δ	declination of the radio source,
b_i	respective baseline component,
$h(t)$	Greenwich hour angle of the radio source.

Actual variances of the observations, which are used for the analysis, are determined during the correlation process coupled with the group delay. Theoretically, the standard deviation of a group delay can be predicted approximately by

$$\sigma_{\tau_{X/S}} = \frac{1}{2\pi \cdot SNR \cdot B_e} \tag{2.21}$$

(Schuh and Campbell 1994) with the effective bandwidth B_e of the receiving system depending on the number of channels n, the individual channel frequencies f_i and the mean frequency f_m

$$B_e = \sqrt{\frac{\sum (f_i - f_m)^2}{n - 1}} \tag{2.22}$$

and the signal-to-noise ratio (SNR) of an interferometer that is the inverse of the phase noise (standard deviation) and can be calculated theoretically as

$$SNR = \eta \frac{F}{2k} \cdot \sqrt{\frac{A_1 \cdot A_2}{T_{S_1} \cdot T_{S_2}}} \cdot \sqrt{2 B_e T}, \tag{2.23}$$

with

η	quality of the digitization and filtering of the signals
F	luminosity of the radio source [Jy]
k	Boltzmann's-constant (1.38×10^{-23} J/K)
A_i	effective antenna areas of the telescopes
T_{S_i}	noise temperatures of receiving systems
T	coherent observing or integration time at the correlation process.

A detailed description of the *SNR*, the effective bandwidth and the aforementioned relationships can be found in Hase (1999).

2.3.4 Scheduling

Since the accuracy and the precision of $\Delta UT1$ estimates heavily depend on the configuration of an observing session, the observation schedule plays a crucial role for improving the $\Delta UT1$ determination. Various authors discuss different scheduling strategies in general and specific scheduling strategies for Intensive sessions, which are described in Chap. 3 in more detail.

2.4 VLBI2010

The IVS is an international service of the International Association of Geodesy (IAG), the leading scientific organization in the field of geodesy. It is involved in reference frames, gravity field, geodynamics and Earth rotation and positioning. The Observing System of the IAG is the Global Geodetic Observing System (GGOS). GGOS integrates different geodetic techniques (SLR, GNSS, VLBI and DORIS – Doppler Orbitography and Radiopositioning Integrated by Satellite), different models and different approaches in order to ensure a long-term, precise monitoring of the geodetic observables and the gravity field (Gross et al. 2009).

Over the last 30 years, the VLBI-system has been upgraded and further developed many times. Nevertheless, it has reached its ultimate accuracy level, not least because of many aging radio telescopes, obsolete electronic and susceptibility to external radio-frequency interference (Niell et al. 2005, Hase et al. 2009). Among other things, this leads to great operational costs as well as costs of maintenance. To remedy these problems and to improve the measuring accuracy, the IVS developed the VLBI2010 concept in order to create the next generation VLBI system needed to meet the goals of GGOS.

The VLBI2010 requirements from antennas to analysis are:

1. 1 mm measurement accuracy on global baselines,
2. continuous measurements for time series of station positions and EOP,
3. turnaround time to initial geodetic results of less than 24 hours.

For achieving long term accuracy at the level of 1 mm or better, the VLBI2010 working group has suggested several strategies (Niell et al. 2005):

- reduce the random component of the delay-observable error, i.e., the per-observation measurement error, the stochastic properties of the clocks, and the unmodeled variations in the atmosphere,
- reduce systematic errors,
- increase the number of antennas and improve their geographic distribution,
- reduce susceptibility to external radio-frequency interference,

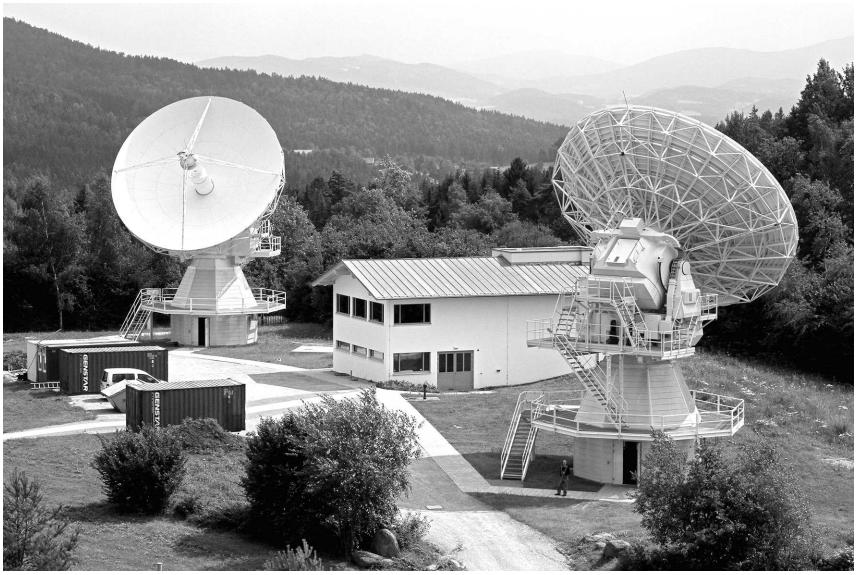

Figure 2.6: The Twin Telescope Wettzell with its new operations building (Photo: Dr. Alexander Neidhardt, TUM).

- increase observation density, i.e. the number of observations per unit of time,
- develop new observing strategies.

Since atmospheric effects remain the dominant error source of VLBI observations, it is intended to improve the determination of the atmospheric parameters. For this purpose, an increased sampling rate of the atmosphere above each radio telescope within an observing session is necessary. As a consequence, the new generation of radio telescopes have to slew faster than the old generation of radio telescopes. This will be achieved by building antennas with a relative small diameter of about 10 – 12 m, what is sufficient for geodetic purposes. Moreover, the operational costs are to be reduced by deploying these new generation of radio telescopes. Further instrumental and technical modifications concern the improvement of the receiving system in terms of its *SNR*, a faster data transfer via the Internet (e-transfer and e-VLBI), the employment of new hydrogen masers with improved frequency standards, and a greater bandwidth.

Side benefits of such low-cost and high-performance radio telescopes are the facilitation of enlarged networks and homogeneously distributed observing sites. Additionally, it may be possible to place multiple antennas at the same site while sharing data recording and transmission resources. This provides an increased observing density, which allows much faster and more diverse sampling of the atmosphere to help reduce systematic atmospheric effects, or may reduce clock stability requirements, as well as correlations between atmosphere, clocks and the local vertical component by observing different sources simultaneously (Niell et al. 2005).

The 20 m radio telescope in Wettzell is participating in geodetic VLBI measurements since 1983. It has been so far the most frequent scheduled VLBI station of the IVS network (Hase et al. 2009). Participating in all regular VLBI sessions, including all types of daily Intensive sessions, the Wettzell radio telescope is one of the most important sites of the IVS. But, serving for more than 25 years, the 20 m radio telescope Wettzell is operating at its technical limits. As continuous observations of Earth orientation parameters contradict with necessary maintenance cycles of the radio telescope more than one radio telescope is needed at one site. Therefore, it was decided to construct two identical radio telescopes at the Fundamental Station Wettzell (FSW). The Twin Telescope Wettzell (TTW) was built at the FSW as a pilot project in order to meet the future requirements of the next VLBI generation. The TTW consists of two identical fast moving radio telescopes with a diameter of 13.2 m and innovative ring focus optics which are optimized for observations with a wide spectrum receiver up to at least 12 GHz (Fig. 2.6; Hase et al. 2008).

If both antennas of a twin radio telescopes are available at the same time, new observation modes are feasible. On the one hand, both radio telescopes can observe the same source simultaneously to increase the sensitivity. On the other hand, the radio telescopes can point two different sources so that different subnets are tied at the same time. Latter can be modified in such a way that one radio telescope observe changing sources, while the other radio telescope is still tracking one source. Which special observing strategies appears for the Intensive series with the TTW will be discussed in Chap. 6.

3. Scheduling VLBI sessions

This chapter gives an overview on the procedure of scheduling VLBI observing plans as well as different optimization approaches. Furthermore, the groundwork for developing a new and improved approach for an automatic scheduling procedure is presented (Ch. 4).

3.1 Introduction on scheduling VLBI sessions

The information content of VLBI observables heavily depends on the configuration of the experiment. The observing configuration in turn depends on the source position and the actual orientation of the source with respect to the baseline. Thus, the observation schedule plays a crucial role in determining the types and precision of parameters that can be estimated. Some observing geometries impose limitations on the estimability and separability of certain parameters, so-called critical baseline configurations (see, e.g., Sovers et al. 1998, or Takahashi 1994).

A VLBI observing plan predefines the observing sequence of all participating radio telescopes of an observing session. Requirements for creating an observing plan are, among others, the station positions of the participating radio telescopes, the positions of suitable radio sources and the observing frequencies. The radio telescopes point at one source at a defined start time and record the emission of the radio source for a while before moving to the next radio source. At least two radio telescopes must observe the same source simultaneously for a geodetic VLBI observation. A network of several stations is able to point at different sources at the same time by forming sub-nets.

The scheduling procedure is embedded in limiting conditions of the system technology. For instance, the different slew times that are needed by the radio telescopes for moving and which depend on individual constructions, weights and engine powers, respectively, have to be taken into account. Even the duration of pointing at one radio source is different for each radio telescope and each radio source. Here, the influencing factors are the correlated flux density of the radio source, the antenna diameter of the radio telescope, the sensitivity of the receiver, and a threshold *SNR*. Further limitations which have to be explicitly taken into account are, e.g., restricted slew distances for azimuth-elevation mounted radio telescopes because of cable wrap, or individual horizon masks of some radio telescopes because of visual obstructions. How this limiting conditions can be considered mathematically can be seen, e.g., in Gipson (2012), or Sun (2013).

3.2 Current scheduling strategies

Up to date, only a few authors have investigated VLBI scheduling methods for geodetic and astrometric purposes. Most VLBI observing plans were created with the software package SKED (Vandenberg 1999), which is continually maintained and updated by John M. Gipson (NASA/GSFC, Gipson 2012). Initially, it helpfully supported to schedule handmade observing plans, later an automatic scheduling procedure was implemented by Steufmehl (1994).

Handmade observing plans needed experienced schedulers. Mainly observations to the strongest sources were chosen, ensuring the highest number observations within a predefined session duration. In contrast, the algorithm of Steufmehl (1994) selects the observations by a dynamic optimization process following the optimization of geodetic networks. As objective function, the covariance matrix of the estimated parameters is minimized. Because of the computational power limitations in the early 1990ties, the searching process was simplified to the point that created observing plans only approximate their optimal solutions. Nevertheless, it was a great step to ease the creation of VLBI observing plans, especially those of costly 24h-sessions. By adjusting several optimization parameters, the procedure can be used for different applications. Those

optimization parameters are, e.g., reduction of the slew time of the telescopes between two observations, reduction of the time pointing at one source, or avoiding to point at a source two times successively.

A further scheduling strategy is also implemented in the software package SKED. At that, the observing plan is optimized in terms of achieving a homogeneous source distribution at the hemispheres of each participating radio telescope in a short time period, solely. Therefore, this method is called uniform sky coverage. The fundamental idea of this method is as follows. One of the biggest influencing factors of VLBI-delay measurements is the troposphere. As described in Sec. 2.3.3, it is necessary to introduce tropospheric parameters, the zenith wet delays, as unknown parameters in the VLBI analysis. Obvious from Eq. 2.10, the entry of the Jacobian matrix that is related to a zenith wet delay is the elevation dependent wet mapping function $m_w(\varepsilon)$. Thus, systematic disturbances can occur because of an insufficient mapping function or weather turbulences. Particularly observations with low elevation angles are affected, because of the longer way through the troposphere. Observing homogeneously distributed over all elevation angles, the influence of an insufficient mapping function is reduced and the estimation of the zenith wet delay will be more reliable. To handle the influence of weather turbulences, an arithmetic averaging over all azimuths is taken place. Therefore, different sky regions should be covered within a short time period (Steufmehl 1994). Because of the homogeneous coverage of elevation angles and azimuths, a homogeneous coverage over the whole hemisphere results.

Recently, a further approach for scheduling with respect to VLBI2010 requirements was released. Sun (2013) developed the scheduling package VIE_SCHED that is part of the Vienna VLBI Software (VIEVS, Böhm et al. 2012). In that package, the uniform sky strategy is implemented as well as a new source-based scheduling strategy. It selects radio sources from a predefined catalog without regard for their direct impact on individual stations. Thus, the distribution of observed sources is optimized in terms of their sky-bound positions solely, which can be applied efficiently for large globally distributed networks with fast moving antennas. Although the scheduling process produces reasonable observing sequences, no improvements in the results were demonstrated (see also Sun et al. 2014).

Since in general all these scheduling strategies have been developed for global station networks which last 24 hours, they can be applied to Intensive sessions only within limits. The special conditions of Intensives, like small networks of two to three radio telescopes, great extents of the observing baselines, consequently quite small common visibilities and short session durations of one hour, have to be considered. Hence, a few authors had focused their efforts on refining the scheduling strategies for Intensive sessions.

Fischer et al. (2003) investigated the scheduling of INT2 sessions first and expressed the following findings:

- The sky coverage of simultaneously visible sources is fairly poor and only up to one third of the full working range of each telescope is covered with observable sources.
- Short duration schedules with only twenty scans react very sensitive to the selection of sources. Replacing in some cases a single scan changes the simulated accuracies for one or all unknown parameters significantly.
- The occurrence of scans with low elevations is absolutely necessary for the estimation of tropospheric path delays and already one single low elevation scan below 20° improves the simulated accuracy for the tropospheric delay considerably.
- The estimation of $\Delta UT1$ itself does not seem to be influenced directly by the existence of low elevation observations.
- Sources near the equator may improve the sensitivity for $\Delta UT1$ and should be included in the schedule if possible. Nevertheless, experiments without any equatorial sources may still lead to reasonable $\Delta UT1$ results.
- To reach uniform sensitivity for all unknown parameters a well balanced sky coverage is needed and the short duration schedules have to be prepared carefully. Longer slew times should be accepted to allow relatively big changes in spatial direction from one scan to the next.

Baver and Gipson focus their investigations on INT1 schedules. Summarizing their findings of several publications, e.g., Baver et al. (2004), Baver and Gipson (2010), Baver et al. (2012) or Baver and Gipson (2013):

- Scheduling strong sources might reduce the $\Delta UT1$ root mean square (RMS).
- The source distribution is important to achieving a low $\Delta UT1$ formal error.
- Better sky coverage is linked with smaller $\Delta UT1$ formal errors.
- Using a restricted source list with the strongest but unevenly distributed sources leads to schedule the same sources repeatedly in one session and, thus, a bad sky coverage, because only a few strong sources are available at some times of the year. The loss of a single source can then lead to dramatic changes in sky coverage, which in turn has a large effect on the $\Delta UT1$ formal errors.
- Using more but weaker sources yields schedules which are more robust but lowers the session observation counts because it takes longer to observe a weaker source.
- To observe source closer to the equator is considered to be important.
- Temporal sky coverage (how frequently areas of the sky are sampled) matters.
- On the one hand, lower elevation observations create better geometry for the estimates, reducing the $\Delta UT1$ estimate scatter. But lower elevation observations also introduce extra noise due to atmospheric turbulence, resulting in larger scatter. The improved geometry dominates until $\sim 20°$, at which point the extra noise dominates.
- Covering key areas might lower the RMS and the formal errors of $\Delta UT1$.

There are some other investigations to assess Intensive schedules, like the work of Uunila (2013), who classifies the spatial distribution of INT1 observing plans with special quality codes (see also Uunila et al. 2012). For this purpose, the source distribution is regarded in the hemisphere of a fictitious baseline reference point that is the projection of the baseline midpoint onto the ellipsoid and serves as the origin of a topocentric system with the tangential plane being the equatorial plane of the system. The horizon limits of both stations and the distribution of the observations are best displayed in a stereographic projection of the baselines midpoint hemisphere. The quality codes describe the geometric distribution of observations with respect to their counts in six defined sections of the stereographic projection. Analyzing the categorized observing plans by means of their $\Delta UT1$ formal error and RMS values lead to the conclusion that observations far down in the baseline sky plot cusps are important. This refers to sources which are observed with low elevation angles at both radio telescopes.

Another interesting regression diagnostic tool that can be used to investigate the design of VLBI experiments has been developed by Vennebusch (2008). Basing on the Singular Value Decomposition (SVD) combined with the Cluster Analysis (CA), this method is able to detect groups of important or less important observations and theirs influence on particular parameters. The method can help to achieve a deeper understanding of the impact of specific observations on the adjustment process and can thus be used to optimize the observation schedule by neglecting less important observations or by supporting observations which highly affect important parameters by appropriate observations. This regression diagnostic tool sounds very promising and may help to find important knowledge for the subject of this thesis. Therefore, the method will be described in the following sections in more detail followed by own investigations.

3.3 Assessment of VLBI observing plans via SVD and CA

The regression diagnostics tool by Vennebusch (2008) analyses the entire design or geometry of an experiment. As the Jacobian matrix contains information on the geometry of the design of an adjustment problem the procedure starts with the SVD of the Jacobian matrix. After applying the SVD, several assessment criteria result and the basis for the cluster analysis can be derived. For the detection of the impact of single or groups of observations on individual parameters a further method, the reduction of parameters, is needed. In the following, the three basic algorithms will be shortly described for a deeper understanding.

3.3.1 Singular value decomposition

The SVD is a tool that enables a detailed analysis of an $m \times n$ matrix $\mathbf{A} \in \mathbb{R}^n$ with rank r by the factorization into three matrices

$$\mathbf{A} = \mathbf{U} \cdot \mathbf{S} \cdot \mathbf{V}^T \tag{3.1}$$

(Trefethen and Bau 1997 or Lay 2003). The first r diagonal entries of $\mathbf{S}$ $(m \times n)$ are the singular values σ_i of $\mathbf{A}$, which are (usually) arranged in descending order $\sigma_1 \geq \sigma_2 \geq \ldots \geq \sigma_r > 0$,

$$\mathbf{S} = diag\begin{pmatrix}\sigma_1 & \sigma_2 & \ldots & \sigma_r & 0 & \ldots & 0\end{pmatrix}. \tag{3.2}$$

The columns of the $m \times m$ orthogonal matrix $\mathbf{U}$ are called left singular vectors $\mathbf{u}_i$ corresponding to the order of the singular values σ_i

$$\mathbf{U} = \left(\begin{array}{cccccccc} \vdots & \vdots & & \vdots & \vdots & & \vdots \\ u_1 & u_2 & \ldots & u_r & u_{r+1} & \ldots & u_m \\ \vdots & \vdots & & \vdots & \vdots & & \vdots \\ \underbrace{\qquad\qquad\qquad}_{\mathbf{U}_r} & & & & \underbrace{\qquad\qquad\qquad}_{\mathbf{U}_0} & & \end{array}\right), \tag{3.3}$$

where the first r columns $\mathbf{U}_r = \{\mathbf{u}_1, ..., \mathbf{u}_r\}$ span a basis for the column space $R(\mathbf{A})$ of the matrix $\mathbf{A}$. The columns of the $n \times n$ orthogonal matrix $\mathbf{V}$ are called right singular vectors $\mathbf{v}_i$

$$\mathbf{V} = \left(\begin{array}{cccccccc} \vdots & \vdots & & \vdots & \vdots & & \vdots \\ v_1 & v_2 & \ldots & v_r & v_{r+1} & \ldots & v_n \\ \vdots & \vdots & & \vdots & \vdots & & \vdots \\ \underbrace{\qquad\qquad\qquad}_{\mathbf{V}_r} & & & & \underbrace{\qquad\qquad\qquad}_{\mathbf{V}_0} & & \end{array}\right), \tag{3.4}$$

where the first r columns $\mathbf{V}_r = \{\mathbf{v}_1, ..., \mathbf{v}_r\}$ span a basis for the row space $R(\mathbf{A}^T)$ of the matrix $\mathbf{A}$.

In the sense of a least-squares adjustment, interpreting the Jacobian matrix $\mathbf{A}$ as a mapping from the space of the model parameters into the data space, the subspace $\mathbf{U}_r$ is related to the data space and the subspace $\mathbf{V}_r$ is related to the model space of $\mathbf{A}$ (Scales et al. 2001). For further details of the SVD see e.g. Golub and Kahan (1965), Kalman (1996) Trefethen and Bau (1997), Lay (2003) or Strang (2003).

Data resolution matrix

A data resolution matrix $\mathbf{H}$ (also known as 'Hat Matrix') being an $m \times m$ projection operator onto the data space of $\mathbf{A}$ can be computed by

$$\mathbf{H} = \mathbf{U}_r \mathbf{U}_r^T. \tag{3.5}$$

Following, e.g. Förstner (1987), the data resolution matrix can also be computed via the design matrix $\mathbf{A}$ and the covariance matrix $\mathbf{\Sigma_{yy}}$ of a least-squares adjustment

$$\mathbf{H} = \mathbf{A}\left(\mathbf{A}^T \mathbf{\Sigma}_{\mathbf{yy}}^{-1} \mathbf{A}\right)^{-1} \mathbf{A}^T \mathbf{\Sigma}_{\mathbf{yy}}^{-1}. \tag{3.6}$$

Impact factors

Since the elements of the data resolution matrix indicate how much weight each observation has on the adjusted observations (Dodge and Hadi 1999, Menke 1984 or Scales et al. 2001), the main-diagonal elements of $\mathbf{H}$ are called impact factors

$$\mathbf{h} = diag(\mathbf{H}). \tag{3.7}$$

The impact factors are closely related to partial redundancies (Förstner 1987). The redundancy numbers

$$r_i = 1 - h_i = (\mathbf{I} - \mathbf{H})_{ii} \quad (\text{for } \boldsymbol{\Sigma}_{\mathbf{yy}} = \mathbf{I}) \tag{3.8}$$

indicate how far errors in an observation show up in the corresponding residuals of the least-squares fit. Observations with large impact factors and thus weakly controlled observations are called high leverage points. These observations are important for the geometrical stability of a least squares solution. High leverage points significantly affect the accuracy of the estimated parameters and are necessary to avoid a defect of the configuration (Niemeier 2002).

Impact co-factors

The off-diagonal elements h_{ij} of $\mathbf{H}$, named impact co-factors, show the similarities between the observations. Small impact co-factors indicate a significantly distinct information content of the respective observations, whereas large impact co-factors show that the respective observations have been performed under similar geometric conditions (see, e.g., Gray and Ling 1984, or Hoaglin and Welsch 1978).

3.3.2 Cluster analysis

Cluster analysis is the most common method for estimating similarities between pairs of things. The cluster analyst's objective is to classify objects that are similar to each other in groups by means of measurable attributes (Romesburg 2004). This section describes the basic calculations of general cluster analysis as well as the cluster analysis for regression diagnostics. Detailed descriptions and a range of different algorithms can be found in, e.g., Duda et al. (2000) or Romesburg (2004).

Procedure

The basis of a general cluster analysis is a data matrix whose columns stand for objects and whose rows stand for attributes, the properties of the objects. As the attributes of the objects can be almost anything they could be measured in a mixture of units. Therefore, it may sometimes be advantageous to convert the original attributes to new dimensionless attributes, thus, standardizing the data matrix. After that the resemblance matrix has to be computed which contains the resemblance coefficients that indicate the degree of similarity between each pair of objects. At the beginning each object is regarded as being in a separate cluster. Now the clustering method can be applied to the resemblance matrix, consisting of a series of steps that incrementally merge similar objects to groups or clusters. In each step of the clustering method the closest two clusters will be grouped into one cluster, followed by a recalculation of the resemblance matrix to consider the new similarity coefficients between the new cluster and all other clusters. Several methods for recalculating the resemblance matrix exist. Here, the most widely used method called the unweighted pair-group method using arithmetic averages (UPGMA) is used. That means that the average value of the similarity coefficients which belong to the two objects that have been last grouped between a third object will be used as new similarity coefficient. Consequently, the resemblance matrix is reduced by one in each step of the clustering method until only one cluster remains that contains all original objects.

In case of regression diagnostics, the design matrix serves as data matrix for cluster analysis and the data resolution matrix $\mathbf{H}$, which can be computed by the design matrix $\mathbf{A}$ and the covariance matrix $\boldsymbol{\Sigma}_{\mathbf{yy}}$ of the observations as shown in Eq. 3.5 or Eq. 3.6, is used as resemblance matrix. As mentioned in Sec. 3.3.1, the elements of the data resolution matrix have two different meanings. The main diagonal entries h_{ii} are called impact factors because they indicate the influence of each observation on the adjusted observations. The off-diagonal elements h_{ij}, named impact co-factors, show the similarities between the observations. Small impact co-factors indicate a significantly distinct information content of the respective observations, whereas large impact co-factors show that the respective observations have been performed under similar geometric conditions. And, thus, the data resolution matrix serves as similarity matrix for the cluster analysis (see, e.g., Gray and Ling 1984, or Hoaglin and Welsch 1978). Table. 3.1 summarizes the three required steps of general cluster analysis and cluster analysis as used for regression diagnostics.

Step	General Cluster Analysis	Cluster Analysis for Regression Diagnostics
1.	obtain the data matrix	setting up the design matrix
2.	compute the resemblance matrix	compute the data resolution matrix
3.	execute the clustering method	execute the clustering method

Table 3.1: Terminology of general cluster analysis steps and for cluster analysis as used for regression diagnostics according to Romesburg (2004) and Vennebusch (2008).

Example For a graphical representation, an example of five coordinated points is used. Thus, the five points are the objects having two attributes, the x- and the y-coordinate, respectively. Having the positions of the points, the Euclidean distances between each pair of objects can be computed, which are presented by the dashed lines in Fig. 3.1. These distances will be interpreted as similarity coefficients in this example. Thus, small coefficients indicate a high similarity between two objects. Figure 3.1 displays the clustering of the five objects step-by-step until all objects have been merged into one common cluster.

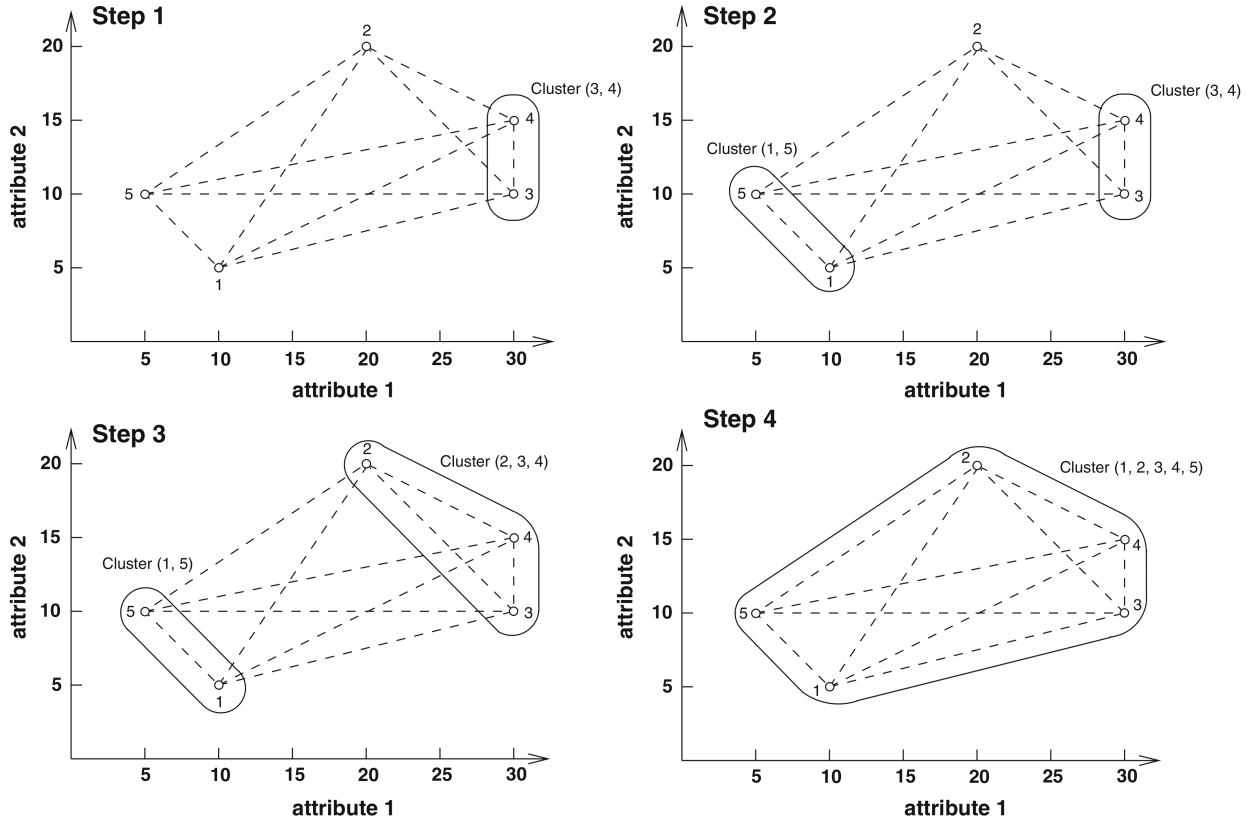

Figure 3.1: Cluster analysis example: clustering steps (Vennebusch et al. 2009).

Dendrogram

The results of the clustering process can be depicted in a map of sorts, called tree or dendrogram (Duda et al. 2000, Romesburg 2004). The x-axis of the dendrogram shows the objects and the y-axis shows the similarity scale at which the clusters have been merged together. Figure 3.2 shows the dendrogram for the example with Euclidean distances.

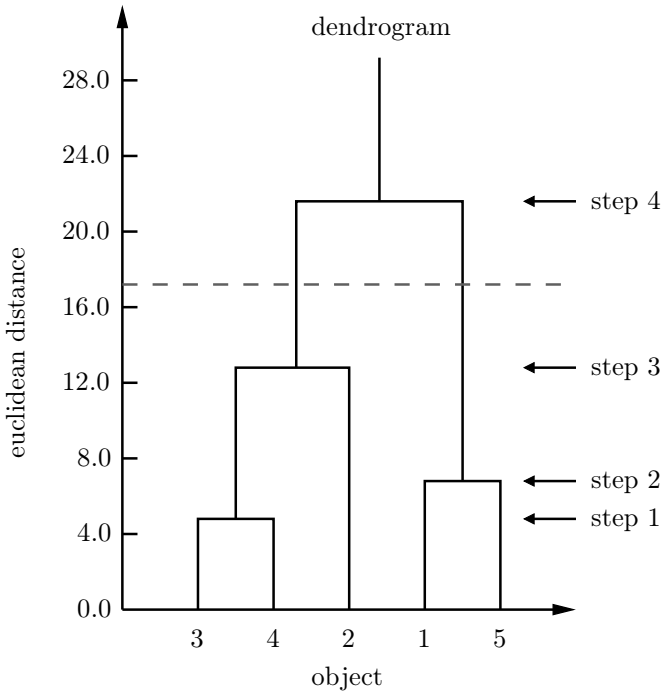

Figure 3.2: Dendrogram for the prior example with a tree cut (dashed line) at a large gap according to Romesburg (2004) and Vennebusch (2008). Beneath the tree cut, two clusters with distinct information contents are obtained.

To obtain groups of observations with significantly distinct information contents and not only one big cluster that contains all observations, the subdivision of the dendrogram at a reasonable height is necessary. This so named tree cut defines the number of final clusters and, therefore, the level of detail. A reasonable height for a tree cut is given by a large gap in the dendrogram, which indicates the clustering of two previously significantly distinct clusters, as shown by the exemplary dendrogram in Fig. 3.2. Nonetheless, the height of the tree cut is a subjective decision.

3.3.3 Parameter reduction

The method of parameter reduction enables the estimation of a subset of the original parameters without changing the original functional model (see, e.g., Teunissen 2000). This method partitions the original linear system (Eq. 3.9) in a way that the parameter vector $\mathbf{x}$ is divided into two vectors, where the parameters of interest $\mathbf{x}_1$ are separated from the others $\mathbf{x}_2$ (Eq. 3.10).

$$\mathbf{A}\mathbf{x} = \mathbf{y} \tag{3.9}$$

$$\begin{bmatrix}\mathbf{A}_1 & \mathbf{A}_2\end{bmatrix}\begin{bmatrix}\mathbf{x}_1\\ \mathbf{x}_2\end{bmatrix} = \begin{bmatrix}\mathbf{y}_1\\ \mathbf{y}_2\end{bmatrix} \tag{3.10}$$

Either a single parameter or a group of parameters can be chosen as parameters of interest. Eqs. 3.11 to 3.14 are used to compute the data resolution matrix and the impact factors for the reduced system.

$$\mathbf{P}^{\perp}_{\mathbf{A}_2} = \mathbf{I} - \mathbf{A}_2\left(\mathbf{A}_2^T\boldsymbol{\Sigma}^{-1}_{\mathbf{y}\mathbf{y}_2}\mathbf{A}_2\right)^{-1}\mathbf{A}_2^T\boldsymbol{\Sigma}^{-1}_{\mathbf{y}\mathbf{y}_2} \tag{3.11}$$

$$\bar{\mathbf{A}}_1 = \mathbf{P}^{\perp}_{\mathbf{A}_2}\mathbf{A}_1 \tag{3.12}$$

$$\bar{\mathbf{H}} = \bar{\mathbf{A}}_1\left(\bar{\mathbf{A}}_1^T\boldsymbol{\Sigma}^{-1}_{\mathbf{y}\mathbf{y}_1}\bar{\mathbf{A}}_1\right)^{-1}\bar{\mathbf{A}}_1^T\boldsymbol{\Sigma}^{-1}_{\mathbf{y}\mathbf{y}_1} \tag{3.13}$$

$$\bar{\mathbf{h}} = diag\left(\bar{\mathbf{H}}\right) \tag{3.14}$$

In this case the impact factors $\bar{\mathbf{h}}$ indicate the influence of each observation on the parameters of interest only.

Alternatively, this can also be computed via the SVD of the partitioned system. With the singular value decomposition of $\mathbf{A}_2 = \mathbf{U}_2\mathbf{S}_2\mathbf{V}_2$, the projector $\mathbf{P}^{\perp}_{\mathbf{A}_2}$ can be computed by

$$\mathbf{P}^{\perp}_{\mathbf{A}_2} = \mathbf{I} - \mathbf{U}_{2_{r_2}}\mathbf{U}^T_{2_{r_2}} \tag{3.15}$$

with r_2 denoting the rank of the matrix $\mathbf{U}_2$ and $\mathbf{U}_{2_{r_2}}$ consisting of the first r_2 columns of $\mathbf{U}_2$. Since $\bar{\mathbf{H}}$ is the projector onto the subspace formed by the columns of $\bar{\mathbf{A}}_1 = \mathbf{P}^{\perp}_{\mathbf{A}_2}\mathbf{A}_1$, it can also be derived by using the singular value decomposition of $\mathbf{A}_1 = \mathbf{U}_1\mathbf{S}_1\mathbf{V}_1$

$$\bar{\mathbf{H}} = \bar{\mathbf{U}}_{1_{r_1}}\bar{\mathbf{U}}^T_{1_{r_1}} \tag{3.16}$$

with r_1 denoting the rank of the matrix $\mathbf{U}_1$ and $\bar{\mathbf{U}}_{1_{r_1}}$ indicating the first r_1 columns of $\bar{\mathbf{U}}_1$.

3.3.4 Investigation of Intensive sessions

Vennebusch (2008) applied the regression diagnostics tool to a fictitious VLBI scenario, mainly. It consists of two stations which form an equatorial baseline and point at nine artificial radio sources that are located at the celestial equator and near the celestial poles. Considering different parametrizations, from single parameters to different composed parameter sets, led to the following findings focusing on Intensives:

- For the sole determination of the clock offset, every observation is of equal importance. For the clock rate, observations at the end of the observing session are most important.
- Observations performed with low elevations are needed in particular for the determination of atmospheric zenith path delays.
- For the sole determination of the Earth rotation angle, observations of equatorial sources lying orthogonal to the baseline (at the time of the observation) are needed. Observations to polar sources can be omitted.
- For the composed parameter set (clock offset, clock rate and Earth rotation angle) different observations are needed: Observations into every direction of the mutually visible part of the celestial sphere is responsible for the clock offset determination. The same observation constellation is needed at the end of the observing session in order to determine the clock rate parameter. For the Earth rotation angle, still observations to equatorial sources are of main importance.
- For more complex parametrizations, the interpretation of the regression diagnostics is complicated by the unavoidable increase of complexity in the relations between the parameters involved.

Since these findings confirm some conclusions of other researchers, the diagnostics tool seems to be promising for deriving specific geometric criteria for optimized Intensive observations.

To verify the validity of these findings for real Intensive sessions, special investigations have been carried out here. For this purpose, different Intensive sessions have been analyzed via cluster analysis. Here, the results of three different representative Intensive observing plans will be interpreted. First, a fictitious Intensive observing plan, at which the result of the clustering can best be seen, has been generated using the scheduling software SKED. In this, the uniform sky scheduling method has been used to create an observing plan with the radio telescopes in Tsukuba and Wettzell using a fictitious source catalog with homogeneously distributed radio sources. The result is an INT2-like session with a uniform cover of the hemisphere above each radio telescope. The other Intensive sessions considered here are a real INT2 and a real INT1 observing plan. For the investigations, the design matrix has been set up using the parametrization for Intensive sessions described in Sec. 2.3.3, i.e., a clock polynomial (cl_0, cl_1 and cl_2), an atmospheric offset per station (at_A and at_B) and the Earth rotation parameter $\Delta UT1$.

The clustered observations will be depicted by means of sky-plots which show the source sample on the hemisphere above each station (Fig. 3.6). In addition, also an alternative way for the presentation of observed sources will be introduced.

Nothnagel and Campbell (1991) developed a procedure which graphically displays the geometric configuration of each observation relative to a fictitious baseline reference point (brp). This reference point is defined as the projection of the baseline midpoint onto the ellipsoid and serves as the origin of a topocentric system with the tangential plane being the equatorial plane of this system (Fig. 3.3).

By using simple rotation matrices, the observation's azimuth α and elevation ε can be transformed in the baseline system. Furthermore, the horizon limits of both stations A and B are transferable to the baseline system. The baseline system can be interpreted as a hemisphere put on top of the ellipsoid at the baseline reference point. Figure 3.4 illustrates the common hemisphere's visibility of both radio telescopes by shifting the horizon lines of the stations to the baseline reference point in parallel. Perpendicular to the baseline, there are narrow but also deep valleys in the common visibility, which will be named cusps in this work. Observed sources in these cusps are those with the lowest common elevations for both radio telescopes. Uunila (2013) used the same depiction for her classification purposes (cf. Sec. 3.2).

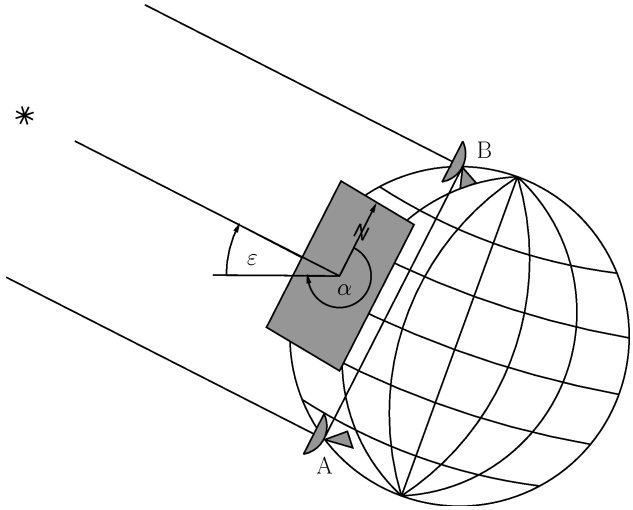

Figure 3.3: Example of the midpoint based reference system (according to Nothnagel and Campbell 1991).

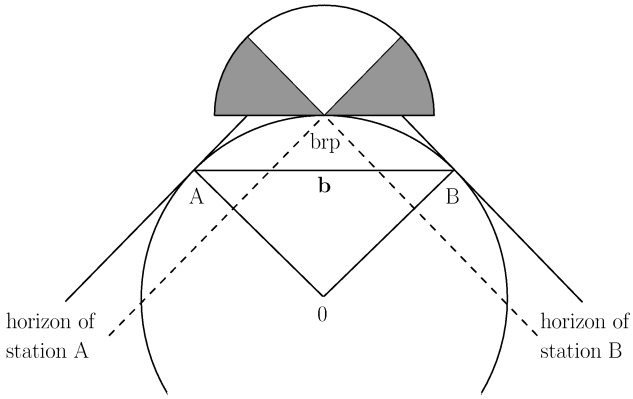

Figure 3.4: Geometry of baseline reference system and horizon mask (according to Nothnagel and Campbell 1991).

Fictitious Intensive observing plan

The regression diagnostics tool has been applied to the fictitious Intensive session with homogeneously distributed observations. In the following, the focus will be on the major results of the comprehensive analysis components, particularly the clustering of the observations and the impact of the clusters on the estimated parameters.

After applying the cluster analysis to the fictitious session and cutting the dendrogram at a reasonable height five clusters emerged which are depicted in Fig. 3.5. The positioning of the different groups of observations are depicted in the skyplots of the hemisphere above each telescope and above the baseline mid-point (Fig. 3.6). The observations of the red cluster and those of the green cluster encircle the observations of the other clusters. These are the observations with the lowest elevation values for either telescope.

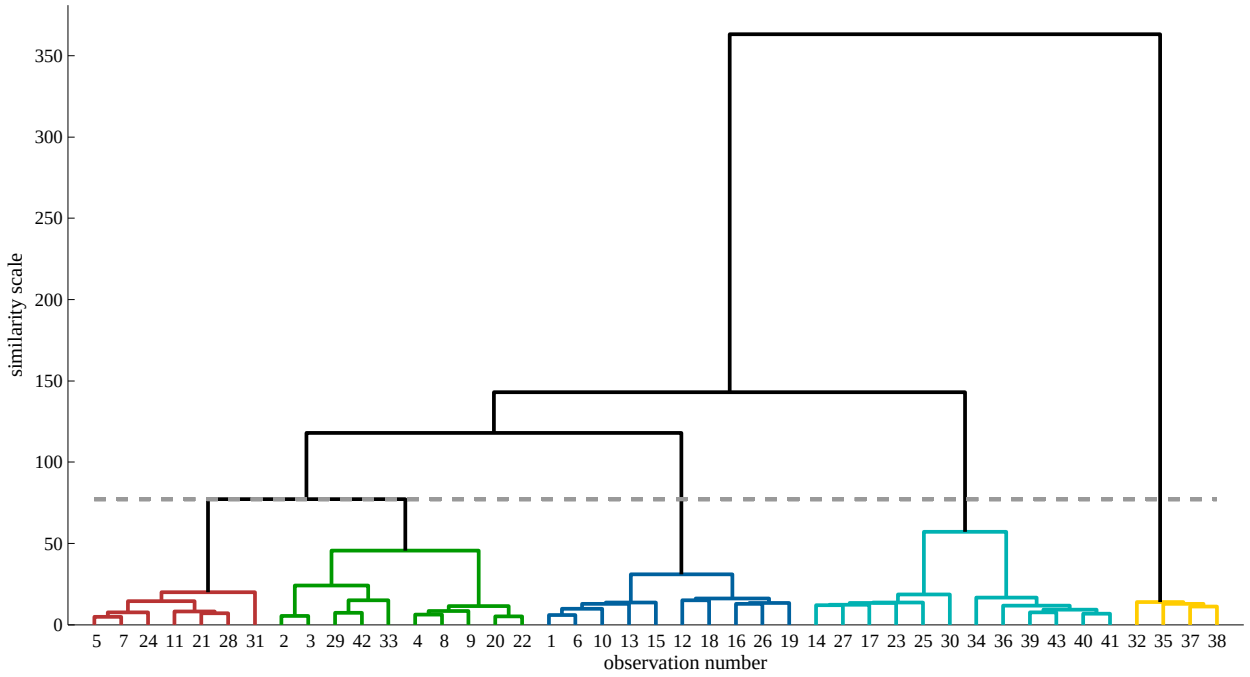

Figure 3.5: Dendrogram of the uniform sky scheduled test session.

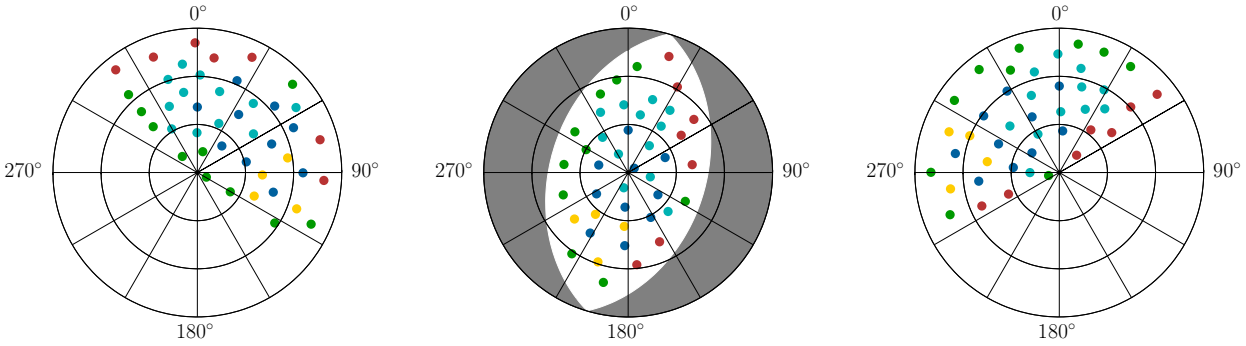

Figure 3.6: Skyplot of Wettzell (left), the baselines mid-point (center) and Tsukuba (right) for the uniform sky scheduled test session with clustered observations.

		cluster					mean IF of one obs.
		7	4	10	12	10	
single parameters	$\Delta UT1$	**0.035**	**0.029**	**0.026**	0.021	0.013	0.023
	cl_0	0.020	0.007	0.022	0.009	**0.051**	
	cl_1	0.023	0.004	**0.033**	0.014	**0.032**	
	cl_2	0.019	0.007	**0.029**	**0.024**	**0.026**	
	at_A	0.010	0.012	**0.056**	0.013	0.016	
	at_B	**0.079**	0.004	0.013	0.006	0.023	
groups of parameters	cl	0.047	0.039	**0.076**	**0.081**	**0.078**	0.070
	at	**0.093**	0.016	**0.075**	0.017	0.032	0.047

Table 3.2: Average impact factors of each cluster for each single parameter and for two groups of parameters, all three clock parameters in the first group and both atmospheric parameters in the second group. Values that are greater than the average impact factor of one observation on the respective number of parameters are highlighted, those average values are listed in the last column of the table. The values in the colored table elements are the number of observation of the respective cluster.

By the method of parameter reduction, average impact factors of each cluster have been computed for each single parameter and for two groups of parameters where the clock parameters and the atmospheric parameters have been merged respectively (Tab. 3.2). By reference to Tab. 3.2 can be seen which clusters have a great influence on individual parameters. The important clusters for the target parameter $\Delta UT1$ are the yellow, red and green clusters, the latter two consist of observations with low elevations (cf. Fig. 3.6). An in-depth study of the observed sources of the yellow cluster revealed that the source positions are located near the equator. The distance between a radio source position and the equator is given by the declination of the radio source. It has been figured out that the distances between the sources of the yellow cluster and the equator amounts between 6° and 34°. The mean source declinations of the other clusters are substantially bigger than those of the yellow cluster. Furthermore the individual declinations of the other clusters are widely distributed. The blue, green and turquoise clusters influence the clock parameters substantially. Observations with low elevations highly influence the atmospheric parameters. Those are arranged in the green cluster in case of station A (Tsukuba) and in the red cluster in case of station B (Wettzell).

To validate the identified relations, the formal errors of the parameters have been examined as well. Within the least-squares adjustment, a priori variances of the observations, taking into account antenna specifications and the geometry of the design (see Eq. 2.21 – 2.23 and Eq. 4.26 – 4.28), are used to populate the covariance matrix of the observations $\mathbf{\Sigma_{yy}}$. With the Jacobian matrix $\mathbf{A}$, the covariance matrix $\mathbf{\Sigma_{xx}}$ of the parameters $\mathbf{x}$, including the squared formal errors on the main-diagonal, can be computed by

$$\mathbf{\Sigma_{xx}} = \left(\mathbf{A}^T \mathbf{\Sigma_{yy}^{-1}} \mathbf{A}\right)^{-1}. \tag{3.17}$$

The variations of the formal errors of the parameters have been analyzed which are due to the respective observations of individual clusters being deleted from the observing plan. These results are shown for the parameters $\Delta UT1$, at_A and at_B in Fig. 3.7. Although the yellow cluster has a greater average impact factor for $\Delta UT1$ than the turquoise and the blue clusters, the increase of the formal error is bigger when these clusters are removed (Fig. 3.7 left). This is the consequence of the greater number of observations in the aforementioned clusters (cf. Tab. 3.2). Taking the square root of the number of observations into account, indeed the $\Delta UT1$ formal error increases most if the observations of the red cluster, which has the greatest average impact factor, would be deleted (Fig. 3.8 left). However, the lost of the observations of the green and the turquoise cluster respectively still cause a greater increase of the formal error than the lost of the observations of the yellow cluster. Surprisingly, the delete of the observations of the blue cluster results in a decrease of the $\Delta UT1$ formal error taking the square root of the number of observations into account.

The previously identified dominating clusters for the atmospheric parameters were also reflected by the changes of the zenith wet delay's formal errors, i.e., the green cluster for Tsukuba and the red cluster for Wettzell (Fig. 3.7 center and right). This is also true if the square root of the number of observations would

be taken into account (Fig. 3.8 center and right). Here, the consideration of the number of observations has a lower influence than for the $\Delta UT1$ formal errors. In the case of station A, the order of increase of the formal errors corresponds to the order of average impact factors of the different clusters exactly. Concerning station B, the delete of the observations of the two most influencing clusters (red and blue) cause the greatest increase of the formal error indeed. However, the order of increase of the formal errors of the other clusters disagree with the order of their average impact factors. Again the *at* formal errors exhibit a decrease if the observations of less important clusters would be deleted and the square root of the number of observations would be applied.

Since the timing of the observations is more important for the clock parameters than the geometry, the changes of the formal errors of the clock parameters are meaningless. Considering the impact factors for the clock parameters in chronological order (Fig. 3.9), colored in theirs respective cluster colors, it is recognizable

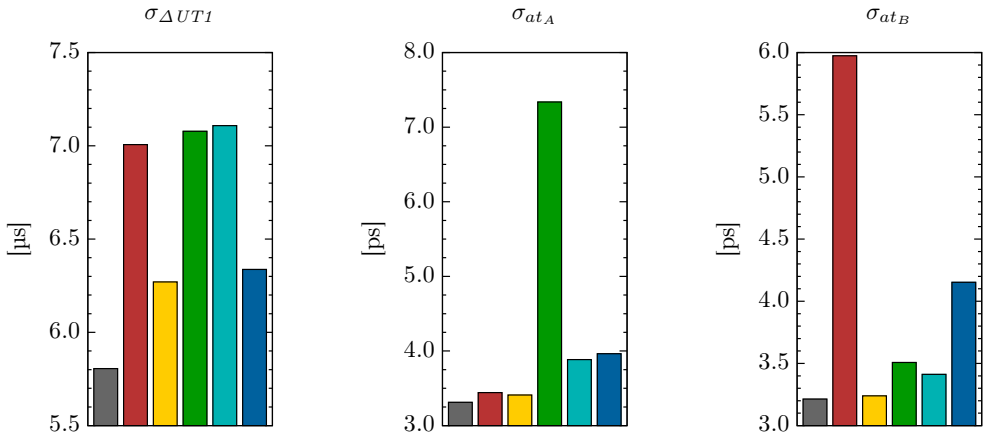

Figure 3.7: Formal errors of $\Delta UT1$ (left), zenith wet delay of station A (center) and zenith wet delay of station B (right). The gray bar represents the formal error determined by the original observing plan. The other bars represent the formal errors determined without the observations of the color-coded cluster.

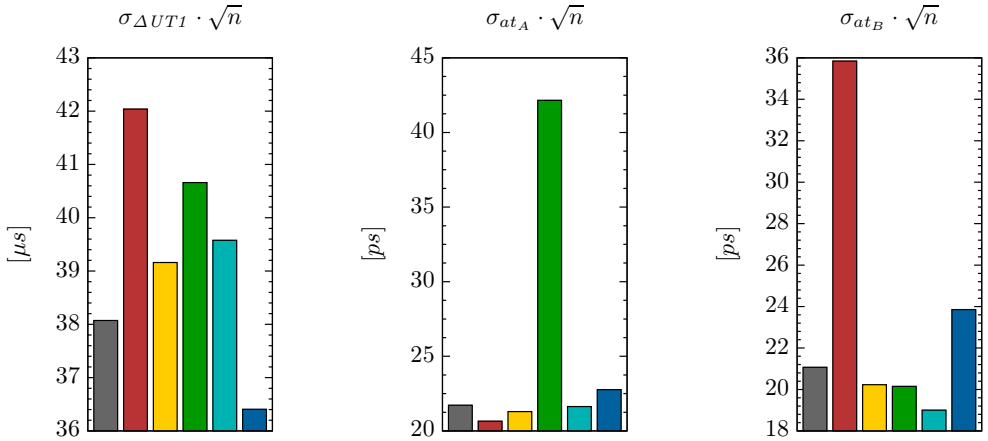

Figure 3.8: Formal errors of $\Delta UT1$ (left), zenith wet delay of station A (center) and zenith wet delay of station B (right) multiplied with the square root of the respective number of observations. The gray bar represents the formal error determined by the original observing plan. The other bars represent the formal errors determined without the observations of the color-coded cluster.

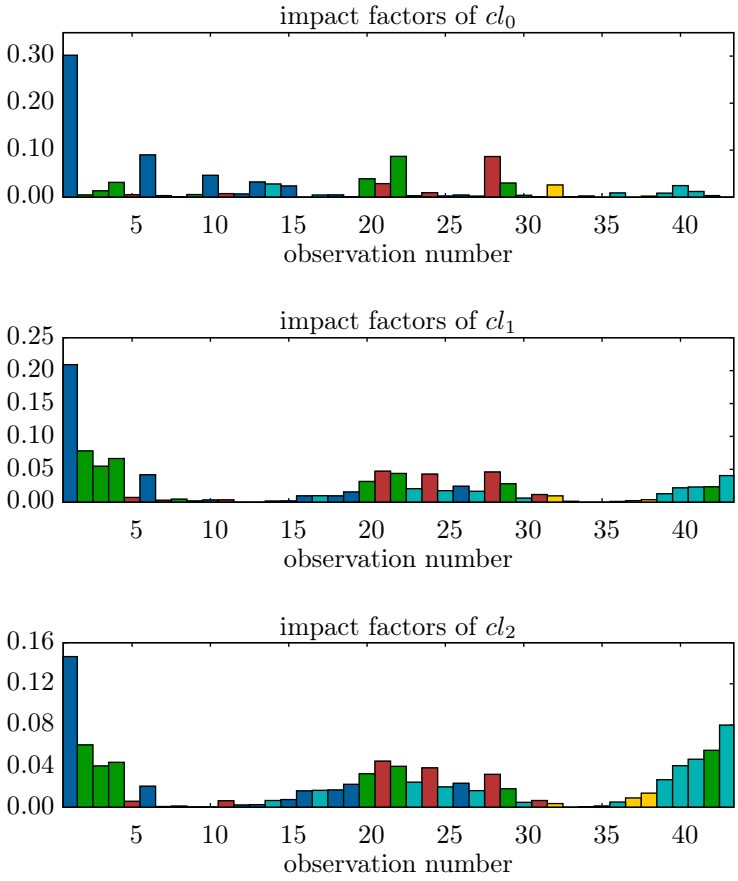

Figure 3.9: Impact factors for the three clock parameters in chronological order, colored in their respective cluster colors as in Fig. 3.5.

that the most influential observations are arranged at the beginning, at the middle and at the end of the session. These observations belong to the blue, green and turquoise clusters in particular.

Real Intensive sessions

In the following, results of the cluster analysis of real Intensive observing plans will be examined. It is necessary to find out if the findings of the test sessions also apply to real Intensive sessions with real source positions. For that purpose, two exemplary sessions will be used – one real INT2 session (K11064) and one real INT1 (I12010) session.

The mid-point skyplots of both sessions with their clustered observations are depicted in Fig. 3.10. Conspicuously, there is no strict geometric distinction as it was the case for the test session. Observations to the same source but time-displaced seem to be associated with different clusters occasionally. Nonetheless, similar distinct clusters are recognizable.

In case of the INT2 session, the low elevation observations are arranged in the red and the yellow cluster and, in fact, these are the main important clusters for $\Delta UT1$ and the atmospheric parameters as the average impact factors, shown in Tab. 3.3, confirm. Sources with short orthodromic distances to the equator are contained in the same clusters. The minimal distances between the sources and the equator are found in the red cluster with a minimal distance of 1.6°, a maximal distance of 15° and a mean distance of 9°. But also the yellow cluster contains observations with short distances between sources and the equator. Here the minimal

distance amounts to 24° and, although the maximal distance amounts to 58°, the average value totals just 38° because the shorter distances prevail. However, also the green cluster is indicated to be important for $\Delta UT1$. But here, the source declination amounts to 48°, thus, this cluster appears to be not important because of sources near the equator. Therefore, it is assumed that there are important low elevation observations, but, only three of eleven observations have elevations below 30° for the station in Tsukuba. Eventually, no evident reason could be found that justifies the impact of the green cluster for $\Delta UT1$.

The situation is more complex for the INT1 session. Again the main important clusters for $\Delta UT1$ are the red, the yellow and the green ones. Two of the three red-clustered sources have a short distance to the equator of less than 40°. Additionally, all three observations have been carried out under relatively low elevations of 22° on average for both radio telescopes. For this reason, it is also an important cluster for the atmospheric parameter at_A. The yellow cluster is a mixture of low elevation observations and observations to sources near the equator. Except of one observation, all of those in the green cluster have very low observations for the station Wettzell, thus, this cluster is of main importance for the parameter at_B. The one exceptional observation is quasi opposites, being a very low elevation observation for the other station (in Kokee Park). Furthermore, the turquoise cluster impacts both atmospheric parameters. Especially two observations of this cluster lie in a cusp of the midpoint sky-plot (cf. Fig 3.10b), indicating low elevations for both stations. Since the blue cluster consists of three observations with very low elevations for the station in Kokee Park (10.7°, 16.2° and 11.4°), is was expected that this cluster has also a great impact on at_A at least, but incomprehensibly that is not the case.

3.3.5 Conclusions of initial investigations

The regression diagnostics tool with cluster analysis has been applied to different Intensive scenarios. The analysis of the fictitious session with homogeneously distributed observations revealed that the cluster analysis is able to detect groups of observations with geometric similarities. Concerning the target parameter $\Delta UT1$, three important groups of observations stand out – the red, yellow and green cluster. While the observations of the red and the green cluster could be classified with low elevation observations of the respective radio telescopes clearly, the observations of the yellow cluster are those to radio sources that are close to the equator. By the reduction of parameters and the examination of the formal errors the influence of different clusters on single parameters has been proven. Therefore, this analysis confirm some of the findings that Vennebusch (2008) has made by means of the analysis of other fictitious VLBI experiments. In addition, it has been found out that observations to sources near the equator and observations with low elevations are of high importance for the determination of the target parameter $\Delta UT1$.

The interpretation of the cluster analysis of real Intensives is very complicated as Vennebusch (2008) predicted. There is no clear geometric distinction as it is for the fictitious session and the assignment of some observations to the clusters seems to be incorrect. A reason for this might be that an observation can fulfill more than one geometric criteria so that it could be assigned to several clusters. Furthermore, even a cluster whose observations fulfill all the same geometric criteria being, e.g., of high impact for the determination of a certain parameter, are not categorized in the same cluster. Eventually, these investigations both partly approve and disagree the before mentioned findings.

Due to this complexity, it might be inadequate to consider just the average impact factor per cluster. Thus, the impact factor of each single observation on different parameters has been examined. Figures 3.11 to 3.13 show individual observations (color-coded according to their corresponding clusters) with high impact factors for single parameters, left $\Delta UT1$, middle at_A and right at_B, of the three examined Intensive sessions. Two things stand out in every sky-plot immediately. First, in no case the entire group of observations of a cluster noted as important has a really high impact on a certain parameter. And second, in every case individual or several observations of a cluster noted as important have also a high impact on a certain parameter. Concerning the parameter $\Delta UT1$, conspicuously, important observations accumulate in the cusps of the midpoint sky-plot leaving a gap in the middle area. In case of the atmospheric parameters at_A and at_B, there is always at minimum one observation, but mostly more, near the center of the sky-plot besides the low elevation observations detected as important. Additionally, there are observations on the opposite site

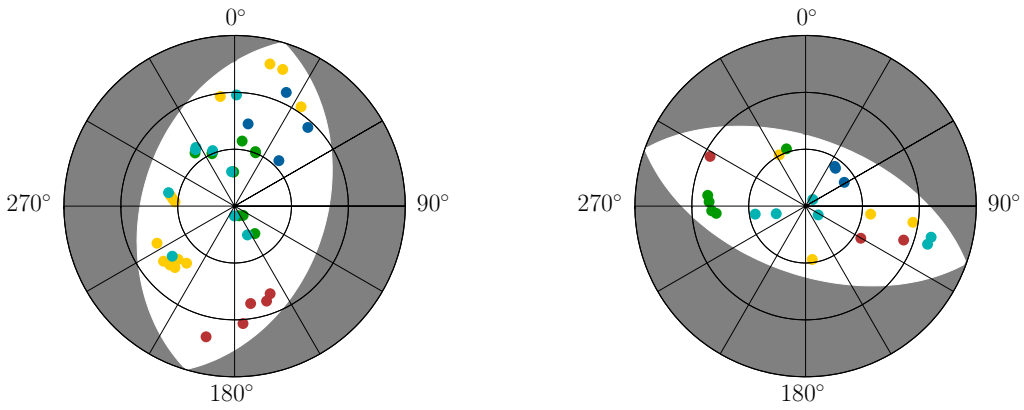

(a) INT2 (K11064). (b) INT1 (I12010).

Figure 3.10: Clustered observations of an exemplary INT2 (a) and an exemplary INT1 (b) session.

	cluster				
	5	13	11	9	4
$\Delta UT1$	**0.036**	**0.029**	**0.026**	0.013	0.012
at_A	0.009	**0.041**	0.022	0.013	0.017
at_B	**0.060**	**0.033**	0.001	0.018	0.022

(a) INT2 (K11064).

	cluster				
	3	4	5	6	3
$\Delta UT1$	**0.087**	**0.063**	**0.054**	0.033	0.006
at_A	**0.053**	0.033	0.015	**0.087**	0.036
at_B	0.009	0.033	**0.086**	**0.057**	0.022

(b) INT1 (I12010).

Table 3.3: Average impact factors of each cluster for $\Delta UT1$ and both atmospheric parameters for the exemplary INT2 (a) and INT1 (b) session. Values that are greater than the average impact factor of one observation on one parameter are highlighted.

of the sky-plot, meaning observations with very high elevations for the respective station and low elevations for the partner telescope. This fact is due to the strategy of the uniform sky scheduling method, described in Sec. 3.2, as observing distributed over different elevation angles and different azimuths is necessary for a reliable determination of the atmospheric parameters.

It can be concluded that the cluster analysis of Intensive sessions is only restrictedly suitable for finding geometric conditions for important observations. The not very strict assignment of observations to different clusters allows just vague assumptions and ambiguous possibilities of interpretation. However, it has been found that the impact factors of single observations offer the possibility of a more detailed analysis of the importance of observations. Since the impact factors take into account the entire design of a VLBI session with respect to the parameters to be estimated, they are more informative than partial derivatives of a functional model which only provide the theoretical sensitivity of single observations on single parameters independently of other observations. Thus, the use of impact factors has great potential for improving the schedules of VLBI sessions.

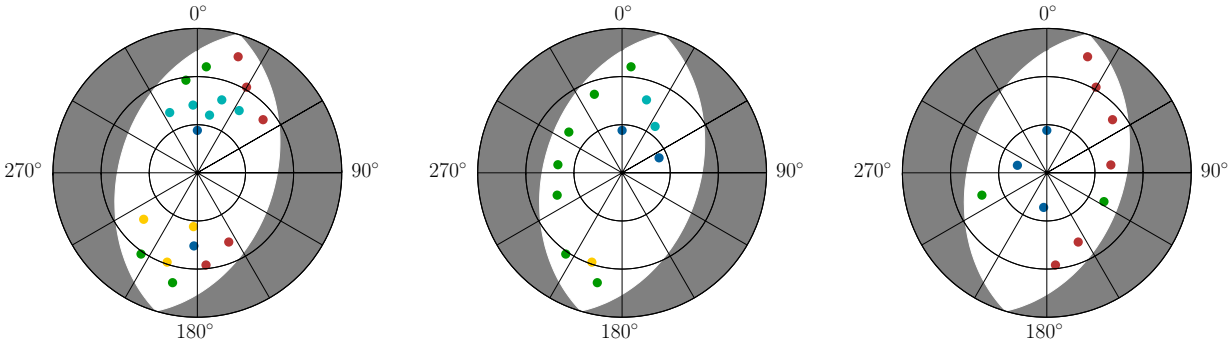

Figure 3.11: Observations with high impact factors for $\Delta UT1$ (left), at_A (middle) and at_B (right) for the fictitious INT2 session.

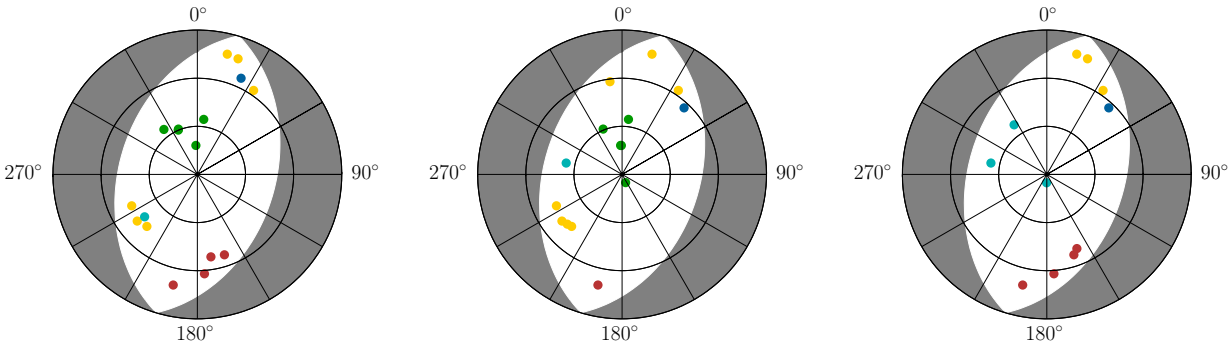

Figure 3.12: Observations with high impact factors for $\Delta UT1$ (left), at_A (middle) and at_B (right) for the examined INT2 session (K11064).

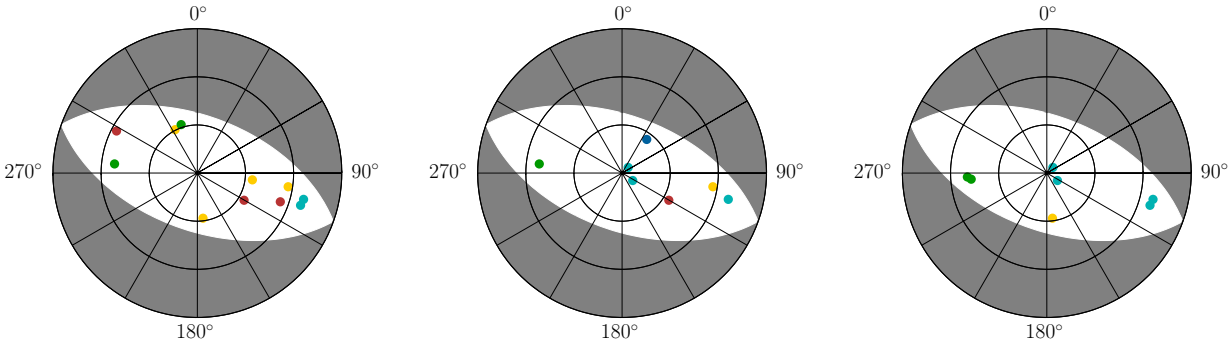

Figure 3.13: Observations with high impact factors for $\Delta UT1$ (left), at_A (middle) and at_B (right) for the examined INT1 session (I12010).

4. Scheduling strategy on the basis of impact factors

There are different reasons for developing a new scheduling procedure. On the one hand, none of the existing scheduling methods has been designed for the optimization of Intensive sessions, which represent a special case of VLBI observing sessions. On the other hand, the goal of this work is the implementation of twin radio telescopes in Intensive observing plans but no existing scheduling program provides the possibility to investigate the potential of twins within Intensives. Thus, in this work a new scheduling procedure for Intensive sessions has been developed.

The requirement for the scheduling procedure is that each observation will be chosen sequentially and automatically under the condition that the entire observing geometry is optimized. Previous investigations, described in Sec. 3.3, have shown that the impact factors of the observations, derived by SVD of the design matrix, are well suited for indicating influential observations for the estimated parameters. Therefore, the impact factors of the observations are used as selection criteria for the VLBI observations. Thus, no subjective idea on how the schedule should look like needs to be introduced for this approach, as only an objective criterion, the geometry, is used.

The observations have to be chosen successively by analyzing the current Jacobian matrix that consists of all previous observations and the potential new observation. This means that each following observation should be chosen in a way that the observing geometry is optimized based on the current state of the observing schedule. Since the geometric improvement can be determined via the impact factors of the potential new observation, they have to be computed several times during the scheduling process. The data resolution matrix, that contains the impact factors on the main-diagonal, can be computed via SVD as described in Sec. 3.3.1 or via the design matrix and the covariance matrix of the observations according to Eq. 3.6. As only the impact factor of the new observation is of interest, the method of recursive least squares adjustment can be used to economize computational costs. This method will be introduced in Sec. 4.1 before the entire concept of the scheduling procedure will be described detailed in Sec. 4.2.

4.1 Recursive least squares adjustment

Suppose the observations are separated into the uncorrelated vectors $\mathbf{y}_1$ and $\mathbf{y}_2$ with their covariance matrices $\mathbf{\Sigma}_{\mathbf{y}\mathbf{y}_1}$ and $\mathbf{\Sigma}_{\mathbf{y}\mathbf{y}_2}$ which have the common unknown vector $\mathbf{x}$ but originate from measurements at different times. It is possible to estimate the unknown parameters in a Gauss-Markoff model with the first observing block $\mathbf{y}_1$ immediately after it is available and to determine the gain of further observations $\mathbf{y}_2$ on the basis of the first result (see, e.g., Koch 1999). This approach enables the determination of impact factors of subsequent observations without computing the SVD of the whole Jacobian matrix. The parameters can be estimated with the first observing block by

$$\hat{\mathbf{x}}_1 = \left(\mathbf{A}_1^T \mathbf{\Sigma}_{\mathbf{y}\mathbf{y}_1}^{-1} \mathbf{A}_1\right)^{-1} \mathbf{A}_1^T \mathbf{\Sigma}_{\mathbf{y}\mathbf{y}_1}^{-1} \mathbf{y}_1, \tag{4.1}$$

their covariance matrix by

$$\mathbf{\Sigma}_{\hat{\mathbf{x}}\hat{\mathbf{x}}_1} = \left(\mathbf{A}_1^T \mathbf{\Sigma}_{\mathbf{y}\mathbf{y}_1}^{-1} \mathbf{A}_1\right)^{-1} \tag{4.2}$$

and the respective residuals by

$$\bar{\mathbf{v}}_1 = \mathbf{A}_1 \hat{\mathbf{x}}_1 - \mathbf{y}_1. \tag{4.3}$$

The common solution of both observing blocks is then composed of the first solution $\hat{\mathbf{x}}_1$ and an additional term for the second observations $\mathbf{\Delta x}$

$$\hat{\mathbf{x}} = \hat{\mathbf{x}}_1 + \mathbf{\Delta x}. \tag{4.4}$$

The redundancies of the second observations are

$$\mathbf{v}_2 = \mathbf{A}_2\hat{\mathbf{x}} - \mathbf{y}_2 \tag{4.5}$$
$$\mathbf{v}_2 = \mathbf{A}_2\hat{\mathbf{x}}_1 + \mathbf{A}_2\mathbf{\Delta x} - \mathbf{y}_2, \tag{4.6}$$

the latter resulting from substituting Eq. 4.4 in Eq. 4.5.

Resolving Eq. 4.6, it can be rewritten in a block matrix equation system (Eq. 4.8)

$$\mathbf{v}_2 - \mathbf{A}_2\mathbf{\Delta x} + \mathbf{y}_2 - \mathbf{A}_2\hat{\mathbf{x}}_1 = 0 \tag{4.7}$$
$$\underbrace{\begin{bmatrix}\mathbf{I} & -\mathbf{A}_2\end{bmatrix}}_{\mathbf{B}} \underbrace{\begin{bmatrix}\mathbf{v}_2 \\ \mathbf{\Delta x}\end{bmatrix}}_{\mathbf{v}^*} + \underbrace{(\mathbf{y}_2 - \mathbf{A}_2\hat{\mathbf{x}}_1)}_{\mathbf{w}} = 0 \tag{4.8}$$
$$\mathbf{B}\quad\mathbf{v}^* + \mathbf{w} = 0 \tag{4.9}$$

and formulated as a model of the adjustment with condition equations (Eq. 4.9), with $\mathbf{v}^* = \left[\begin{smallmatrix}\mathbf{v}_2 \\ \mathbf{\Delta x}\end{smallmatrix}\right]$ being the "residuals" of $\mathbf{y} = \left[\begin{smallmatrix}\mathbf{y}_2 \\ \hat{\mathbf{x}}_1\end{smallmatrix}\right]$ with $\mathbf{\Sigma_{yy}} = \left[\begin{smallmatrix}\mathbf{\Sigma}_{\mathbf{yy}_2} & \mathbf{0} \\ \mathbf{0} & \mathbf{\Sigma}_{\hat{\mathbf{x}}\hat{\mathbf{x}}_1}\end{smallmatrix}\right]$.

The normal equation system of this model is

$$\mathbf{B\Sigma_{yy}B}^T\mathbf{k} + \mathbf{w} = 0 \tag{4.10}$$

where

$$\mathbf{B\Sigma_{yy}B}^T = \begin{bmatrix}\mathbf{I} & -\mathbf{A}_2\end{bmatrix}\begin{bmatrix}\mathbf{\Sigma}_{\mathbf{yy}_2} & \mathbf{0} \\ \mathbf{0} & \mathbf{\Sigma}_{\hat{\mathbf{x}}\hat{\mathbf{x}}_1}\end{bmatrix}\begin{bmatrix}\mathbf{I} \\ -\mathbf{A}_2^T\end{bmatrix} = \mathbf{\Sigma}_{\mathbf{yy}_2} + \mathbf{A}_2\mathbf{\Sigma}_{\hat{\mathbf{x}}\hat{\mathbf{x}}_1}\mathbf{A}_2^T. \tag{4.11}$$

Solving Eq. 4.10 according to $\mathbf{k}$ and inserting Eq. 4.11 and Eq. 4.8 results in

$$\mathbf{k} = -\left(\mathbf{B\Sigma_{yy}B}^T\right)^{-1}\mathbf{w} \tag{4.12}$$
$$\mathbf{k} = -\left(\mathbf{\Sigma}_{\mathbf{yy}_2} + \mathbf{A}_2\mathbf{\Sigma}_{\hat{\mathbf{x}}\hat{\mathbf{x}}_1}\mathbf{A}_2^T\right)^{-1}(\mathbf{y}_2 - \mathbf{A}_2\hat{\mathbf{x}}_1). \tag{4.13}$$

Then the wanted residuals of $\mathbf{y}_2$ and the addition of the estimated parameters $\mathbf{\Delta x}$ can be computed by

$$\begin{bmatrix}\mathbf{v}_2 \\ \mathbf{\Delta x}\end{bmatrix} = \mathbf{v}^* = \mathbf{\Sigma_{yy}B}^T\mathbf{k} = \begin{bmatrix}\mathbf{\Sigma}_{\mathbf{yy}_2} & \mathbf{0} \\ \mathbf{0} & \mathbf{\Sigma}_{\hat{\mathbf{x}}\hat{\mathbf{x}}_1}\end{bmatrix}\begin{bmatrix}\mathbf{I} \\ -\mathbf{A}_2^T\end{bmatrix}\mathbf{k} = \begin{bmatrix}\mathbf{\Sigma}_{\mathbf{yy}_2}\mathbf{k} \\ -\mathbf{\Sigma}_{\hat{\mathbf{x}}\hat{\mathbf{x}}_1}\mathbf{A}_2^T\mathbf{k}\end{bmatrix}. \tag{4.14}$$

To determine the impact factors of the second observing vector $\mathbf{y}_2$, the covariance matrix of the residuals is necessary. In this case, this covariance matrix is

$$\mathbf{\Sigma_{vv}} = \mathbf{\Sigma_{yy}B}^T\left(\mathbf{B\Sigma_{yy}B}^T\right)^{-1}\mathbf{B\Sigma_{yy}} \tag{4.15}$$
$$= \begin{bmatrix}\mathbf{\Sigma}_{\mathbf{yy}_2} & \mathbf{0} \\ \mathbf{0} & \mathbf{\Sigma}_{\hat{\mathbf{x}}\hat{\mathbf{x}}_1}\end{bmatrix}\begin{bmatrix}\mathbf{I} \\ -\mathbf{A}_2^T\end{bmatrix}\left(\mathbf{\Sigma}_{\mathbf{yy}_2} + \mathbf{A}_2\mathbf{\Sigma}_{\hat{\mathbf{x}}\hat{\mathbf{x}}_1}\mathbf{A}_2^T\right)^{-1}\begin{bmatrix}\mathbf{I} & -\mathbf{A}_2\end{bmatrix}\begin{bmatrix}\mathbf{\Sigma}_{\mathbf{yy}_2} & \mathbf{0} \\ \mathbf{0} & \mathbf{\Sigma}_{\hat{\mathbf{x}}\hat{\mathbf{x}}_1}\end{bmatrix} \tag{4.16}$$
$$= \begin{bmatrix}\mathbf{\Sigma}_{\mathbf{vv}_2} & \mathbf{\Sigma}_{\mathbf{v}_2\mathbf{\Delta x}} \\ \mathbf{\Sigma}_{\mathbf{\Delta x}\mathbf{v}_2} & \mathbf{\Sigma}_{\mathbf{\Delta x}\mathbf{\Delta x}}\end{bmatrix}. \tag{4.17}$$

From this follows that the needed covariance matrix of the second observing block explicitly is

$$\mathbf{\Sigma}_{\mathbf{vv}_2} = \mathbf{\Sigma}_{\mathbf{yy}_2}\left(\mathbf{\Sigma}_{\mathbf{yy}_2} + \mathbf{A}_2\mathbf{\Sigma}_{\hat{\mathbf{x}}\hat{\mathbf{x}}_1}\mathbf{A}_2^T\right)^{-1}\mathbf{\Sigma}_{\mathbf{yy}_2}. \tag{4.18}$$

The general equation for computing the data resolution matrix from the covariance matrix of the residuals is

$$\mathbf{H} = (\mathbf{\Sigma_{yy}} - \mathbf{\Sigma_{vv}})\,\mathbf{\Sigma_{yy}}^{-1} = \mathbf{I} - \mathbf{\Sigma_{vv}}\mathbf{\Sigma_{yy}}^{-1}. \tag{4.19}$$

Thus, the data resolution matrix for the second observing block $\mathbf{y}_2$ only is

$$\mathbf{H}_{\mathbf{y}_2} = \mathbf{I} - \mathbf{\Sigma_{vv}}_2\mathbf{\Sigma_{yy}}_2^{-1} \tag{4.20}$$

with the respective impact factors

$$\mathbf{h}_{\mathbf{y}_2} = diag\,(\mathbf{H}_{\mathbf{y}_2})\,. \tag{4.21}$$

Consequently, the impact factors for the second observing block can be easily computed by using Eqs. 4.2, 4.18, 4.20 and 4.21.

4.2 Scheduling Concept

As mentioned before, the observations will be chosen by means of their impact factors with the aim of optimizing the entire observing geometry. Preferably, each observation of the schedule contributes a new information content ensuring to estimate the parameters by observations that are as individual, meaning uncorrelated, as possible. For this reason, observations with the greatest impact factors at a respective current state of the observing plan will be chosen in particular.

Usually, geodetic measurements require a good controllability for obtaining reliable results. This contradicts the demand for observations with great impact factors. However, in the course of the sequential scheduling procedure of the complete VLBI observing session, the number of observations increases and, thus, leads to an overdetermined equation system, where each observation contributes more or less to the determination of the unknown parameters. From this, a good mutual control of the observations is normally given automatically. This is particularly true for Intensive sessions because of the very limited option of feasible observations due to the restricted common visibility area.

4.2.1 Main schedule

At each step of the scheduling process, the suitability of all available sources is tested with respect to the participating baselines. The relevant criteria for which the sources are tested for are

1. the visibility of the source,
2. the distance angle between the current source and Sun positions,
3. the source was not observed from both stations of the respective baseline immediately prior,
4. the elapsed time since the source was last observed,
5. the slew times of the radio telescopes does not exceed a predefined limit,
6. the observing duration does not exceed a predefined limit.

One might assume that some of these criteria do not need to be recalculated in each step of the scheduling process, especially point 1. and 6., but can rather be computed once before starting the scheduling process for sorting out useless radio sources. This is true in case of point 1., but since the actual orientation of the Earth is needed for the scheduling procedure anyway, it does not cost much making a simple retrieval for the source visibility at each step. Therefore, the computational cost would not be decreased significantly. The situation is different, however, for the observing duration which depends among others on the strength of the source signal. In turn the receiving signal strength depends on the antenna sensitivity that includes an

elevation dependent term. Consequently, the actual observing elevation of both antennas to a radio source is needed to calculate the respective observing duration.

Points 1. to 3. of the source criteria are basic necessities whereas points 4. to 6. are optional criteria which can be adjusted individually. If a source fulfills all criteria, it is considered a candidate for the following observation. Thus, the partial derivatives are built and the Jacobian matrix, which contains all prior observations of the schedule, is extended with the new observation. Subsequently, the impact factor of the new observation has to be computed. This could be done via the SVD of the hole Jacobian matrix (Sec. 3.3.1), or via the method of recursive least squares adjustment (Sec. 4.1).

This procedure is repeated until all available sources are tested and their respective impact factors are computed. Finally, a certain number of potential next observations results. As the geometry of the schedule should be optimized, the observation with the greatest impact should be chosen at any time. Thus, the impact factors of all potential new observations have to be compared to each other.

For observations of a single baseline, as it is mostly the case for Intensive sessions, only one impact factor per possible observation occurs, so that the observation with the maximal impact factor is easy to find. To reduce memory capacity requirements, only the latest observation with the greatest impact factor is stored as long as another tested source reaches a better impact factor. Then, the new observation to the better source is stored and the old one is discarded. The algorithm is depicted in a flow chart in Fig. 4.1.

An observation is defined as two radio telescopes forming a baseline and observing the same radio source at one epoch. If more than two radio telescopes, thus a network of radio telescopes, observe the same radio source at the same epoch, they form all possible baseline combinations $n_{bl} = \frac{n_{st} \cdot (n_{st}-1)}{2}$, with n_{st} being the number of radio telescopes, and exactly the same number of observations as baselines occur. This set of observations at an instance of time is denoted by a scan.

In case of a two station network (e.g. INT1 and INT2) one scan contains always one observation because the two participating radio telescopes always form one baseline. But, for observing sessions with more than two telescopes pointing at the same source together (which is the case for INT3 sessions) more than one observation is obtained at an instant of time. For example, if the three radio telescopes of an INT3 session observe the same radio source together, one scan containing three observations occurs. The more radio telescopes observe together, the more observations are included in a scan.

Considering a scan with multiple observations, multiple impact factors occur at an instant of time by observing one source. These multiple impact factors have to be compared to each other in order to find the next radio source that have to be observed. As these groups of impact factors imply several single impact factors with different values, the mixture of the values can be very different. For instance, one group of impact factors may imply extremely high values as well as extremely low values while another group of impact factors consists of several average values only. Thus, various cases occur whose values differ in range and magnitude. So, which of these cases provide the greatest benefit for the current constellation is not easy to decide.

Furthermore, observing sessions with multiple radio telescopes provide the possibility of sub-netting. A subnet consists of a subset of stations of the entire station network that are participating in a VLBI session. Sub-netting refers to a scheduling strategy where different sets of stations simultaneously participate in different scans. One aspect of sub-netting is the reduction of idle times of the participating radio telescopes (Gipson 2012). The slew times, which radio telescopes need to point at the next source of an observing plan, differs as a function of the slew speed of the antenna and the distance the antenna must travel. Antennas that arrive first on a source have to wait for the arrival of all other telescopes before they can begin to observe. Thus, during this waiting time the respective radio telescopes are idle. Therefore, sub-netting is a convenient possibility for reducing these idle times and, thus, raising the number of observations. Another aspect of sub-netting is the optimization of the observing geometry. Extensive station networks have a severely limited common visibility of the sky. Sub-netting offers the possibility to observe different areas of the sky that cannot be observed by the entire network. Due to this fact, more radio sources can be observed in a session improving the sky coverage of each site. For instance, this benefit was utilized by Sun (2013) in a source-based scheduling strategy.

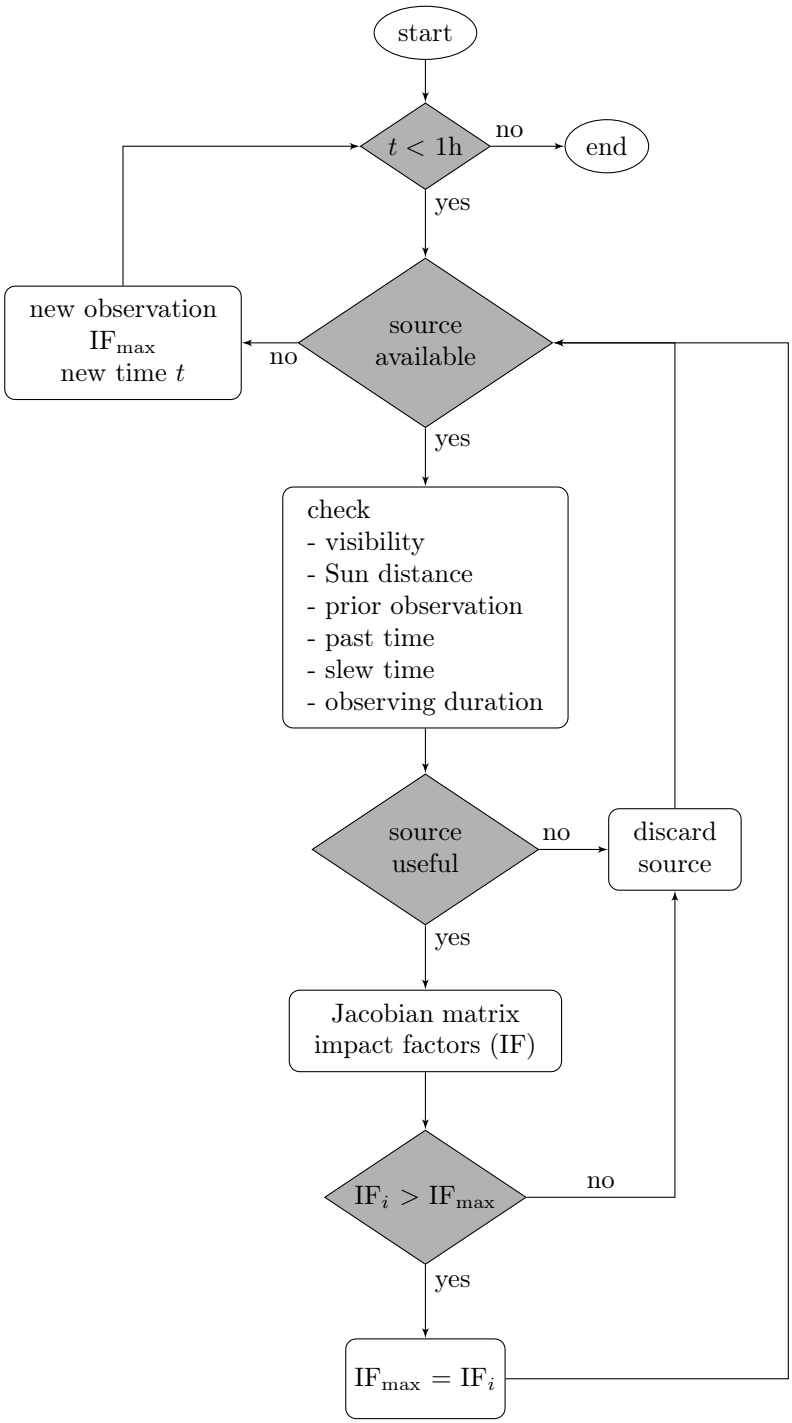

Figure 4.1: Procedure of the automatic scheduling method based on the observations' impact factors for one hour long VLBI Intensive sessions: The main scheduling process starts at a time t defined by the last initial observation. If the time since the start of the scheduling process is less than one hour - following the VLBI Intensive concept - all sources are checked for their suitability at this time. If a source is useful, the Jacobian Matrix is built and the impact factors are computed. If the impact factor of the new source is larger than that of all previous sources of the loop, the source will be earmarked as the new observation. When all sources are checked the new observation with the largest impact factor is found. With the slew time of the radio telescopes and the scan length of the observation, the start time of the next selection process is computed. While this new time is less than one hour, the process of finding the next observation with the largest impact factor is repeated.

The consequence of sub-netting for the scheduling method using impact factors is a further complication of choosing the next scan, as sub-nets with varying numbers of baselines and, thus, varying numbers of impact factors can be built. Using the example of a three station network, it may happen that observing one source by only two radio telescopes while the third radio telescope is idle leads to better results than observing another source by all three radio telescopes simultaneously. In this case one impact factor has to be weight up against three impact factors. Concerning a network of four radio telescopes several more cases occur that have to be taken into account. Pointing at the same radio source together by all radio telescopes leads to six observations. If one radio telescope is idle while the others observe together, three observations occur. If two radio telescopes are idle while just two radio telescopes observe a source, one observation occurs. Otherwise, the idle pair of radio telescopes can observe another source at the same time, so that two scans with one observation respectively, therefore two observations in total, result. The more radio telescopes participate in one session the more observing combinations are possible increasing computational costs immensely.

To make unequal numbers of impact factors, which belong to different sized sub-nets, comparable, was a first major challenge of this work. Matters were complicated further by the fact that the greater the number of observations the lower the values of the impact factors because the total redundancy increases. Extensive investigations have been done for finding a reasonable way to compare the impact factors of different sized sub-nets. The examinations are presented in detail in Appendix A. The conclusion of these investigations for deciding on the best procedure is that the average impact factor of the respective observations is calculated which is further scaled by the square root of the number of impact factors. The latter step accounts for the increasing redundancy with the increase of number of observations.

This scheduling approach offers opportunities for refinement or variation. One of those possible refinements that obviously makes sense will also be presented here. Since $\Delta UT1$ is the target parameter of Intensive sessions and the absolute values of the other parameters are not of interest, another criterion for the selection of the observations is the impact factor for the parameter $\Delta UT1$ only. This is a separate special case compared to the one at which all parameters of the solutions are taken into account. It is possible to determine the impact factor of each observation on the parameter $\Delta UT1$ separately by the concept of reduction of the parameters as described in Sec. 3.3.3. In this work both kinds of impact factors, the general impact factors for all parameters and the impact factors for $\Delta UT1$ alone, have been tested extensively (see Ch. 5).

4.2.2 Initial observations

At the beginning of the IF scheduling process, an initial normal equation system is needed which is composed of as many observations as parameters. Otherwise, the normal matrix $\mathbf{N} = \mathbf{A}^T\mathbf{\Sigma}_{\mathbf{yy}}^{-1}\mathbf{A}$ is singular and, thus, not invertible. This is due to the fact that each observation is uncontrolled and a negative redundancy exists. The SVD regularize the Jacobian matrix so that it is possible to determine the impact factors of the observations. But, as the influences of the observations on the unknown parameters are not separable, each impact factor amounts to 1. If and only if $\mathbf{N}$ is regular one can determine meaningful impact factors. For this reason, a sufficient number of initial observations must be chosen first with other criteria.

Hence, the number of required initial observations or scans depends on the number of the participating radio telescopes and the number of unknown parameters. The following applies to Intensive sessions with the parametrization that is chosen for this work (see Sec. 2.3):

$$n_{obs} = (n_{st} - 1) \cdot u_{cl} + n_{st} \cdot u_{at} + u_{\Delta UT1}, \tag{4.22}$$

$$n_{bl} = \frac{n_{st} \cdot (n_{st} - 1)}{2}, \tag{4.23}$$

$$n_{scan} = \left\lceil \frac{n_{obs}}{n_{bl}} \right\rceil, \tag{4.24}$$

with

n_{st}	number of stations,
n_{bl}	number of baselines,
n_{obs}	number of necessary observations,
n_{scan}	number of necessary scans involving all radio telescopes,
u_{cl}	number of clock parameters per station,
u_{at}	number of atmospheric parameters per station,
$u_{\Delta UT1}$	number of $\Delta UT1$ parameter ($= 1$).

The question of how to handle the initial observations is only important if the additional number of observations is small compared to the initial number. In case of VLBI sessions the initial observations are only a small fraction of the total number of observations. It should be emphasized here that concerning VLBI Intensives an optimal selection of the initial observations is also mandatory in terms of economical usage of observing time because this is generally restricted to one hour. The following describes two different approaches for choosing the initial observations that have been developed in this work.

Geometric consideration

The initial observations can be chosen subject to special geometric considerations. The approach developed here produces reasonable results for scheduling observing plans with a single baseline. Since the observing geometry of a single baseline is well presented by the baseline's midpoint sky-plot, that have been introduced in Sec. 3.3.4, this geometric approach bases on the special baseline representation.

Figure 4.2 shows stereographic projections of the baseline reference system for the east-west extended baseline between Tsukuba and Wettzell, where the central white area (best seen in Fig. 4.2 middle and right) is the common visibility of both radio telescopes. The dashed lines in Fig. 4.2 (left) lie in the direction of the baseline and orthogonal to it. In order to stabilize the geometry of a VLBI Intensive session at the very beginning, the approach is to select initial observations with minimal distances to the dashed lines, whereby the elevations of these observations are constricted to the lower half of the common visibility of the telescopes, which is indicated by the white area in Fig. 4.2 (left).

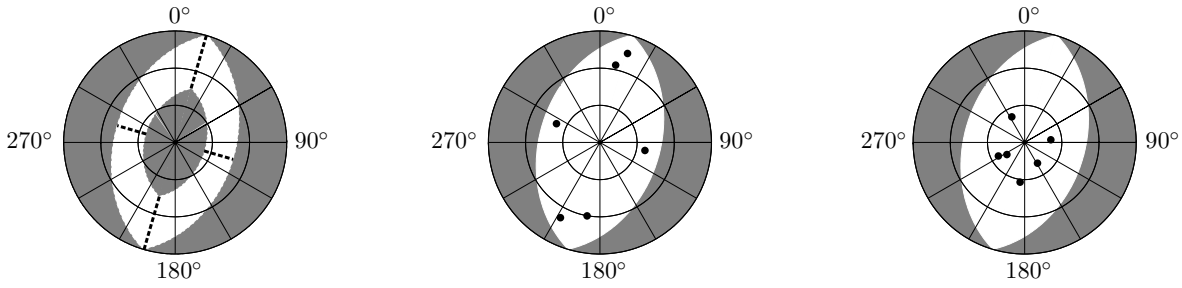

Figure 4.2: Locations of initial sources depicted at the skyplot of the baseline's mid point. Left: schematic geometric criteria. Middle: example for geometric criteria. Right: example for predicted precision of the observations.

Figure 4.2 (middle) shows an example of initial observations which are selected with this concept. Considering the findings of other authors concerning Intensive schedules (cf. Sec. 3.2), the advantages of this approach are:

- including low elevation observations which are necessary for the estimation of tropospheric path delays according to Fischer et al. (2003) and own investigations (Sec. 3.3), and for the reduction of the $\Delta UT1$ estimate scatter according to Baver and Gipson (2013),
- including some observations to sources near the equator which is considered to be important by Fischer et al. (2003), Baver and Gipson (2013) and own investigations (Sec. 3.3),

- including observations far down in the baseline sky plot cusps indicating best categorized observing plans according to Uunila (2013),
- the temporal sky coverage is comparatively good because all four cardinal directions are covered at the very beginning.

Disadvantages of the approach may be:

- long slew times are necessary to cover the four cardinal directions reducing the remaining duration and, thus, the observations' count of the session,
- weaker sources may be chosen which need a longer observing time and, thus, causing or tightening the time problem,
- low elevation observations introduce extra noise due to atmospheric turbulence resulting in larger scatter what may outweigh the advantages of those observations.

Predicted precision

Since INT3 sessions use a network of three radio telescopes and the scheduling program should be designed foresightfully concerning twin radio telescopes, the selection process for initial observations has to work out with several radio telescopes as well. For this reason, a further approach for selecting initial observations has been developed which bases on the predicted precision of the observations. This is a universal approach that can be used for both single baseline schedules and multiple station schedules.

Here, initial observations are selected by means of their a priori standard deviations. The standard deviation of the observed group delay $\sigma_{\tau_{X/S}}$ is useful for scheduling observing plans (Schuh and Campbell 1994) and can be predicted by the *SNR* and the effective bandwidth B_e (see Eq. 2.21). Here, a refined standard deviation for an observation is used that consists, apart from the standard deviation of the group delay, of contributions of the ionospheric influence as well as of atmospheric refraction effects.

VLBI observations are usually carried out in X-band and S-band separately. The recorded data of the S-band are used to calibrate the data of the X-band for the ionospheric refraction effect $\Delta\tau_{ion,X}$ (Ma 1978)

$$\Delta\tau_{ion,X} = (\tau_X - \tau_S)\,\frac{{f_S}^2}{{f_X}^2 - {f_S}^2} \tag{4.25}$$

with the group delay of the X/S-band $\tau_{X/S}$ and the frequency of the respective band $f_{X/S}$. The variance law of error propagation leads to the standard deviation $\sigma_{\Delta\tau_{ion,X}}$ of this adjustment to the X-band data

$$\sigma_{\Delta\tau_{ion,X}} = \sqrt{{\sigma_{\tau_X}}^2 + {\sigma_{\tau_S}}^2}\,\frac{{f_S}^2}{{f_X}^2 - {f_S}^2}. \tag{4.26}$$

According to Gipson et al. (2008) it is assumed that the standard deviation mentioned above is too optimistic. There must be some other noise sources or incorrect modelings of the system. As a consequence of atmosphere mis-modeling, delay residuals are larger at lower elevations. For this reason, a station dependent noise term $\sigma_{\tau_{atm,i}}$ which is proportional to the mapping function is added

$$\sigma_{\tau_{atm,i}} = a_{at} \cdot m_i\,(\varepsilon_i) \tag{4.27}$$

with a noise coefficient a_{at}, the mapping function m_i and the elevation angle ε_i at station i. Gipson et al. (2008) studied the effect of adding a station dependent noise term on the basis of continuous VLBI campaign (CONT05) sessions. One of their evaluation criteria was baseline scatter. In contrast to re-weighting the observations by adding identical additional noise for all baselines until $\chi^2 \approx 1$, which is the standard approach, adding a station dependent noise term without re-weighting better reduces baseline length scatter. Varying

a_{at} from 0 ps to 15 ps yield the best results, meaning the greatest reduction of baseline length scatter, at $a_{at} = 6$ ps. Hence, here the elevation dependent noise term is implemented with a coefficient of 6 ps and the Global Mapping Function (GMF, Böhm et al. 2006a).

Finally the standard deviation of an observed delay amounts to

$$\sigma_\tau = \sqrt{{\sigma_{\tau_X}}^2 + {\sigma_{\Delta\tau_{ion,X}}}^2 + {\sigma_{\tau_{atm,1}}}^2 + {\sigma_{\tau_{atm,2}}}^2}. \tag{4.28}$$

In the approach for the initial observations, the standard deviations of all possible scans including all participating radio telescopes will be determined via Eq. 4.28. Eventually, the scans with the lowest average standard deviations are chosen as initial observations.

Table 4.1 gives some examples for the respective components of the final standard deviation which is depicted in the first column. The standard deviation of a group delay for the X-band σ_{τ_X}, shown in the second column, depends on the *SNR* and the effective bandwidth. Thus, differences between σ_{τ_X} of a defined baseline mainly depends on the source flux. In the shown examples, the σ_{τ_X} decreasing from above to below is related to increasing source fluxes. The standard deviation of the ionospheric correction $\sigma_{\Delta\tau_{ion,X}}$ is mostly lower than the standard deviation of a group delay for the X-band, but, may also exceed it, as it is the case in the last row of Tab. 4.1, because of different source fluxes at X- and S-band. The atmospheric noise terms $\sigma_{\tau_{atm,1}}$ and $\sigma_{\tau_{atm,2}}$ mainly depend on the observing elevation. For the first row, both elevation angles are about 30° resulting in similar noise terms. The elevation angles of the second row amount to 20° and 6° which are the lowest ones of the shown examples and, thus, leading to the highest amounts of $\sigma_{\tau_{atm,1}}$ and $\sigma_{\tau_{atm,2}}$. The two last rows are related to relatively high elevation angles of 49° and 44°, and 55° and 40° respectively. It can be recognized that the finial standard deviation of the first row is dominated by the great σ_{τ_X} because of a very low source strength. The low elevations and, thus, great atmosphere noise terms most influence the finial standard deviation in the second row. In the last row, the ionospheric part predominates the finial standard deviation. Therefore, the third row, which is highlighted in gray, exhibits the smallest final standard deviation σ_τ as the single components are well balanced.

σ_τ [ps]	σ_{τ_X} [ps]	$\sigma_{\Delta\tau_{ion,X}}$ [ps]	$\sigma_{\tau_{atm,1}}$ [ps]	$\sigma_{\tau_{atm,2}}$ [ps]
28.83	21.67	9.36	11.85	11.57
57.74	7.20	3.42	17.82	54.34
14.48	6.90	4.75	7.99	8.70
16.27	5.93	9.49	7.37	9.23

Table 4.1: Examples for the standard deviation components.

Figure 4.2 (right) shows an example of initial observations which are selected with this concept. Summarizing the advantages of this approach:

- depending on the *SNR*, mainly strong sources will be chosen that might reduce the *ΔUT1* root mean square (RMS) according to Baver and Gipson (2013),
- strong sources need shorter observing duration, so that more time remains for more observations,
- low elevation observations will be avoided, reducing extra noise due to atmospheric turbulence which would produce larger *ΔUT1* estimate scatter (Baver and Gipson 2013),
- including observations at mid elevations are as important as low elevation observations for a reliable determination of the atmospheric parameters according to the investigations in Sec. 3.3,
- since no geometric criterion is used for this approach, it is most useful for sessions with multiple baselines.

Considered as disadvantage of this approach is the total absence of geometric conditions in a scheduling method which aims at optimizing the geometry. As a consequence, the use of low elevation observations or observations near the equator is not supported by choosing the initial observations through this method. However, in a more complicated scenario of multiple baselines, it is a very sensible option.

5. Examination of the scheduling method

To examine the scheduling algorithm developed here, several observing plans have been created by computing the impact factors via singular value decomposition and via recursive least squares adjustment. Comparing the created observing plans reveals that both algorithms, using the SVD and the recursive least squares adjustment, lead to the same results as intended. It can therefore be concluded that the algorithms are on a par. Using the recursive least squares adjustment has only the advantage of reducing the run-time of the scheduling program. Creating an Intensive observing plan with two participating radio telescopes lasts just a few seconds ($\leq$ 2.5 s) with both algorithms. Precisely, the algorithm including the recursive least squares adjustment on average needs only 90 % of the runtime of the algorithm applying the singular value decomposition. Therefore, the advantage of the recursive least squares adjustment is hardly noticeable. Increasing the number of participating radio telescopes of a VLBI session raises the number of possible observations that have to be taken into account and, thus, leads to a longer run-time. For testing purposes, observing plans including a set of five radio telescopes have been created. Here, the difference in run-time between the two algorithms is clearly perceptible, as it lasts several minutes. In this case, the algorithm including the recursive least squares adjustment on average lasts just 0.6 as long as the algorithm including the singular value decomposition. In summary, it can be stated that both algorithms are on a par concerning standard Intensive sessions with two or three radio telescopes and a total observing duration of one hour. The creation of observing plans with more participating radio telescopes or a longer session duration or both is faster managed by the algorithm including the recursive least squares adjustment.

To assess the created observing plans by the scheduling method, the standard IVS schedules of all Intensive session types have been taken as reference. All of these observing plans have been created using the uniform sky method, with some handmade corrections from time to time. It is conspicuous that a radio source selection of the whole source catalog is predefined in every schedule file. The program SKED provides a tool for preselecting radio sources that appear to be best with respect to a given station network and the observing duration. Presumably, the source selection of the schedules have been done with this routine. The number of predefined sources varies from time to time and between Intensive types. For INT1 sessions this number ranges from 45 to 90. For INT2 sessions it amounts to between 90 and 150 and in the case of INT3 sessions from 40 to 150.

For comparison reasons, observing plans which are scheduled with the new scheduling method use the same time windows as the IVS schedules. As the basis for these investigations the Intensive sessions of the years 2009 to the middle of 2013 were used. To distinguish the different Intensive schedules, the reference schedules of the IVS will be labeled with IVS for short, the schedules created with the new scheduling method are labeled with IF in case of using the general impact factors and $\mathrm{IF}_{\Delta UT1}$ in case of using the impact factors for the parameter $\Delta UT1$ alone.

The scheduling procedure using the impact factors offers three minor selection options that are listed in Sec. 4.2.1 (items 4. to 6.). For all Intensive setups (INT1, INT2 and INT3) and both IF scheduling methods, the options have been defined as follows:

- The minimum time between observations of the same source is set to 10 minutes.
- The maximum time to allow an antenna to slew is set to 2 minutes.
- The maximum scan length is set to 200 seconds.

These definitions originate from experimental and logical reasons. The scan length depends on the observed source strength, the sensitivity of a VLBI receiver (System Equivalent Flux Density, SEFD) and the total number of recording bits. Stronger sources give higher *SNR* and consequently decrease the scan length. The lower *SNR* limits of 25 in case of X-band and 20 in case of S-band have been adopted from the IVS schedules. But, concerning INT1 these minimum *SNR* values are less suited. Probably the main reason for this is the

very big extent of the INT1 baseline because the observed source strength depends on the length of the baseline, thus, longer baselines lead to lower correlated flux densities due to source structure effects which in turn decrease the *SNR*. Hence, lower *SNR* limits have been defined for INT1 sessions, namely 20 for X-band and 15 for S-band. However, the scan length also includes extra time that has to be added to the end of an observation for helping the correlators to synchronize the recorded signals. On this account, a further parameter that defines the minimum scan length has to be defined. Since the minimum scan length varies in the different INT setups and in course of time, a medium value of 30 seconds has been imposed for all cases. Available radio sources for the scheduling program are taken from the source catalog of SKED, specifically those that are marked as geodetic. No predefined selection of radio sources is done before the scheduling process, therefore, all sources of the catalog are available during the scheduling procedure.

In the following investigations, a data gap is visible in the time series of all Intensive session types between the end of August to the end of November 2010 because of a breakdown of the 20 m radio telescope in Wettzell. A second but much smaller data gap in INT1 sessions occurs in April 2013, since seven sessions have been scheduled with the station in Tsukuba instead of Kokee Park. Two different data gaps in INT2 and INT3 sessions from March to the beginning of May 2011 and from February to the middle of April 2012 result from breakdowns of the radio telescope in Tsukuba. In the following sections, the schedules will be compared by different criteria.

5.1 Number of observations

First of all the statistics, in particular the number of observations, the number of scheduled sources, the observing durations and the slewing times of the radio telescopes, are taken into account. It is also advantageous that on this basis, the peculiarities of the different Intensive types and special irregularities in the examined time span can best be seen.

INT1

Figure 5.1 show the observation numbers of the different schedules for INT1 sessions. Occasionally, INT1 sessions have been scheduled with an additional observing station. Most times the third station is Svetloe (Russia), except of the middle of 2010 when the station in Ny-Ålesund was used. These sessions have been taken out of the time series shown in Fig. 5.1 for a clearer presentation. But Tab. 5.1 lists the average values of the different scheduling cases for both station networks.

The number of observations of the IVS schedules reduces from an average of about 25 to about 17 until May 2010 with a gradual increase towards 20 in 2013 (black curve in Fig. 5.1). It behaves similarly in case of schedules with a three station network. Apparently, a change in the IVS scheduling strategy has taken place at this date as both the observing durations and the slewing times of the radio antennas between two consecutive observations increase. The increase of the observing duration concerns both station networks in equal measure and amounts on average to 105 s before the change and 141 s after, thus, an extension of approximately 25 %. However, the predefined minimum observing duration remains unchanged over the investigated time period and amounts to 40 s. An increase of the antenna slewing times is perceivable for the two station network schedules and amounts to 10 % (from 45 s to 50 s on average). These attributes indicate the change of the scheduling strategy using mainly strong sources to the uniform sky scheduling strategy, where also weaker sources will be observed, which results in longer observing durations. So, longer slewing times are necessary to reach a regular sky coverage both in the spatial and in the temporal domain.

Obviously, the scheduling method using impact factors leads to almost twice as many observations as IVS schedules for a 2 station network. However, the IF schedules reach slightly more observations than the $\mathrm{IF}_{\Delta UT1}$ schedules (cf. Tab. 5.1). The minimum observing duration of the schedules using impact factors amounts to 30 s, which is slightly lower than the 40 s of IVS schedules. Additionally, the *SNR* value that has to be achieved for X-band is a little bit lower for IVS schedules (18) which can lead to longer observing

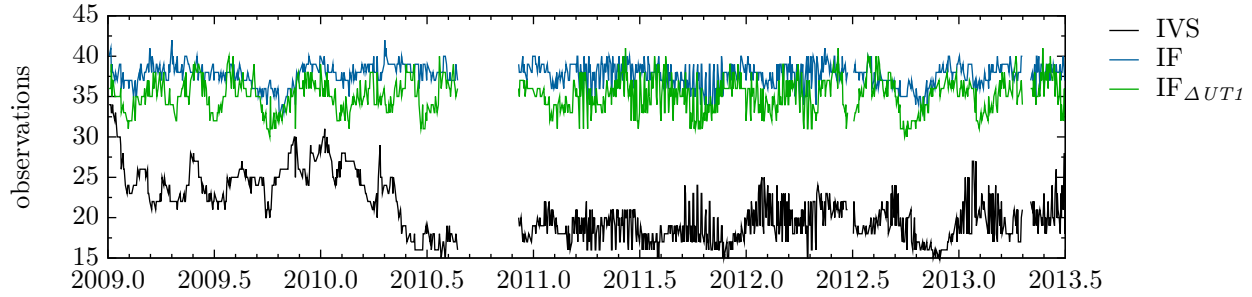

Figure 5.1: Observation numbers of the different schedules for INT1 sessions (2 station network).

	2 stations (1027 sessions)		**3 stations** (97 sessions)		
	scans/obs.	sou.	scans	obs.	sou.
IVS	20.7	10.9	20.2	44.9	10.6
IF	37.7	14.3	26.6	79.0	10.8
IF$_{\Delta UT1}$	35.1	16.5	31.4	43.1	15.8

Table 5.1: Average numbers of scans, observations and used sources of the different schedules for INT1 sessions excluding and including sessions with the additional station Svetloe/Ny-Ålesund.

durations and, thus, fewer observations within one hour. These might be the reasons for the greater number of observations in these cases. Investigations of the observing durations (not shown here) have revealed an average duration of 36 s for the IF schedules and 39 s for the IF$_{\Delta UT1}$ schedules valid for both station networks. These average durations are under one third of the observing duration of IVS schedules, which is an enormous difference. In contrast, the slewing times of the schedules using the impact factors are longer than those of the IVS. Furthermore, there are different average slewing times for the different station networks. In case of a two station network, the mean slewing time amounts to 60 s for the IF schedules and 66 s for the IF$_{\Delta UT1}$ schedules which is just slightly longer than for IVS schedules, indicating that radio sources which are far away from each other will be observed consecutively more often. Among other reasons, this might be caused by an, on average, greater number of different sources that are observed within one session (cf. Tab. 5.1). But, since the increase of the slewing times is small compared to the decrease of the observing durations, the latter increase the realizable number of observations within one hour eventually.

Concerning the three station network, the slewing times of the schedules using the impact factors extend substantially. In contrast to IVS schedules that have slewing times of 50 s on average, the mean slewing time of IF schedules amounts to 107 s and 79 s for IF$_{\Delta UT1}$ schedules. Nevertheless, the average number of scans of both impact factor schedules exceeds the one of the IVS. Thus, the very short observing durations lead to more realizable scans again. Regarding the number of observations, IF$_{\Delta UT1}$ schedules are very similar to IVS schedules. In both cases the third station of the network is only involved in a few scans of a session. Since the number of scans is higher for IF$_{\Delta UT1}$ but the number of observations is lower, the third station is least involved here. The case is very different for IF schedules. Here, the mean number of observations is approximately tripling the mean number of scans, thus, all of the three radio telescopes are involved in nearly every scan. However, radio sources that are observable by a three station network are rarer than those that are observable by a single baseline. This might be the reason for extremely long slewing times compared to both other cases and a relatively low number of observed sources compared to IF$_{\Delta UT1}$ schedules.

INT2

Following the time series of the IVS schedules in Fig. 5.2, there are several irregularities concerning the observation numbers. This characteristic is highly correlated to a varying minimum observing duration. First the minimum observing duration is set to 60 s, causing a mean number of observations of 35. After October 2009 the minimum observing duration is reduced to 40 s, raising the number of observations abruptly up to 44 on average. In February 2012 the minimum observing duration is reduced again to 30 s. The observing durations also change over time following the time steps of the varying minimum observing durations. Average observing durations first amount to 61 s, decrease between October 2009 and February 2012 to 41 s, and finally increase again to 51 s. The last increase of the average observing duration is the reason for the decrease of the number of observations in the last part of the time series. Similar to the observation numbers, the observing durations are characterized by strong fluctuations in the last part of the time series. Therefore, a strong correlation between observing durations and observation numbers exists. The different intervals are not reflected by the slewing times of the antennas between observations, which amount to 42 s on average.

For both the IF schedules and the $\mathrm{IF}_{\Delta UT1}$ schedules, a constant minimum observing duration of 30 s has been used. Therefore, the behavior of the graphs is more constant than those of the IVS. Hence, the observation numbers of IF schedules are first slightly greater than those of the IVS, after October 2009 it is reversed and starting from April 2012 there is no great difference. The observation numbers of the $\mathrm{IF}_{\Delta UT1}$ schedules fluctuate most. At the beginning of the time series, the observation numbers lie between those of the IF and the IVS, but after October 2009 the $\mathrm{IF}_{\Delta UT1}$ curve exhibits the lowest values. The mean observing duration of the IF and the $\mathrm{IF}_{\Delta UT1}$ schedules amounts to 33 s and 37 s respectively. Both mean slewing times are longer than those of the IVS, namely 58 s and 63 s, whereas the slewing times of the $\mathrm{IF}_{\Delta UT1}$ show great fluctuations.

Compared to the IVS, the IF schedules have shorter observing durations but longer slewing times. The differences of both time spans are very similar, so that on average nearly the same number of observations results (see Tab. 5.2). The $\mathrm{IF}_{\Delta UT1}$ schedules have the longest average slewing time of the antennas, and an average observing duration lying between those of the IVS and IF. Longer slewing times might also be caused by more different sources that are observed within one session. Since the slewing times fluctuate similar to the observation numbers as well (not shown here), the slewing time seems to be the most influencing factor in this case.

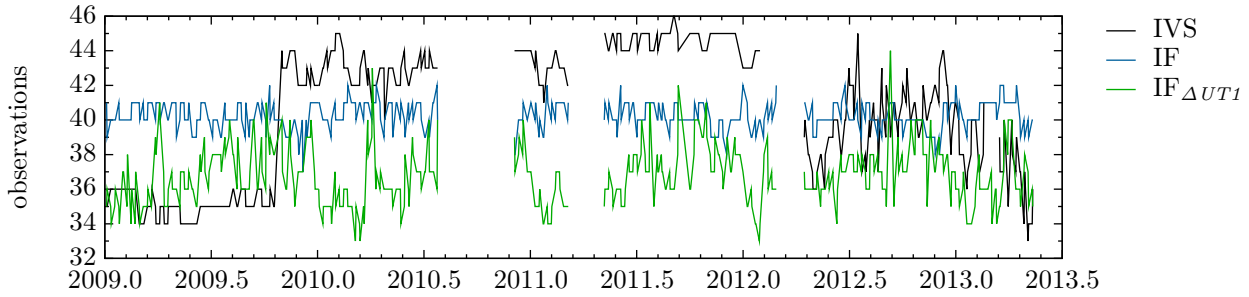

Figure 5.2: Observation numbers of the different schedules for INT2 sessions.

	scans/obs.	sou.
IVS	40.4	20.9
IF	40.2	18.4
$\mathrm{IF}_{\Delta UT1}$	36.8	23.7

Table 5.2: Average numbers of scans, observations and used sources of the different schedules for INT2 sessions (374 sessions).

INT3

Similar to INT1 sessions, INT3 sessions have been performed with an additional station, thus, a forth station in this case, occasionally. But since this happened only seldom, these special cases have been excluded for the following investigations, so that only the normal case of a three station network is considered.

The minimum observing duration changes quite often for IVS-INT3 schedules, while it remains constant at 30 s for both scheduling strategies using the impact factors. In the beginning of the investigated time series the minimum observing duration amounts to 40 s for IVS schedules, then it is reduced to 30 s in the middle of November 2011, further increased to 20 s in the middle of January 2012, once again much reduced to 13 s in June 2012 and after that slightly raised to 15 s in the middle of March 2013. Regarding the unsteady behavior of the IVS time series in Fig. 5.3, no conspicuous effects at the before mentioned epochs attract attention. Also the actual observing durations and the slewing times of the telescopes, that on average amount to 61 s and 55 s respectively, show no jumps or noticeable changes.

Concerning the IF schedules, the mean observing duration amounts to 33 s, thus, about one-half of those of the IVS. But in contrast, the mean slewing time is much longer than those of the IVS and amounts to 83 s. Although, this is not twice of those of the IVS, the same average number of scans is scheduled (31.6, see Tab. 5.3).

The IF$_{\Delta UT1}$ schedules stand out because of their very low observation numbers compared to both other cases, even though the mean observing duration and the mean slewing time lie between the two other schedules. The mean observing duration amounts to 38 s and is, thus, much shorter than those of the IVS, while the mean slewing time of 72 s lies approximately in the middle of the IVS and the IF. Comparing the number of scans and the number of observations in Tab. 5.3 clarifies that the same happened as for INT1 sessions using a three station network. In case of the IF schedules, all of the three radio telescopes are involved in nearly every scan, because the mean number of observations is approximately the triple of the mean number of scans. One of the telescopes will be excluded from a scan occasionally in IVS schedules, and, since the observation numbers of IF$_{\Delta UT1}$ schedules are not much greater than its scan numbers indicate that one station of the three station network is idle mostly. Using a two station network, more different radio sources could be observed in IF$_{\Delta UT1}$ schedules.

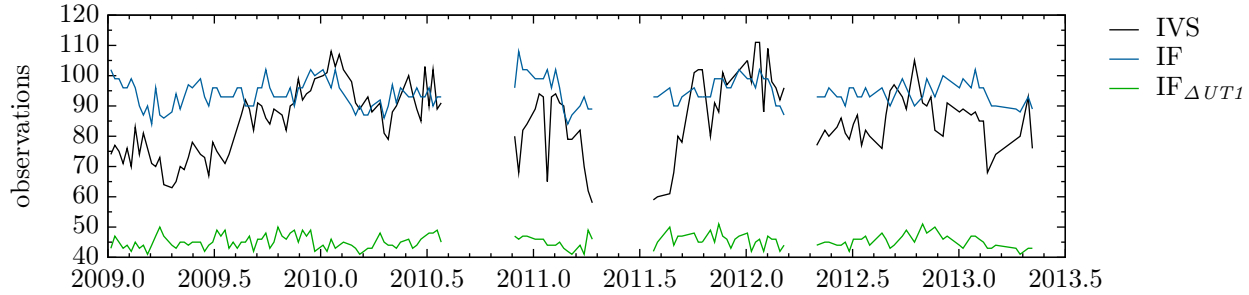

Figure 5.3: Observation numbers of the different schedules for INT3 sessions.

	scans	obs.	sou.
IVS	31.6	85.0	19.9
IF	31.6	94.3	12.2
IF$_{\Delta UT1}$	33.8	45.2	20.6

Table 5.3: Average numbers of scans, observations and used sources of the different schedules for INT3 sessions (174 sessions).

5.2 Sky coverage

In this section, the sky coverage of the different observing plans is evaluated. Since there is no clear definition of uniform sky or the evaluation of the sky coverage, a definition of sky coverage must be discussed first.

Several authors made several efforts for reaching uniformly distributed observations. One possibility to reach uniform sky coverage during the scheduling process is to select the next source to be the one that is furthest away from its nearest neighbor. In other words, filling the largest hole in the current source distribution (Petrachenko et al. 2008). A further consideration is to observe always two sources simultaneously, which are as close to 180 degrees apart as possible. But this approach is only viable for networks of stations which are able to build sub-nets and not for Intensives.

Baver et al. (2012) evaluate sky coverage indirectly by determining the sky emptiness. Therefore, the sky is evenly sampled at one degree intervals to calculate the angular distances between each sampled point and its nearest observation. These angular distances are summed up. A smaller sum indicates less emptiness, or more coverage. For their investigations of INT1 sessions, Baver et al. (2012) used the averages of the sky emptiness of both participating stations as sky coverage or emptiness criterion.

Another perspective of sky coverage is given, e.g., by Sun (2013), who divided the sky above an antenna in 13 segments (see Fig. 5.4). The elevation is separated in three segments, low, middle and high. The middle elevation part is further divided into four azimuthal segments and the low elevation part into eight segments. Specifying a certain time span, the best sky coverage can reach category 13, while the worst case is of category 1 if all observations are concentrated in only one segment.

This approach seems to be inappropriate for Intensives, regarding the extremely limited common visibility of the Intensive stations. Figure 5.5 shows a skyplot of the station in Wettzell of an INT2 session with the gray area being the unscannable sky area above Wettzell by the partner telescope in Tsukuba. Obviously, only nearly half of the segments defined by Sun (2013) can be populated in case of INT2 sessions. For the baseline between Kokee Park and Wettzell of the INT1 sessions which is about 2000 km longer, the visible area is even smaller. Conceivably, the segments could be adapted to the visible areas of Intensives, but, this must been done for each baseline respectively.

Thus, a reasonable method for validating the sky coverage of Intensive sessions is needed to be developed. For this purpose, the Delaunay triangulation is employed in this thesis. The Delaunay triangulation is a method for meshing non-gridded points with triangles (Delaunay 1934). The triangulation is arranged in the way that no point is inside the circumcircle of any triangle. In the triangulation process, the minimum

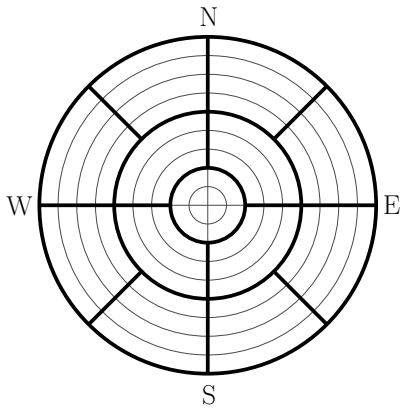

Figure 5.4: Segmentation of the sky above an antenna (according to Sun 2013).

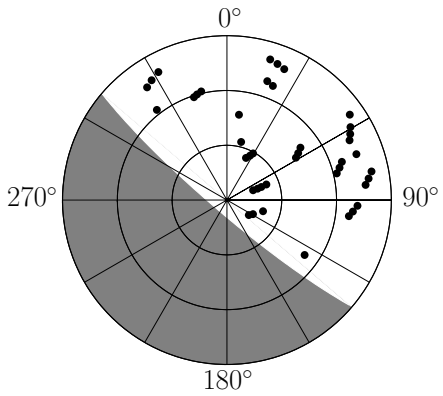

Figure 5.5: Skyplot of the station Wettzell of an INT2 session with the gray area being the unscannable sky area of the partner telescope in Tsukuba.

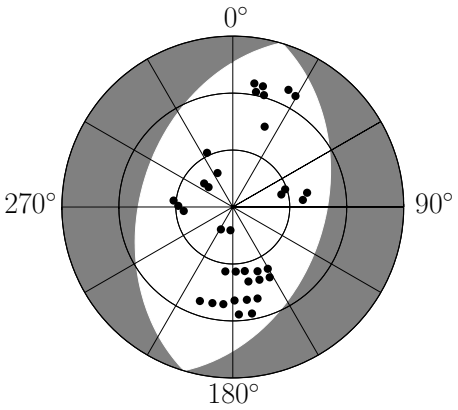

(a) Midpoint skyplot of the baseline Ts – Wz.

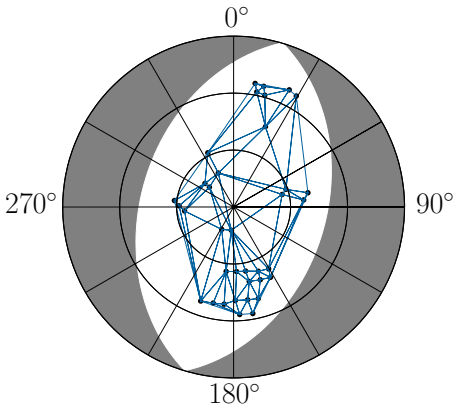

(b) Delaunay triangulated network.

Figure 5.6: A midpoint skyplot of the baseline Tsukuba – Wettzell showing the observed sources of a typical IVS-INT2 session (a) and its Delaunay triangulated network (b).

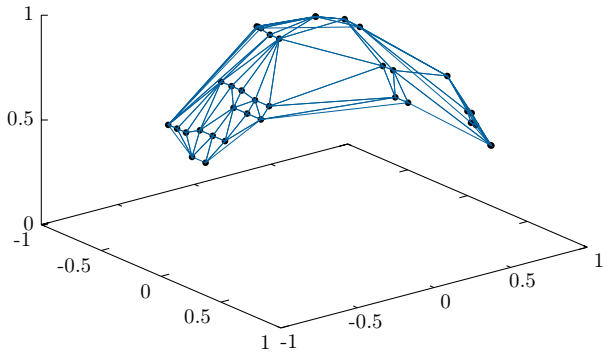

(a) Triangulated network.

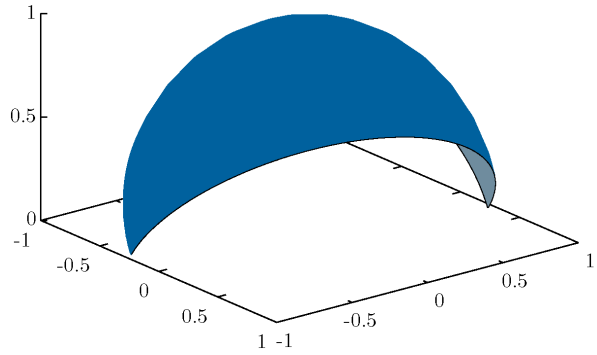

(b) Coverable surface.

Figure 5.7: Three-dimensional depiction of the triangulated network shown in Fig. 5.6b (a) and three-dimensional depiction of the coverable surface for the baseline Tsukuba – Wettzell (b).

angle of all the angles of the triangles in the triangulation are maximized so that skinny triangles are avoided. For more information about the Delaunay triangulation see de Berg et al. (2008), Hjelle and Dæhlen (2006) or Du and Hwang (1992). Applying the Delaunay triangulation on skyplots of VLBI sessions, the surface spanned by the observations can be approximated.

For the purpose of this thesis, it is considered to be more appropriate applying the Delaunay triangulation to the baseline-based skyplots of Intensives, which have been introduced in Sec. 4.2.2, instead of the station-based skyplots. This avoids computing averages of two stations and gives a symmetrical basis.

An example for such a triangulation is given in Fig. 5.6a-5.7a for a INT2 baseline between Tsukuba and Wettzell. The first skyplot (Fig. 5.6a) shows the distribution of the observed sources of a typical IVS-INT2 session by the baselines center point of view. Meshing these observed sources with the Delaunay Triangulation results in the triangulated network shown in Fig. 5.6b. Assuming a unit sphere, three-dimensional Cartesian coordinates of the source positions can be calculated and, thus, the triangulated network can also be presented three-dimensionally (Fig. 5.7a). Through this approach, it can be seen, how well the observed sources of an

INT1		INT2		INT3	
Kokee Park – Wettzell	0.40	Tsukuba – Wettzell	0.54	Tsukuba – Wettzell	0.54
Kokee Park – Svetloe	0.46			Tsukuba – Ny-Ålesund	0.66
Svetloe – Wettzell	0.91			Ny-Ålesund – Wettzell	0.83
Kokee Park – Ny-Ålesund	0.56				
Ny-Ålesund – Wettzell	0.83				

Table 5.4: Coverable surface of the hemispheres in percentage terms for all investigated baselines.

Intensive session cover the surface of a hemisphere. Expressing this by the sum of the surface areas of all three-dimensional triangles, permits to characterize an observing session with a single quantity.

The spanned surface of the observed sources cannot complete the whole surface of the hemisphere because of the obstructed common visibility of both radio telescopes. The fraction of coverable surface depends on the length of the respective baseline, hence, it is different for the three Intensive types. The coverable fraction of the hemisphere's surface can be determined per baseline and is depicted in Fig. 5.7b for the example of the baseline Tsukuba – Wettzell. Table 5.4 lists the coverable fraction of the hemisphere's surface in percentage terms for all baselines which occur in the investigated test sessions. According to Tab. 5.4, the smaller common visibility of the baseline Kokee Park – Wettzell (0.40) compared to the baseline Tsukuba – Wettzell (0.54), as mentioned before, is clearly recognisable.

A surface determined by the triangulation of the observed sources per session can then be expressed as percentage of the baseline-depended maximal coverable surface as well. In case of a multiple station network, as is usually the case for INT3 sessions and occasionally the case for INT1 sessions, the surfaces of the different baselines represented by the triangulation will be added and evaluated in relation to the total area of all baselines. Thus, the maximal attainable sky coverage amounts to 1 for every session independently from the station network. In this manner, all session types can be compared to each other.

Figures 5.8 to 5.10 show the sky coverages of the differently scheduled sessions of the investigated time span computed in this way. For a better readability, Fig. 5.8 depict the sky coverage of INT1 sessions with the two station network only. Noticeably, there are strong distinctions between the three Intensive types. Concerning INT1 sessions the scheduling methods using impact factors, IF and $\mathrm{IF}_{\Delta UT1}$, seem to reach nearly always a better sky coverage as the IVS scheduled sessions (see Fig. 5.8). But, the sky coverage of the $\mathrm{IF}_{\Delta UT1}$ scheduled sessions varies very much, while the sky coverage of the IF sessions shows the most stable behavior and nearly always the best results. The not depicted sessions with a three station network reach a sky coverage of about merely 0.1. The previous section (Sec. 5.1) reveals that a third station contributes just a few observations. This is confirmed by the sky coverage as the use of a third radio telescope within the INT1 setup decreases the entire sky coverage substantially. As can be seen by the average values of the sky coverages in Tab. 5.5, this is especially true for IVS and IF schedules. In these cases, the sky coverage reaches only a third (IVS) or a quarter (IF) of that of the sessions scheduled with just two stations, while the $\mathrm{IF}_{\Delta UT1}$ sessions reach a little bit more than half of it at maximum.

In case of INT2 sessions, the IF schedules reach the best sky coverage again, which is also reflected by the average values in Tab. 5.5. The table also reveals an identical average sky coverage of IVS and $\mathrm{IF}_{\Delta UT1}$ schedules. Considering Fig. 5.9, the $\mathrm{IF}_{\Delta UT1}$ time series is more erratic than that of the IVS and reaches better and worse sky coverages.

Much different than INT1 and INT2, the best sky coverage of INT3 sessions is achieved by the IVS schedules (Fig. 5.10). The next best sky coverage is related to IF schedules and the $\mathrm{IF}_{\Delta UT1}$ sky coverage is the worst of all almost constantly.

Regarding the average values in Tab. 5.5 it is clearly seen, that the IF and the $\mathrm{IF}_{\Delta UT1}$ schedules reach better sky coverages than those of the IVS, except for INT3 sessions. However, it is notable that all average values are far from the maximal reachable value of 1. Especially all values of INT3 sessions not even reach half of the maximum sky coverage. The best general sky coverage is achieved for INT2 sessions in all three cases.

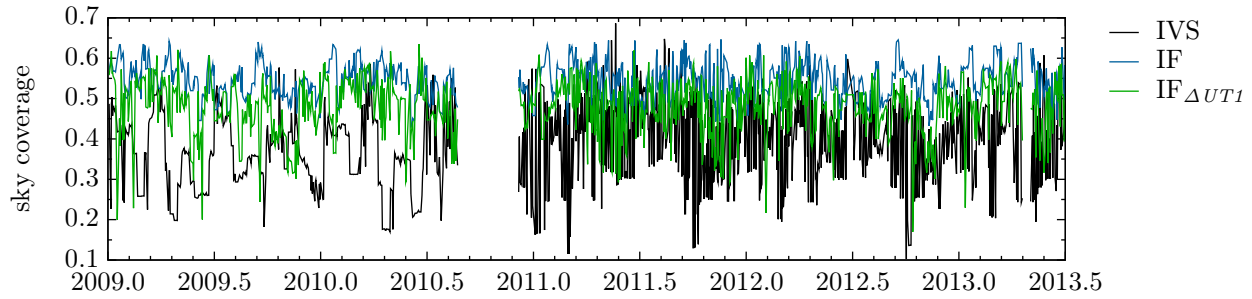

Figure 5.8: Sky coverage of INT1 sessions (2 station network).

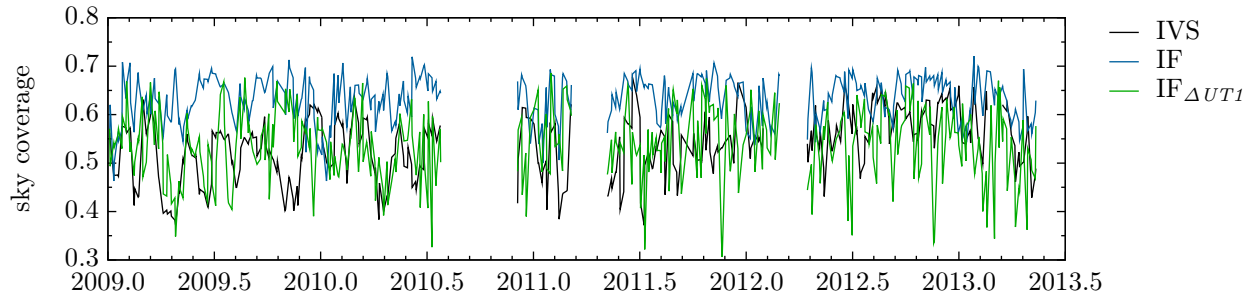

Figure 5.9: Sky coverage of INT2 sessions.

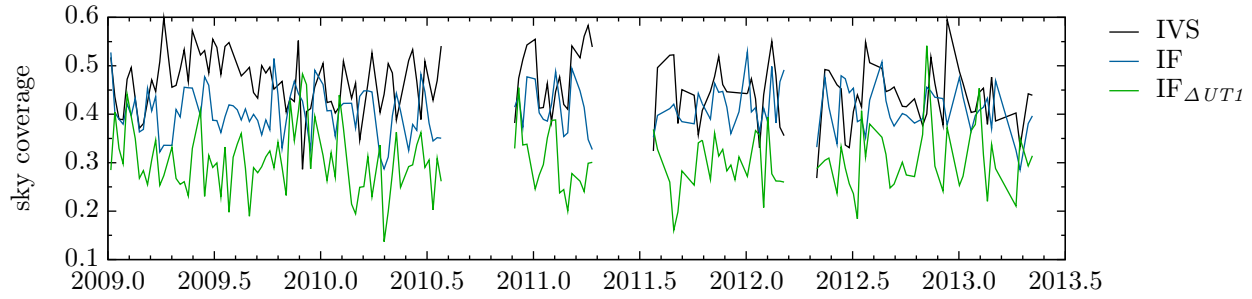

Figure 5.10: Sky coverage of INT3 sessions.

	INT1 (2 stations)	**INT1** (3 stations)	**INT2**	**INT3**
IVS	0.39	0.12	0.54	0.46
IF	0.55	0.14	0.63	0.41
IF$_{\Delta UT1}$	0.48	0.26	0.54	0.30

Table 5.5: Average sky coverage of the investigated sessions with the different scheduling methods.

5.3 Correlations

Another criterion for evaluating the different scheduling methods are the correlation coefficients between the estimated parameters. A correlation coefficient as a measure of separability between the estimated parameters

is a quality feature for the session geometry and for the reliability of the results. Within the least-squares adjustment, the correlation coefficients can be derived. A priori variances of the observations, taking into account antenna specifications and the geometry of the design (see Eq. 2.21 – 2.23 and Eq. 4.26 – 4.28), are used to populate the covariance matrix of the observations $\mathbf{\Sigma_{yy}}$. With the Jacobian matrix $\mathbf{A}$ the covariance matrix of the parameters $\mathbf{x}$ can be computed by

$$\mathbf{\Sigma_{xx}} = \left(\mathbf{A}^T \mathbf{\Sigma_{yy}^{-1}} \mathbf{A}\right)^{-1}. \tag{5.1}$$

The covariance matrix of the parameters $\mathbf{\Sigma_{xx}}$ contains the variances of each parameter σ_i^2, that are arranged at the main-diagonal, and the covariances of the parameters σ_{ij} as off-diagonal elements. These elements are used to calculate the correlation coefficients between the estimated parameters

$$\rho_{ij} = \frac{\sigma_{ij}}{\sigma_i \sigma_j}. \tag{5.2}$$

Since both the a priori variances of the observations and the Jacobian matrix can be derived just by scheduling a session, no actual observations are needed and the three scheduling cases IVS, IF and IF$_{\Delta UT1}$ can be investigated in the same manner. Due to the fact that $\Delta UT1$ is the only objective of Intensive sessions, solely the correlation coefficients between $\Delta UT1$ and the auxiliary parameters are of interest, while the correlations between the auxiliary parameters are rather uncritical.

Due to the fairly large quantity of investigated observing plans, the whole correlation matrix cannot be regarded in detail for each session. Picking out a single correlation coefficient of one Intensive type and plotting it for the three different scheduling methods over the investigated time interval produces various time series, exemplarily depicted by the correlation coefficient $\rho_{cl_0,\Delta UT1}$ between the clock offset and $\Delta UT1$ of the investigated INT1 sessions in Fig. 5.11 to 5.13 on page 62. By this example it can be seen, that the correlation coefficients are scattered about zero for all scheduling cases, however, a small offset to zero might be recognized in all cases. These offsets are listed in Tab. 5.6 to 5.8. For INT1 sessions (Tab. 5.6), the absolute offsets do not exceed a negligible correlation coefficient of 0.3. In case of INT2 and INT3 sessions (Tab. 5.7 and 5.8), some of the absolute offsets are greater than 0.3 but lower than 0.7 and, thus, belong to moderate correlation coefficients.

	cl_0	cl_1	cl_2	at_A	at_B
IVS	0.09	0.01	0.00	0.12	0.08
IF	0.17	-0.01	0.01	0.14	0.08
IF$_{\Delta UT1}$	0.14	-0.02	0.01	0.10	0.03

Table 5.6: Mean correlation coefficients between the respective auxiliary parameter and $\Delta UT1$ for INT1 sessions scheduled with the three different methods.

	cl_0	cl_1	cl_2	at_A	at_B
IVS	-0.32	-0.06	0.02	-0.48	-0.10
IF	-0.39	0.03	-0.02	-0.29	0.00
IF$_{\Delta UT1}$	-0.31	0.03	-0.02	-0.15	-0.01

Table 5.7: Mean correlation coefficients between the respective auxiliary parameter and $\Delta UT1$ for INT2 sessions scheduled with the three different methods.

Regarding the behavior of the correlation coefficients over time (Fig. 5.11 to 5.13), it is conspicuous, that the scattering is lower for both the IF and IF$_{\Delta UT1}$ schedules compared to the IVS schedules in this example. To assess all determined correlation coefficients between $\Delta UT1$ and the auxiliary parameters, the standard deviations of the respective correlation coefficients using zero as mean value as measure of dispersion are

	cl_{0_A}	cl_{1_A}	cl_{2_A}	cl_{0_B}	cl_{1_B}	cl_{2_B}	at_A	at_B	at_C
IVS	0.31	-0.03	0.04	-0.16	0.03	-0.03	-0.14	-0.47	0.02
IF	-0.50	0.01	-0.00	-0.28	-0.01	0.01	-0.50	0.23	-0.05
$IF_{\Delta UT1}$	-0.29	0.00	0.01	-0.22	0.01	-0.01	-0.23	-0.01	-0.17

Table 5.8: Mean correlation coefficients between the respective auxiliary parameter and $\Delta UT1$ for INT3 sessions scheduled with the three different methods.

taken into account. These values are listed in Tab. 5.9 to 5.11, whereas the lowest value per column is highlighted.

Concerning INT1 and INT2 sessions (Tab. 5.9 and 5.10), both the IF and the $IF_{\Delta UT1}$ scheduling method exhibits lower values than those of the IVS. For some parameters, the differences to the IVS standard deviations are quite great. However, the situation of INT3 sessions is quite different, as the standard deviations mostly differ only slightly, so that the best values occur in each scheduling case for different parameters and, thus, no significant benefit can be detected by using the IF or $IF_{\Delta UT1}$ scheduling method.

As only standard deviations of correlation coefficient were considered, it cannot be concluded whether $\Delta UT1$ is well separable from the other parameters or not. The standard deviations signify merely the size of the respective scatter about zero. From this can be inferred which scheduling method exhibit a steadier behavior of the correlation coefficients as indicated by Fig. 5.11 to 5.13.

	cl_0	cl_1	cl_2	at_A	at_B
IVS	0.36	0.22	0.22	0.39	0.38
IF	0.24	0.07	0.08	0.21	0.23
$IF_{\Delta UT1}$	0.19	0.09	0.09	0.16	0.12

Table 5.9: Standard deviations of the correlation coefficients between the respective auxiliary parameter and $\Delta UT1$ for INT1 sessions scheduled with the three different methods for a two station network.

	cl_0	cl_1	cl_2	at_A	at_B
IVS	0.40	0.33	0.33	0.51	0.24
IF	0.40	0.06	0.06	0.31	0.13
$IF_{\Delta UT1}$	0.32	0.07	0.07	0.17	0.09

Table 5.10: Standard deviations of the correlation coefficients between the respective auxiliary parameter and $\Delta UT1$ for INT2 sessions scheduled with the three different methods.

	cl_{0_A}	cl_{1_A}	cl_{2_A}	cl_{0_B}	cl_{1_B}	cl_{2_B}	at_A	at_B	at_C
IVS	0.35	0.14	0.14	0.20	0.14	0.14	0.17	0.50	0.23
IF	0.51	0.07	0.08	0.28	0.05	0.05	0.51	0.30	0.09
$IF_{\Delta UT1}$	0.32	0.11	0.11	0.25	0.08	0.08	0.27	0.11	0.31

Table 5.11: Standard deviations of the correlation coefficients between the respective auxiliary parameter and $\Delta UT1$ for INT3 sessions scheduled with the three different methods.

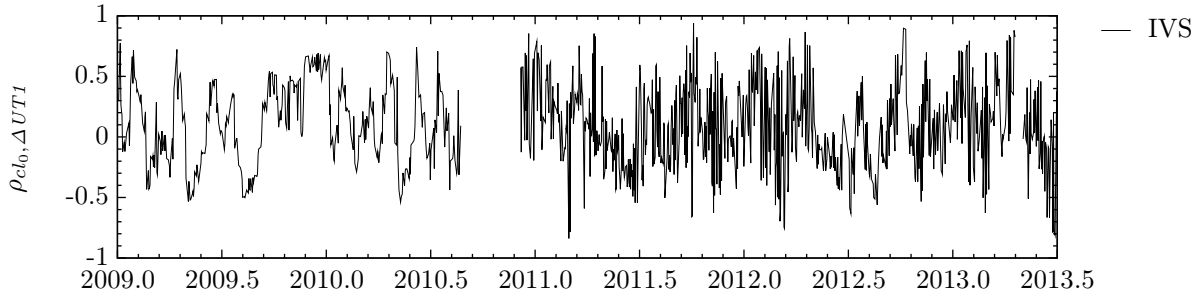

Figure 5.11: Correlation coefficient between the clock offset cl_0 and $\Delta UT1$ for IVS-INT1 observing plans.

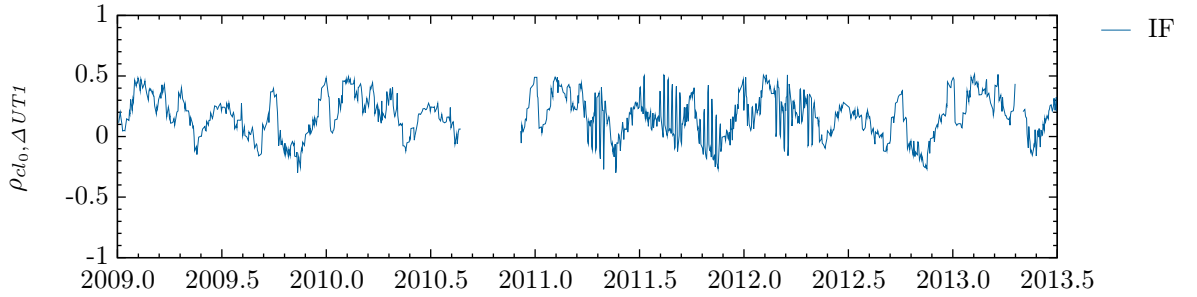

Figure 5.12: Correlation coefficient between the clock offset cl_0 and $\Delta UT1$ for IF-INT1 observing plans.

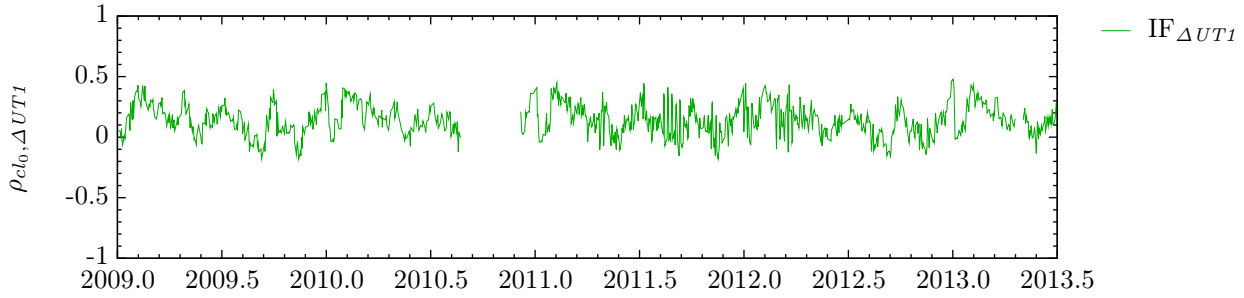

Figure 5.13: Correlation coefficient between the clock offset cl_0 and $\Delta UT1$ for IF$_{\Delta UT1}$-INT1 observing plans.

5.4 Formal errors

Since improving $\Delta UT1$ formal errors is a goal of scheduling Intensive sessions, the reached $\Delta UT1$ formal errors of the different scheduling methods are subject of this section. The computed $\Delta UT1$ formal errors $\sigma_{\Delta UT1}$, determined from the covariance matrix of the parameters (see Eq. 5.1), are depicted for the three Intensive types in Fig. 5.14 to 5.16 with their respective mean values shown in Tab. 5.12. It should be noted that the resulting formal errors simply represent the geometry produced by the observation schedules still neglecting the post fit scatter of the observations, which is dealt with in Sec. 5.5.

The $\Delta UT1$ formal errors resulting from the IF and IF$_{\Delta UT1}$ scheduling method are extremely better than those of the IVS in case of INT1 and INT2 sessions (Fig. 5.14 and Fig. 5.15). Due to visualization reasons, the y-axes of Fig. 5.14 had to be truncated. The largest $\Delta UT1$ formal error of the IVS schedules, which is not visualized, appears in the second quarter of 2011 and amounts to 125.20 µs. Probably, the main reason

for this is the small number of observed radio sources, which amounts to 5, and theirs disadvantageous distribution over the sky. Concerning INT1 sessions, the mean formal errors of both the IF and $\mathrm{IF}_{\Delta UT1}$ are improved by a factor of about 2 compared to IVS in case of a two station network and a slightly smaller factor for a three station network. (see Tab. 5.12). In case of INT2 sessions, this factor amounts to about 1.5. Moreover, the scatter of the IF and $\mathrm{IF}_{\Delta UT1}$ $\Delta UT1$ formal errors is essentially reduced over the whole investigated time span of INT1 and INT2 compared to IVS.

The situation slightly differs for INT3 sessions, as an improvement of the $\Delta UT1$ formal errors is only reached by the IF scheduling method (Fig. 5.16). This improvement is also confirmed by the mean values listed in Tab. 5.12, as the improvement amounts to a factor of about 1.2. Table 5.12 also reveals a slight improvement for the $\mathrm{IF}_{\Delta UT1}$ scheduling method. But this value must be interpreted with caution because of the great scatter of the respective $\Delta UT1$ formal errors (see Fig. 5.16). Several formal errors exceed those of the IVS significantly. However, the $\mathrm{IF}_{\Delta UT1}$ scheduling method also reaches the smallest $\Delta UT1$ formal errors for several INT3 sessions.

It can be concluded that both scheduling methods using the impact factors of the observations improve the $\Delta UT1$ formal errors for the three Intensive types. The greatest improvement is reached for INT1 sessions, closely followed by INT2 sessions. Concerning INT3 sessions, only by using the IF scheduling method a constant improvement with respect to IVS schedules can be achieved.

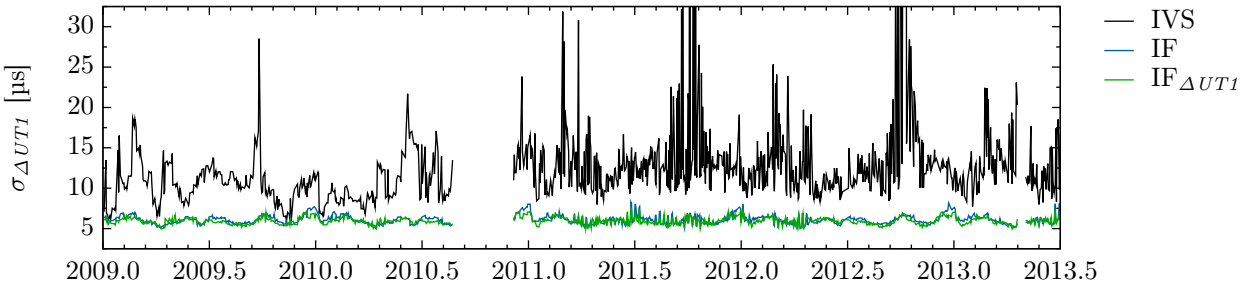

Figure 5.14: $\Delta UT1$ formal errors for INT1 sessions (2 station network).

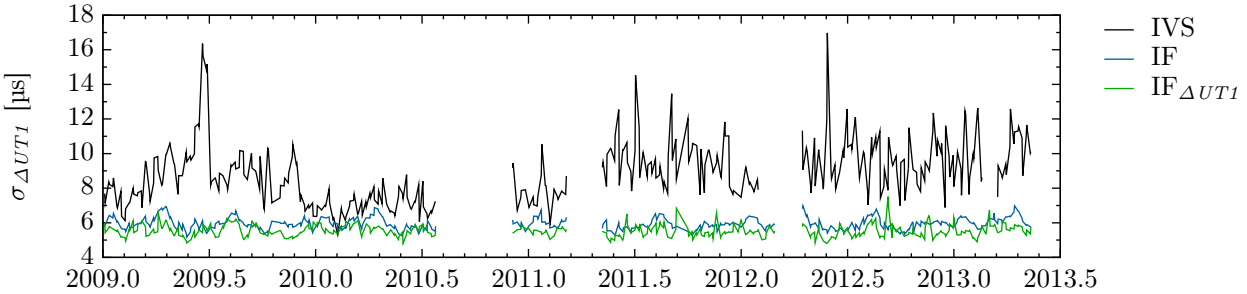

Figure 5.15: $\Delta UT1$ formal errors for INT2 sessions.

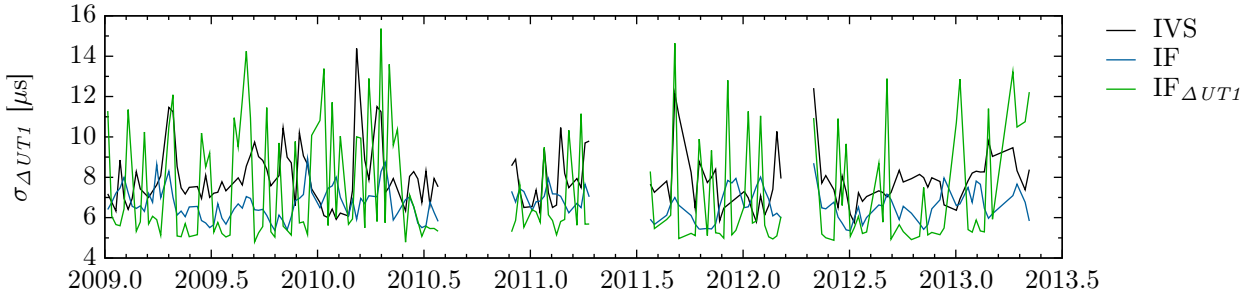

Figure 5.16: $\Delta UT1$ formal errors for INT3 sessions.

	INT1 (2 stations)	**INT1** (3 stations)	**INT2**	**INT3**
IVS	12.59	11.76	8.86	7.87
IF	6.09	7.01	5.95	6.65
IF$_{\Delta UT1}$	5.93	6.24	5.53	7.30

Table 5.12: Mean $\Delta UT1$ formal errors in µs for all Intensive types scheduled with the three different methods.

Taking the formal errors of the auxiliary parameters into account reveals the difference between the IF and the IF$_{\Delta UT1}$ scheduling method. Figures 5.17 and 5.18 show examples of the formal errors of two auxiliary parameters, a clock offset cl_0 and an atmospheric parameter at, of the investigated INT2 sessions. These figures show impressively that the IF scheduling method improves the formal errors of the other estimated parameters as well, while the IF$_{\Delta UT1}$ scheduling method in most cases produces enormous formal errors for the auxiliary parameters. Table 5.13 gives an overview of all auxiliary parameters of the INT2 sessions by their mean formal errors. These mean values confirm the improvement of the formal errors of most parameters by the IF scheduling method and worse results for the IF$_{\Delta UT1}$ scheduling method. Here, the formal errors have a similar magnitude as those of the IVS schedules.

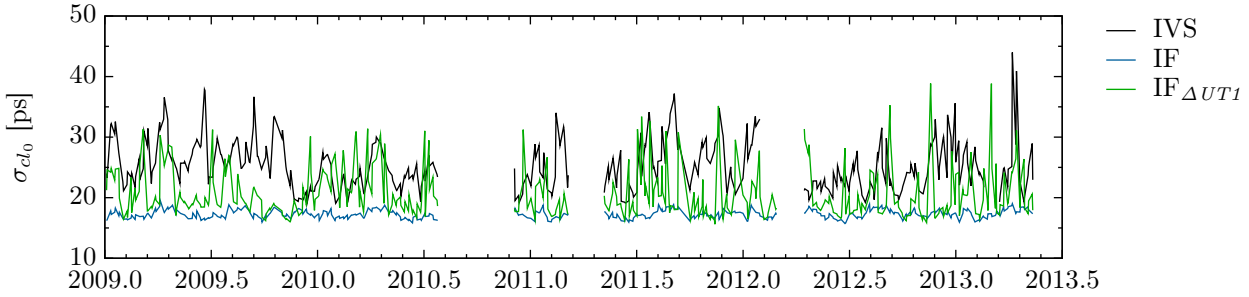

Figure 5.17: cl_0 formal errors for INT2 sessions.

	σ_{cl_0} [ps]	σ_{cl_1} [10^{-14}]	σ_{cl_2} [10^{-14}/d]	σ_{at_A} [ps]	σ_{at_B} [ps]
IVS	25.25	2.32	55.20	5.31	4.27
IF	17.28	1.87	44.25	3.58	2.21
IF$_{\Delta UT1}$	20.80	2.58	59.76	7.16	4.74

Table 5.13: Mean formal errors of the auxiliary parameters for INT2 sessions scheduled with the three different methods.

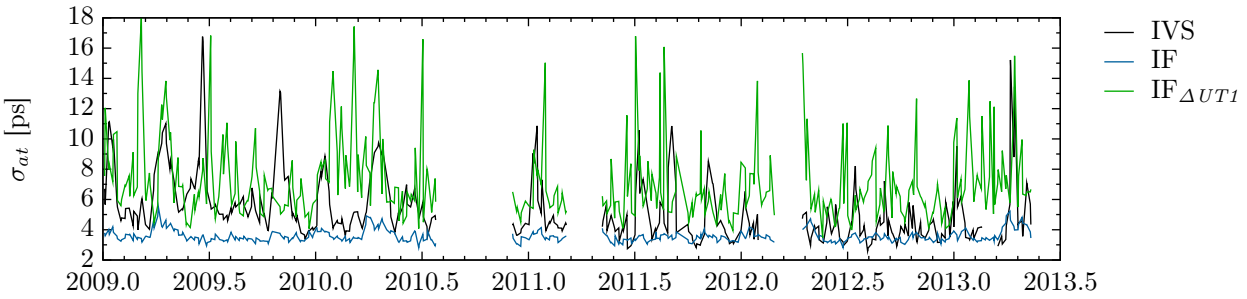

Figure 5.18: *at* formal errors for INT2 sessions.

5.5 Repeatability

An advanced approach to assess VLBI observing plans is to simulate stochastic factors, since a session is termed robust if its $\Delta UT1$ estimate does not change much with random noise, from e.g. atmospheric fluctuations. For this purpose, the three greatest stochastic errors of VLBI observations – slant wet delays, station clock behavior and white noise – are taken into account as it was also done for VLBI2010 simulations (e.g. Wresnik et al. 2009). The influence of these stochastic errors can best be determined by using a Monte Carlo simulation (MCS, Metropolis and Ulam 1949).

Simulations are abstractions of reality with the aim of gaining knowledge about the real system which is imitated. The MCS is a simulation method for modeling random variables to calculate characteristics of their distribution functions. The "law of large numbers" constitutes the mathematical justification for a MCS. Performing a MCS n times resulting in a random sample with n different solutions which can be analyzed statistically. The results, like the sample mean and the sample variance, are the more probable the more simulations n will be done.

Here, the MSC is used to simulate a full VLBI least squares adjustment. However, since the geometry stays the same in all simulation runs, the variability needs to be reflected only in the reduced VLBI observation vector $o - c$ (observed minus computed). This reduced observation vector should be simulated as a composition of the three greatest stochastic errors of VLBI observations mentioned before in the form of

$$o - c = (zwd_B \cdot m_B(\varepsilon_B) + cl_B) - (zwd_A \cdot m_A(\varepsilon_A) + cl_A) + wn_{bl}, \tag{5.3}$$

with $zwd_{A,B}$ being the zenith wet delay at the participating stations A and B, $m_{A,B}$ denotes the mapping function wet and $\varepsilon_{A,B}$ the elevation at the respective station, $cl_{A,B}$ is the respective station clock and wn_{bl} denotes a baseline dependent white noise. It is not necessary to simulate the total delay, since it will be reduced by deterministic models for the least squares adjustment.

Atmospheric fluctuations The simulation of slant wet delays follows the turbulence model developed by Nilsson et al. (2005), who further developed the turbulence model of Treuhaft and Lanyi (1987). Both models base on the Kolmogorov turbulence theory (Kolmogorov 1941a and Kolmogorov 1941b). The variation in wet delays is simulated as a function of direction and time and results from the integration of the refractive index along the signal path. For detailed information about this modeling see Nilsson et al. (2007), Nilsson and Haas (2008), Nilsson et al. (2009) and Nilsson and Haas (2010). The simulations in this work assumed a refractive index structure constant of $C_n^2 = 1 \cdot 10^{-14}\,\mathrm{m}^{-\frac{2}{3}}$ and individual wind speeds for the different VLBI stations. The method for calculating the slant wet delays is modified in a way, that the simulated turbulence starts 12 hours before the start time of the session. Thus, preventing an assumed running-in of the turbulence simulation. To visualize the mentioned effect, simulations of the troposphere have been done for the first 24 hours of the CONT11 campaign with and without a forerun of 12 hours. The respective 50 realizations of the simulated zenith wet delay of the station in Kokee Park are shown in

Fig. 5.19. The running-in is clearly visible (Fig. 5.19 left), as the simulated zenith wet delays are close to a constant initial value at the beginning and spread out over the session. This behavior will be well avoided by the forerun which can be seen in Fig. 5.19 (right).

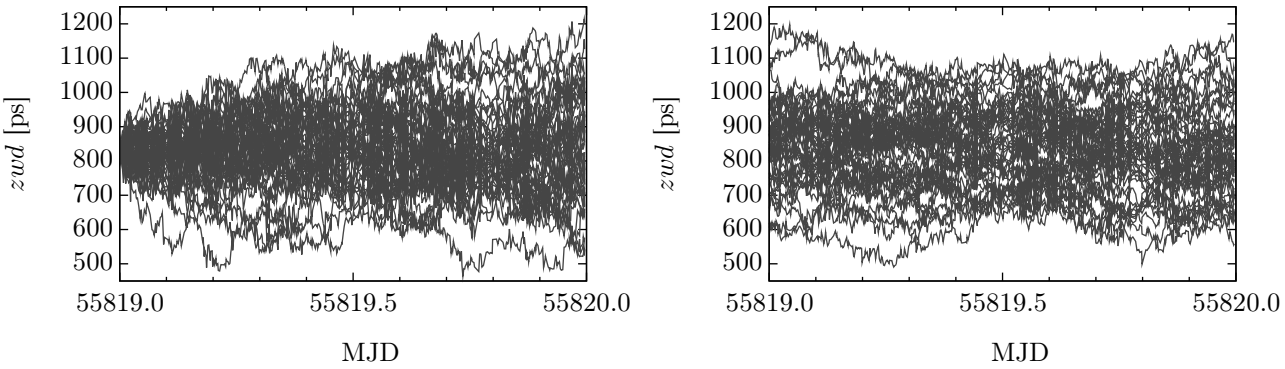

Figure 5.19: 50 realizations of the simulated zenith wet delay for the station in Kokee Park for the first 24 h of the CONT11 campaign. Left without forerun of the simulation, right with a forerun of 12 h.

Clock behavior In range measurements where the signals are phases compared relative to a reference signal, as is the case with VLBI measurements, instabilities in any of the oscillators involved introduce an uncertainty in the range estimate. Those phase and frequency instabilities include both random and deterministic components and define the limits of stability of the clock. Thus, accurate simulation of the instabilities is necessary. In this work, the clock variations have been modeled by a power-law process (Kasdin 1995) including five common types of noise that are considered to affect clocks and clock measurements: random walk frequency noise, flicker frequency noise, white frequency noise, flicker phase noise and white phase noise (Rutman 1978). The power-law noise is particularly suitable for clock simulations as it results in non-stationary noise sequences that are also scale-invariant and causal and have the proper autospectral densities and Allan variances (Kasdin and Walter 1992). For the required simulations, the clock variations have been modeled by a power-law process that has been adjusted to reach an Allan standard deviation (ASD) of $1{\cdot}10^{-14}$@50 min. Although atomic clocks are more precise by about one order of magnitude (e.g. Giordano et al. 2011), the chosen ASD is reasonable as the simulations represent variations due to thermal and other physical responses of the cabling between the active hydrogen maser and the receiving system as well. As can be seen in Fig. 5.20 (bottom on page 67) different components are dominating the process on different time scales. For instance white and flicker phase modulation are dominating on short time scales, while on time scales below one hour, flicker and random walk frequency modulation is dominating. In the final analysis, the generated processes have the desired noise shape. For demonstration purposes, the process shown in Fig. 5.20 has been generated for a longer time span ($\sim$130 000 s = $\sim$36 h).

White noise Baseline dependent white noise with a standard deviation of 10 ps simulates instrumental errors.

The simulated reduced observations, given by the stochastic components, were finally used in a least squares adjustment. This enables the estimation of the adjusted parameters. Several iterations of Monte-Carlo simulations of a single session can be used to calculate the repeatability s of an estimated parameter

$$s = \sqrt{\frac{1}{n-1}\sum_{i=1}^{n}(x_i - \overline{x})^2} \tag{5.4}$$

with n simulation iterations, x_i denoting a single parameter and $\overline{x}$ the mean value of n parameters.

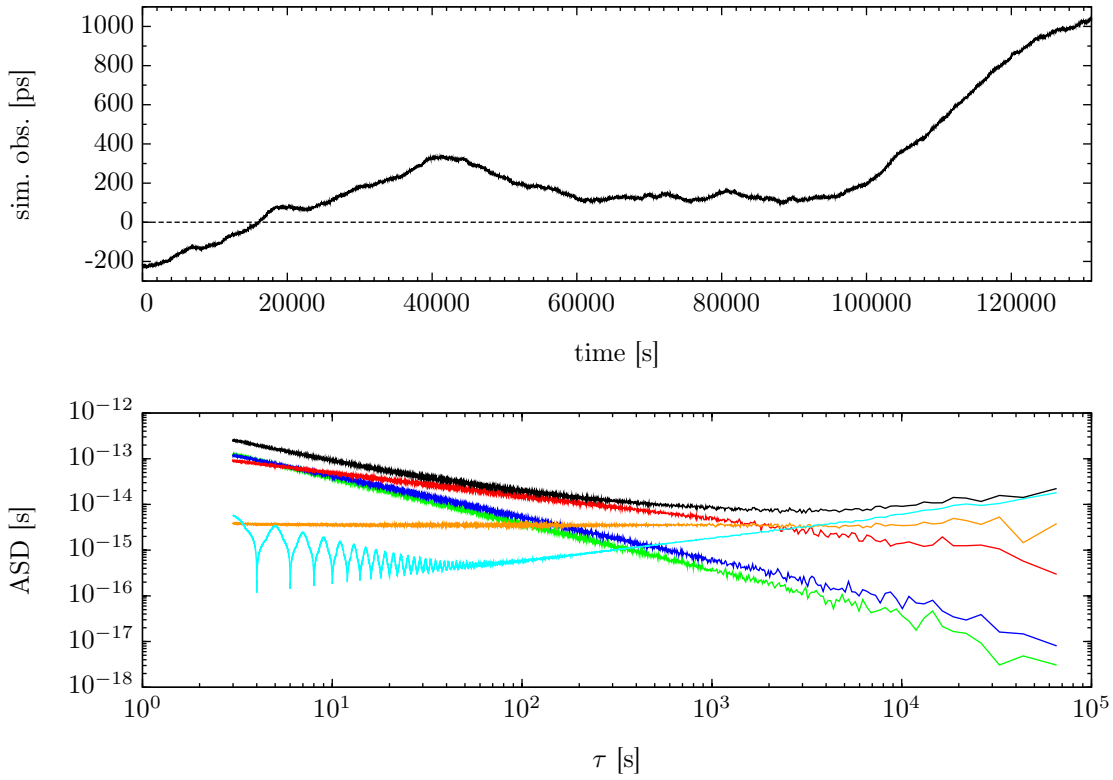

Figure 5.20: A single generated noise sequence with a total number of 2^{17} points (top). Allan standard deviation estimates of the five particular types of noise, random walk frequency noise (cyan), flicker frequency noise (orange), white frequency noise (red), flicker phase noise (blue) and white phase noise (green), and the composite Allan standard deviation estimate (black line) having its minimum near by the predetermined Allan standard deviation of $1{\cdot}10^{-14}$@50 min (bottom).

Since the "law of large numbers" constitutes the mathematical justification for a MCS the question concerning a reasonable number of simulation iterations n arises. The answer of this question represents a compromise between a tolerable expenditure of time (that depends on the respective computing capacity) and the reliability of the result. Wresnik (2009) suggested an iteration number of 25 accounted for by his examinations. As the state of facts differs from that of Wresnik (2009), e.g., in contrast to his work only Intensive sessions with a minor data volume are used and moreover a new simulation algorithm has been written in C++ compared to using the analysis software OCCAM (Titov et al. 2004), the question of a suitable number of simulation runs was posed again. For this purpose, several Intensive sessions have been simulated with 1000 iterations followed by least squares adjustments so that 1000 estimated $\Delta UT1$ parameters per session exist. The $\Delta UT1$ repeatabilities $s_{\Delta UT1}$ have been computed according to Eq. 5.4 using 2 to 1000 realizations. These repeatabilities are depicted for four randomly chosen sessions in Fig. 5.21, whereby the x-axis is limited to 500 simulation iterations due to readability reasons. Obviously, the repeatability does not change significantly from 150 realizations onwards, marked by the vertical dashed line. The expenditure of time for 150 simulation iterations of one Intensive session is within acceptable limits as well and, thus, all following investigations in this work concerning simulations will be done with 150 iterations.

Figure 5.22 depicts the relation between $\Delta UT1$ repeatability $s_{\Delta UT1}$ and $\Delta UT1$ a posteriori standard deviations $\tilde{\sigma}_{\Delta UT1}$ for the example of the investigated IVS-INT2 sessions. Here, the real observations of the respective INT2 sessions have been analyzed with the software package Calc/Solve (Ma et al. 1990, Baver 2013) with particular attention to $\Delta UT1$ a posteriori standard deviations. A posteriori standard deviations of the parameters are also obtained by the least squares adjustment of the simulated reduced observing vectors. As intended, these simulated a posteriori standard deviations of $\Delta UT1$ (Fig. 5.22 gray line) are on

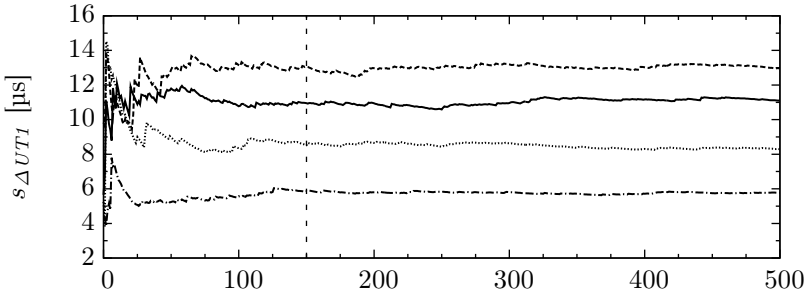

Figure 5.21: Representative $\Delta UT1$ repeatabilities calculated from 2 to 500 simulation iterations of four randomly chosen sessions.

the same level as those of the real data (black line). This confirms the success of the simulation strategy. The simulated time series is a little less noisy than the real time series what may be due to the fact that just a few errors of the whole VLBI error budget are simulated. That is the reason for taking just the $\Delta UT1$ repeatabilities into account for valuation purposes. Furthermore, it can be seen that the $\Delta UT1$ repeatabilities determined from several simulation iterations (gray line) follows a similar trend than the a posteriori standard deviations, but on a slightly higher level.

$\Delta UT1$ repeatabilities, determined by $n = 150$ simulation iterations, are depicted in Fig. 5.23 to 5.25 for the three Intensive types. The $\Delta UT1$ repeatabilities of the IF schedules are mostly better than those of the IVS schedules or at a comparable level. This is also confirmed by the mean values listed in Tab. 5.14, which also reveal an improvement of about 20 % for INT1 sessions and only slight improvements for INT2 and INT3 sessions.

The IF$_{\Delta UT1}$ schedules show a great improvement for INT1 sessions, since the mean $\Delta UT1$ repeatability amounts to 10.75 µs for a two station network which is even lower than those of the IF schedules, in particular about 30 % better compared to IVS. For a three station network the improvement is still about 15 %. No such good results are achieved for INT2 and INT3 sessions with the IF$_{\Delta UT1}$ scheduling method. In case of INT2 the $\Delta UT1$ repeatability is very noisy and partially shows the best results but also the worst results. On average, the improvement is again a little bit bigger than that of the IF schedules but must be treated with caution because of the great fluctuations. As suggested in the previous section, the IF$_{\Delta UT1}$ scheduling method is not always convenient for sessions with multiple stations. This is also reflected by the $\Delta UT1$ repeatabilities of INT3 sessions (Fig. 5.25). Here, the $\Delta UT1$ repeatabilities exceed those of the IVS almost constantly. The values are so big that the average value shows a degradation of about 30 % compared to IVS schedules.

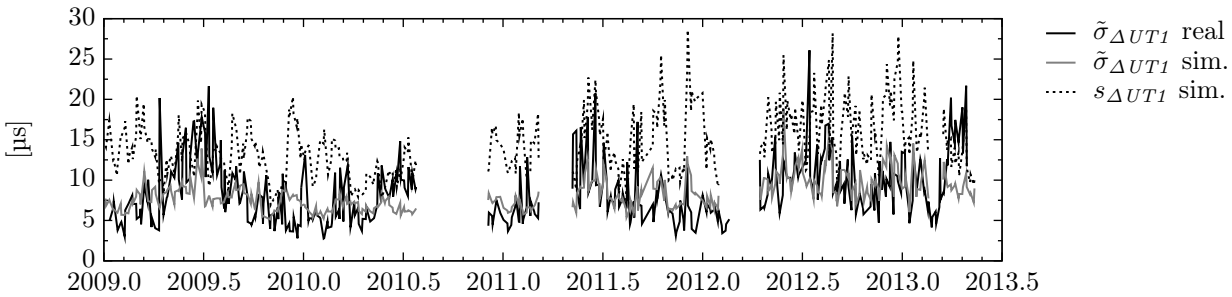

Figure 5.22: Comparison of a posteriori standard deviations of $\Delta UT1$ from real IVS-INT2 sessions, simulated IVS-INT2 sessions and $\Delta UT1$ repeatabilities determined from 150 MCS for INT2 sessions.

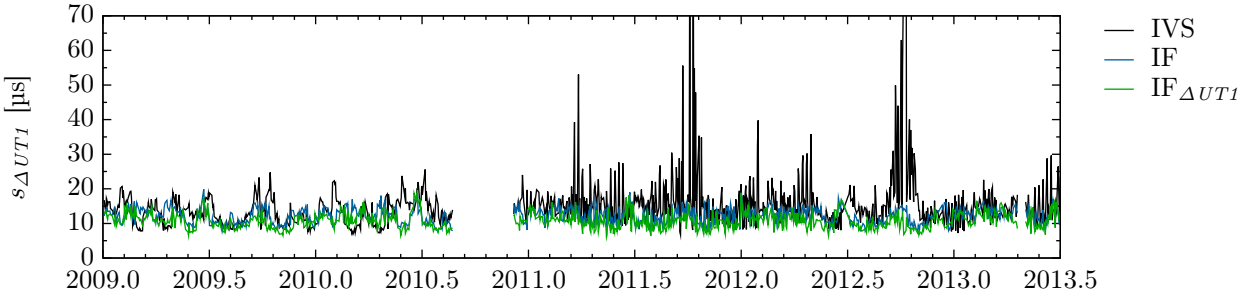

Figure 5.23: $\Delta UT1$ repeatabilities for INT1 sessions (2 station network).

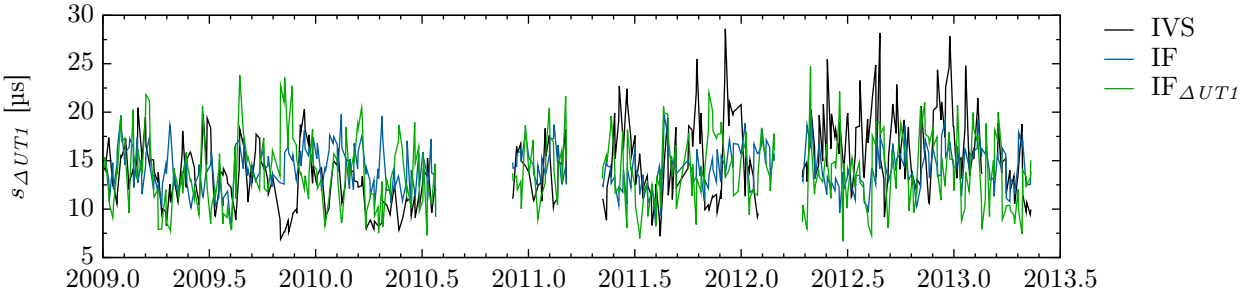

Figure 5.24: $\Delta UT1$ repeatabilities for INT2 sessions.

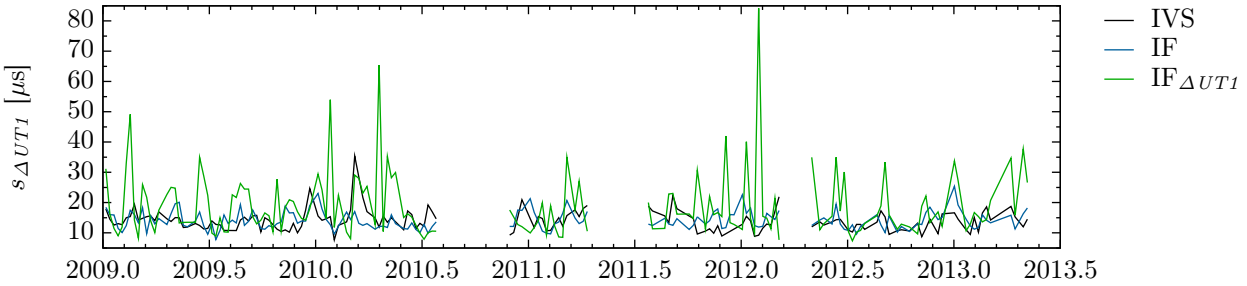

Figure 5.25: $\Delta UT1$ repeatabilities for INT3 sessions.

	INT1 (2 stations)	**INT1** (3 stations)	**INT2**	**INT3**
IVS	15.10	14.69	14.38	14.16
IF	12.23	11.28	14.17	14.10
IF$_{\Delta UT1}$	10.75	12.49	13.85	18.92

Table 5.14: Mean $\Delta UT1$ repeatability in µs for all Intensive types scheduled with the three different methods.

5.6 Conclusions of the examination

Summarizing the last section, correlations between the investigated assessment criteria might be detected. Concerning the number of observations, the IF scheduling method mostly achieves a greater quantity on average compared to both other scheduling methods. This is particularly noticeable for multi station sessions, like INT3 or the INT1 sessions with an additional station. In contrast, the $\text{IF}_{\Delta UT1}$ scheduling method exhibit a greater mean number of observations than IVS sessions only for standard INT1 sessions with a single baseline. In case of INT2 sessions the number is just slightly smaller than that of the other scheduling methods. But scheduling multi-station networks by the $\text{IF}_{\Delta UT1}$ scheduling method leads to significantly lower observation numbers. However, the lowest $\Delta UT1$ formal errors are achieved by the $\text{IF}_{\Delta UT1}$ schedules except for INT3, where it reached the second best result after the IF scheduling method. This indicates that a great number of observations is not so important for improving $\Delta UT1$ formal errors. Instead, the number of scans could be more important, as the $\text{IF}_{\Delta UT1}$ scheduling method produces the greatest number of scans for multi-station sessions. Observing just with the one long east-west baseline of the 3 baseline network, that is most sensitive to the Earth's rotation, seems to suffice for getting low $\Delta UT1$ formal errors. Integrating observations of the third station located in the north, like IVS and IF do, may improve the formal errors of the auxiliary parameters instead. Since also the IF scheduling method produces more or an equal number of scans than the IVS method, the $\Delta UT1$ formal errors consequently decrease in each case.

A further criteria for improving the $\Delta UT1$ formal errors might be the number of used sources, as those of the $\text{IF}_{\Delta UT1}$ schedules exceed those of the other methods in all cases. As already mentioned, observing many different radio sources within a session increases the sky coverage automatically. Earlier investigations, e.g. Fischer et al. 2003 or Baver and Gipson 2010, have shown that a better sky coverage is linked to smaller $\Delta UT1$ formal errors. This is also affirmed by the determined sky coverage in Sec. 5.2. Here again, both scheduling methods using the impact factors show better results than the IVS scheduling method except for INT3 sessions. Due to this, the improvement of $\Delta UT1$ formal errors are not so convincing for INT3 sessions as for the other Intensive setups by the IF and $\text{IF}_{\Delta UT1}$ schedules. Surprisingly, the best sky coverage for INT1 sessions including a third station is reached by $\text{IF}_{\Delta UT1}$ schedules although the third station is hardly involved in the scans. This is another evidence for a well balanced sky coverage of the two major stations in these cases.

The investigations of the correlations between $\Delta UT1$ and the auxiliary parameters, taking into account the scatter of the correlation coefficients, revealed a most steady behavior of both the IF and $\text{IF}_{\Delta UT1}$ schedules for all Intensive setups. Only with respect to INT3 sessions, the IVS schedules exhibit some lower correlation coefficients. Since low correlation coefficients are important for a distinct estimation of the unknown parameters, the scheduling methods using the impact factors have a further advantage.

As both scheduling methods using the impact factors outclass the IVS method in most of the investigated criteria, the interaction of the different features seems to be important for improving the $\Delta UT1$ formal errors.

Concerning the $\Delta UT1$ repeatabilities, which have been determined by simulations of stochastic influences in Sec. 5.5, the $\text{IF}_{\Delta UT1}$ schedules exhibit the best results in case of single baseline Intensives, whereas the IF schedules seems to be most appropriate for multi station sessions. Comparing the ratio between $\Delta UT1$ formal errors and $\Delta UT1$ repeatabilities, the IVS schedules show the smallest value. Therefore, the IVS schedules seem to be most robust towards the simulated influences. On the contrary, the $\text{IF}_{\Delta UT1}$ schedules react very sensitive to the simulated stochastic errors. One reason for this could be the presence of very many observations with very low elevations in these schedules which are highly affected by atmospheric fluctuations. Nevertheless, the $\Delta UT1$ repeatabilities of all scheduling methods have the same magnitude and those of the scheduling methods using the impact factors exhibit lower values than those of the IVS in all cases except of INT3, where just the IF schedules are superior than those of the IVS. In conclusion of the investigations concerning the existing INT sessions, it can be stated that the IF scheduling method is evidently the best one to use and shows the greatest promise to improve the determination of the Earth's rotation.

With regard to the next step, including twin radio telescope in Intensive sessions, the prior investigations can be summarized that the $\mathrm{IF}_{\Delta UT1}$ scheduling method seems to be inappropriate for multi station sessions. Although, the IF scheduling method seems to be more robust towards the simulated influences, this advantage is not transferred to the quality of the observing schedules. Furthermore, also all other criteria that had been investigated in this section show superior results for the IF schedules. Consequently, the IF scheduling method will be applied to Intensive sessions including twin radio telescopes, as it is expected to be the most appropriate strategy.

6. Intensive schedules including twin radio telescopes

This chapter discusses the handling of twin radio telescopes replacing the single radio telescopes of Intensive sessions. Different twin telescope scenarios will be examined, as well as special twin telescope features that have to be considered.

6.1 Twin telescope scenarios

Imagine the 20 m radio telescope in Wettzell would be replaced by the new TTW for performing the Intensives. In case of current single baseline Intensives, like INT1 and INT2, the only gain of the TTW would be a second baseline observing exactly the same as the single baseline (see Fig. 6.1). Solely in case of INT3 sessions, this scenario enables the possibility of forming two baselines observing two different radio sources simultaneously. However, if one radio telescope of the TTW would observe together with the radio telescope in Ny-Ålesund, a north-south oriented baseline would be built (see Fig. 6.2). Since such baselines are not sensitive to $\Delta UT1$, the target parameter of Intensives, this constellation does not make sense.

The case is very different if there would be additional twin radio telescopes in Kokee Park as well as in Tsukuba, the other two important sites of Intensive sessions. For INT1 or INT2 sessions, two almost identical baselines but with the possibility of observing different sources at an instant of time would be formed (see Fig. 6.3 middle and right). These scenarios would increase the number of realizable observations within one hour substantially. This also applies to INT3 sessions with the particularity of enabling more combinations observations in a five station network (a twin telescope in Wettzell, a twin telescope in Tsukuba and a single telescope in Ny-Ålesund). For this reason, the following investigations were done assuming twin radio telescopes at the three most important sites of Intensive sessions.

A conceivable alternative for the scenario depicted in Fig. 6.3 would be a combination of INT1 and INT2 setups including the TTW. This offers also the possibility to form two independent pairs of radio telescopes, which observe two different radio sources simultaneously (Fig. 6.4). A further advantage of this scenario is its immediate practicability, because just the existing single radio telescopes in Tsukuba and Kokee Park and the already constructed TTW in Wettzell is needed. Therefore, this scenario will also be examined in the following sections and will be denoted by INT4.

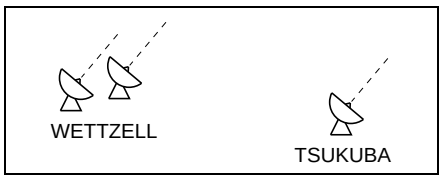

Figure 6.1: Observing scenario using the TTW within the INT2 setup (INT1 analogous).

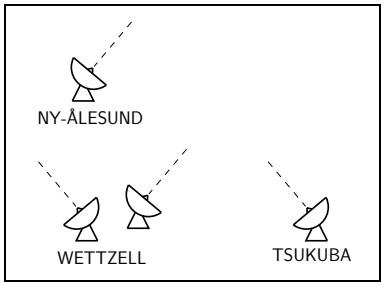

Figure 6.2: Possible observing scenario using the TTW within the INT3 setup.

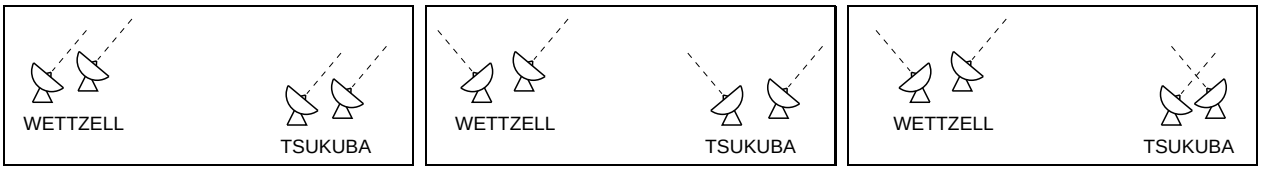

Figure 6.3: Possible observing scenarios using two twin telescopes within the INT2 setup (INT1 analogous).

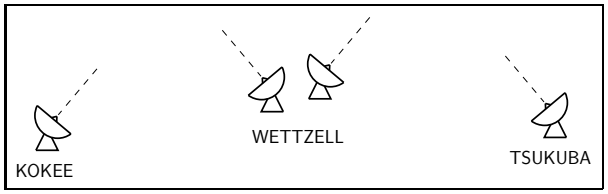

Figure 6.4: INT4 observing scenario composing INT1 and INT2 setups by using the TTW.

6.2 Adjustment of the scheduling program

Since the scheduling method using the impact factors of the observations can already handle multiple station sessions with the possibility of building sub-nets, only the parametrization of the twin telescopes have to be adjusted. Because of the spatial proximity of twin radio telescopes just one atmospheric parameter should be estimated from both single telescope observations. That means, that also simultaneous observations in different directions of the two telescopes of a twin contribute to the same atmospheric parameter. In practical terms, this means that the corresponding columns of the Jacobian matrix will be added together, reducing the set of unknown parameters by one. Taking into account the fact that twin radio telescopes should share one frequency normal and an appropriate calibration of the time and frequency distribution system will be developed, also the clock parameters can be reduced. Here again the corresponding columns of the Jacobian matrix will be added together, but since a polynomial clock function including three parameters will be estimated per station, the set of unknown parameters would be reduced by three per twin telescope. This parameter reduction leads to greater redundancies compared to single telescope Intensive sessions.

What has not yet been mentioned at all is the correlation between VLBI observations. It is a fact, that VLBI observations are correlated due to systematic errors between groups of observations and the functional model (Tesmer 2004). One of the greatest effect is the tropospheric influence and its mismodeling. Especially observations which have been performed by neighboring baselines in a short interval and under similar topocentric directions, thus, observation with similar paths through the troposphere are affected by correlations. Nevertheless, any kind of correlation between VLBI observations is neglected in current VLBI analyses although several authors have done investigations in this field (e.g. Schuh and Wilkin 1989, Schuh and Tesmer 2001, Tesmer 2003, Tesmer 2004, Tesmer and Kutterer 2005, Gipson 2006, Gipson 2007, Gipson et al. 2008), the modeling of correlations is still insufficient or affect the results only slightly. Since particularly twin telescopes fulfill the criteria mentioned before, their observations are certainly high correlated. Presently, investigations in this field are taking place, but unfortunately the model is not yet so sophisticated that it could be used in this thesis. Therefore, in the following investigations about twin radio telescopes correlations between their observations will be neglected.

6.3 Adjustment of the simulation

Also the MCS, simulating the reduced observing vector, has to be adjusted for using twin radio telescopes. Since a twin telescope uses a common frequency standard just one clock simulation has to be performed which applies for both radio telescopes of the twin. Therefore, all observing epochs of both telescopes will

be combined for a consistent clock simulation and afterwards the simulated clock behavior will be assigned to the respective telescope.

The situation is a bit more complicated concerning the simulation of zenith wet delays for the twin telescopes. The applied procedure is similar to that of the clock simulation with the peculiarity that both telescopes might observe in two different directions at the same time. In this case, both observations have to contribute to the computation of the respective zenith wet delay.

6.4 Twin telescope observing plans

In contrast to the investigated sessions in the previous chapter, INT1 sessions will be scheduled including twin telescopes just for the standard set of stations, meaning without the occasionally participating additional radio telescope in Svetloe. Due to the findings of the previous chapter, all twin telescope schedules will be made using the IF scheduling method. For that reason the IF schedules with single radio telescopes are taken as reference for comparisons with twin radio telescope schedules. In the following the schedules of the single telescope sessions will be labeled 'single' and will be displayed in figures with the same color as before and the new schedules including two twin telescopes will be labeled 'twins' and will be displayed in red. Since INT4 is a special case, those schedules will be specially treated.

To get a better idea of the dimension of occurring numbers of scans, observations and observed sources, the respective average values are listed in Tab. 6.1. The mean number of scans is raised by a factor of about 1.7 for the typical three Intensive types. Detailed examination of the created schedules shows that mostly two couples of telescopes form two large east-west baselines which observe two sources simultaneously in case of INT1 and INT2 sessions. The couples always change their respective partner, so that no risk of a rank deficiency occurs. The scheduling method is designed to avoid coupling the two telescope of one twin, since those very short baselines do not contribute extra geometrical information, except if occasionally all radio telescopes point at one source together. Concerning INT3 sessions, it is very interesting that very often a triple of radio telescopes, including one of the twins in Wettzell, one of the twins in Tsukuba and the single telescope in Ny-Ålesund, is built while the remaining telescopes build a large east-west baseline. For this reason, a single scan with Ny-Ålesund and Wettzell, is also avoided by the scheduling method itself. This demonstrates the efficiency of the developed scheduling method. As a consequence, the mean numbers of observations are also raised by using two twin telescopes. For INT1 and INT2 sessions the number of observations are increased on average by a factor of about 2.5 and a factor of 1.8 for INT3 sessions (cf. Tab. 5.1, 5.2 and 5.3 on pages 53, 54 and 55).

As INT4 is a combination of INT1 and INT2 setups, the observing plans of the INT4 sessions have been scheduled for both time windows with the only difference being the different UT time frames of INT1 and INT2. The resulting observation numbers are depicted in Fig. 6.5 with their computed moving averages represented by the smoothed dashed and dotted lines. The moving averages have been computed every 7 days using a window length of 90 days. Apparently, the periodic fluctuations of both smoothed lines show a phase-shifted behavior, indicating that the best source distribution occurs at different time frames. For the following investigations, both cases will be taken together and will be regarded as one time series, as it was already done for calculating the average numbers of scans, observations and observed sources in Tab. 6.1. Surprisingly, the observation number exceed those of INT1 and INT2 sessions including twin telescopes

	INT1	INT2	INT3	INT4
scans	64.1	71.0	55.4	44.4
obs.	94.6	101.2	166.7	114.7
sou.	13.0	22.8	20.2	19.3

Table 6.1: Average numbers of scans, observations and used sources of Intensives scheduled with twin radio telescopes.

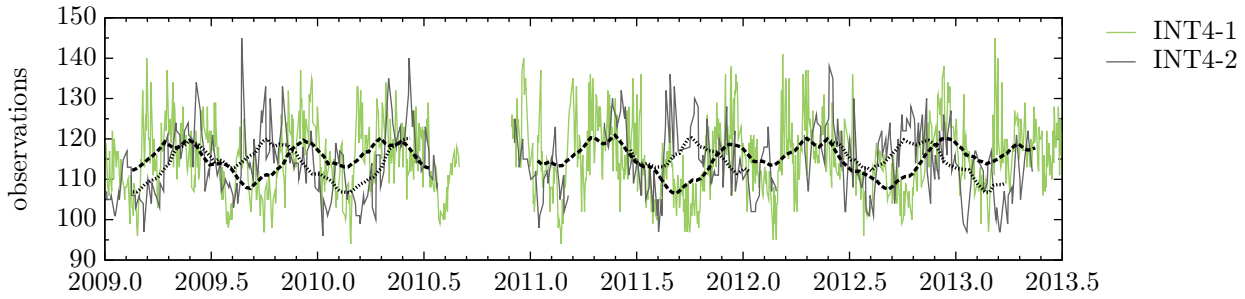

Figure 6.5: Observation numbers of INT4 sessions with the respective moving averages scheduled at 18.30 – 19.30 UT (INT4-1, dashed line) and 07.30 – 08.30 UT (INT4-2, dotted line).

significantly although all types include a set of four radio antennas. This is due to the fact that in case of INT4 sessions, all telescopes observe the same radio source together more often than in case of INT1 and INT2, what is consistent with a smaller number of scans compared to INT1 and INT2. Nonetheless, also pairs of radio telescopes are built between the TTW and the single telescopes in Kokee Park and Tsukuba which observe two sources simultaneously. The number of observed sources is comparable to INT2 sessions, thus exceeding those of INT1 setups.

Concerning the $\Delta UT1$ formal errors, an improvement by using twin telescopes due to the larger numbers of observations is expected. The mean $\Delta UT1$ formal errors are shown in Tab. 6.2a for the Intensive sessions with twin telescopes compared to the IF single telescope values of Sec. 5.5 and, in fact, the mean $\Delta UT1$ formal errors are improved by approximately a factor of $\sqrt{2}$, except for INT2 sessions, where the improvement is just a little less. However, the $\Delta UT1$ repeatabilities that are gained from the MCS and shown in Fig. 6.6 – 6.8 are much more improved by using twin telescopes in all cases. The mean values in Tab. 6.2b reveal a reduction by about 53 % for INT1, 59 % for INT2 and even 49 % for INT3 sessions respectively, what is more than expected and, thus, a great success. Furthermore, the scatter of the depicted time series of $\Delta UT1$ repeatabilities is reduced by a factor about 1.8 for INT1 and 1.7 for the other cases.

Further positive results are accomplished by the INT4 sessions. Here, the $\Delta UT1$ formal errors have the same magnitude on average as the standard Intensives including twin radio telescopes (Tab. 6.2a). Admittedly, the mean $\Delta UT1$ repeatability of INT4 sessions is not as good as those of INT1 and INT2 sessions with twin telescopes, but almost as good as the mean $\Delta UT1$ repeatability of INT3 sessions including twins. Further it reveals an even lower scatter than the other Intensive types including twin telescopes. However, the improvement compared to sessions with single telescopes amounts to nearly 1.8 as well.

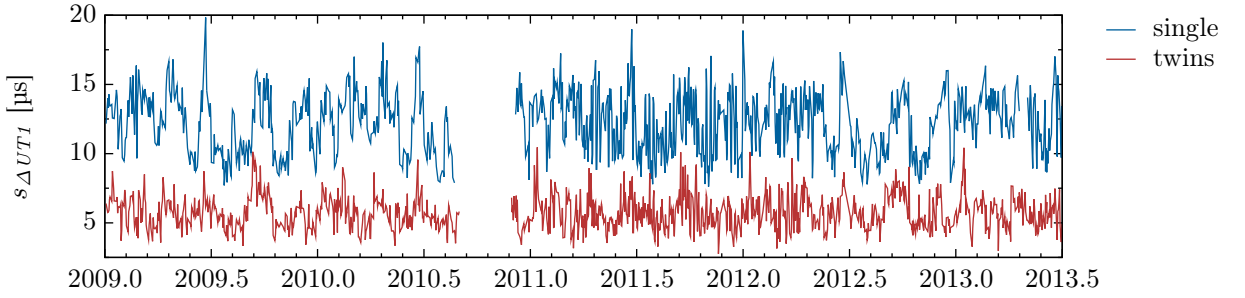

Figure 6.6: Comparison of $\Delta UT1$ repeatabilities with single and twin telescopes for INT1 sessions.

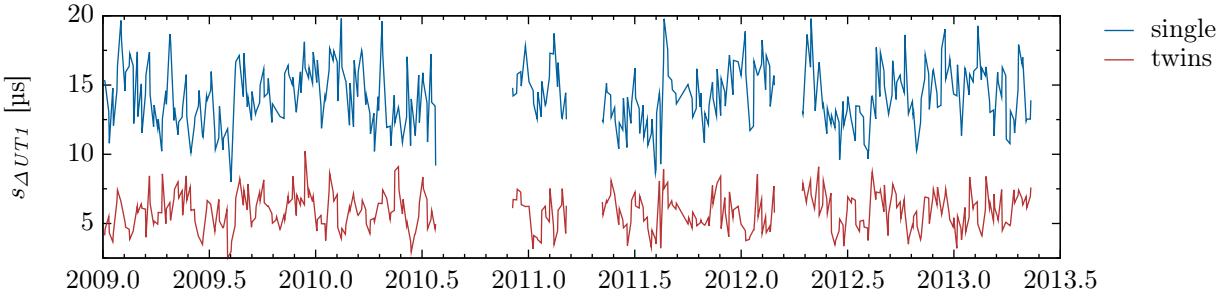

Figure 6.7: Comparison of $\Delta UT1$ repeatabilities with single and twin telescopes for INT2 sessions.

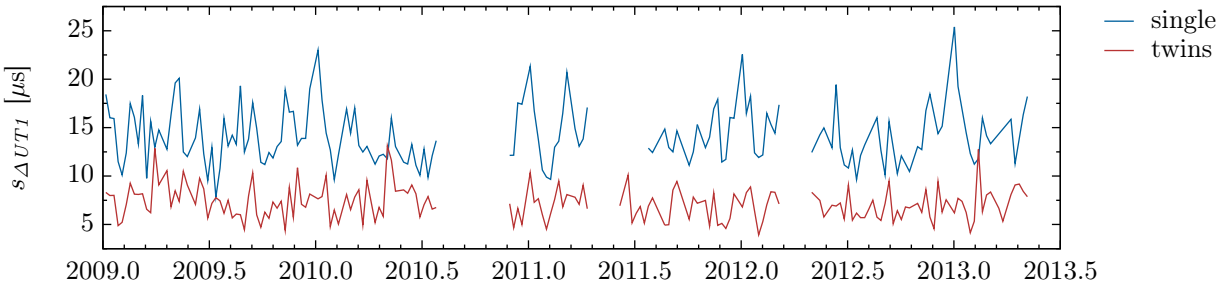

Figure 6.8: Comparison of $\Delta UT1$ repeatabilities with single and twin telescopes for INT3 sessions.

	INT1	INT2	INT3	INT4
single	6.09	5.95	6.65	
twins	4.44	4.64	4.64	4.68

(a) $\Delta UT1$ formal errors.

	INT1	INT2	INT3	INT4
single	12.23	14.17	14.10	
twins	5.71	5.86	7.20	7.59

(b) $\Delta UT1$ repeatability.

Table 6.2: Mean $\Delta UT1$ formal errors (a) and mean $\Delta UT1$ repeatability (b) in µs of Intensive sessions scheduled with twin radio telescopes compared to the IF schedules with single radio telescopes.

6.5 Conclusions of Intensives including twin telescopes

The investigations have shown that a powerful method for scheduling Intensive sessions with twin radio telescopes has been developed. Special features of twin telescopes resulting from theirs spatial proximity, like using the same frequency normal and sample the same atmosphere, reduce the parameters that have to be estimated. Thus, the total redundancy will be raised by more than twice as many observations than for single telescopes (INT1 and INT2) and by an unchanged set of unknown parameters. The developed scheduling program exploits the advantages of twin telescopes as it uses the possibility to build similar or rather equal sub-nets which observe different sources at the same time and, thus, extend the observing geometry within the limited observing duration of one hour. Otherwise, the scheduling method avoids building sub-nets that form single north-south oriented baselines which would bring no benefit for the determination of the target parameter of Intensive sessions, the Earth rotation angle. Beside a reduction of the $\Delta UT1$ formal errors, the greatest benefit of twin radio telescopes can be seen by the $\Delta UT1$ repeatabilities that exhibit improvements by 50 % and more.

7. Assessment of VLBI scheduling with impact factors and its alternatives

It has been proven that the scheduling method developed in this work is an appropriate method for generating regular VLBI Intensive observing plans as well as Intensive observing plans including twin radio telescopes. As this scheduling method is designed for optimizing the observing geometry of VLBI sessions with regard to the parameters to be estimated, a conceivable alternative would be to find out important observing geometries beforehand and to try to cover these geometries with currently available radio sources. However, the examination in Sec. 3.3 has shown that finding important observing geometries for Intensives is not a trivial problem. The necessity of estimating auxiliary parameters that might be correlated with the target parameters complicates the detection of required observations and their repetition rate. One of the advantages of scheduling with impact factors is that actually possible observations with large influence will be chosen automatically.

A direct comparison with the uniform sky scheduling method in Sec. 5 revealed that the developed scheduling method mostly performs better with regard to the examined criteria. This is especially true for the scheduling method using the impact factors which reached a better sky coverage in three out of four examined cases. For using the uniform sky method, a predefined list of radio sources that have to be take into account for the observing session has to be preselected, while the scheduling method using the impact factors takes all available sources into consideration at any time.

A comparison with other scheduling methods will just be made theoretically. Considering the scheduling method by Steufmehl (1994) the main advantage of the scheduling method developed in this thesis are the lower computational costs. As the covariance matrix of the estimated parameters has to be minimized in the scheduling procedure of Steufmehl (1994), a full matrix including information about previous observations as well as potential new observations has to be inverted for each possible observing geometry in each step of the scheduling procedure. Additionally, the objective function of the process is expressed as a gain function that includes the covariances of the estimated parameters of three different steps of the scheduling process, the original condition, the prior step and the present step. This method causes considerable computational costs. On the contrary, using the recursive least squares adjustment for the scheduling method using the impact factors, the covariance matrix of the parameters has to be computed only once per scheduling step with the prior observations. The impact factors for each possible new observation can then be computed with minor computing time. Nonetheless, since the number of possible observing combinations increases exponentially with a rising number of participating radio telescopes the developed scheduling method is accompanied by proportional computational costs while for the Steufmehl method the computational costs increase by the square of the possible combinations.

All of the scheduling methods mentioned above have in common that the observations are chosen sequentially. That means that none of the algorithms selects the observing sequence out of the entirety of all possibilities but rather on the basis of the prior observations. Certainly it would be desirable to define a 'global' optimum so that all observations will be selected collectively instead. A theoretical possibility for realizing such a method would require a discretization of feasible observations in time. Depending on the increment of the discretization an enormous number of combinations of observations have to be compared to each other, the smaller the increment the more possibilities exist. Selecting a whole set of observations this way leads to the problem that the slewing times of the radio telescopes remain uncared for. Ensuring that all observations are viable yet, the increment of the discretization have to be great enough that a maximal slewing time can take place between each observation. However, this would cost much unexploited time since the maximal slewing time is needed extremely seldom. Since VLBI Intensives last just one hour, observing time is very precious and should not be misspent. Taking this into account, a sequential scheduling method appears to be unavoidable for Intensive sessions. The counterargument for the case of 24h-VLBI sessions against a collective selection of the observations is the gigantic computational costs resulting from the numerous combination possibilities.

8. Conclusions and Outlook

This thesis is concerned with scheduling methods for VLBI Intensive sessions. Besides the development of new scheduling strategies, the inclusion of future-oriented twin radio telescopes plays a dominant role.

The first part of this work deals with current VLBI scheduling methods and the assessment of Intensive observing plans. Further investigations have been done using singular value decomposition of the design matrix and cluster analysis on the basis of the observations' impact co-factors with the aim of finding out geometrical characteristics of observations that are important for the parameter determination. The characteristics found by means of fictitious observing plans cannot be confirmed by real Intensive sessions. The unclear grouping of geometrically similar observations complicates the interpretation of the results. Furthermore, the average impact factors of the clusters seemed to be insufficient for reliably detecting really important observations for certain parameters. However, the potential of the observations' impact factors for improving VLBI observing plans has been perceived.

Therefore, a scheduling method which is based on the impact factors of the observations has been developed. The method profits from the feature of impact factors that they are related to the entire design or the entire geometry of an VLBI session with respect to the parameters to be estimated. This is a great advantage compared to partial derivatives of the functional model which only provide the sensitivity of single observations on single parameters without taking into account other observations. As observations with the greatest impact factors will be chosen in each step of the scheduling process, the respective observations of the greatest influence with respect to all previous observations will be added to the design. According to this concept, an automatic scheduling program was developed for this thesis which optimizes the geometry of the experiment for the parameters to be estimated and, thus, is independent of subjective criteria. In order to direct the schedule in one or the other direction, some extra options have been integrated in the program.

Two theoretically similar but essentially different scheduling methods that are based on the impact factors of the observations has been examined thoroughly in Sec. 5. The one method is based on the general impact factors of all estimated parameters in the design and the other method is based on the impact factors for $\Delta UT1$ only, which can be separated by the method of parameter reduction. Concerning many criteria, which have been previously detected to be important for a reliable determination of the target parameter $\Delta UT1$, the results of both scheduling methods developed here outclass those of the standard scheduling method of the IVS. For example the $\Delta UT1$ formal errors, that reflect the geometry of the design with respect to the $\Delta UT1$ determination, have been improved by more than 50 % for a standard INT1 setup by both scheduling methods. In case of INT2 sessions, this improvement on average amounts to between 33 % and 38 % and at least between 7 % and 15 % for the INT3 setup. These results were compared to those of a Monte Carlo simulation with the three greatest stochastic influence factors of VLBI observations – slant wet delays, station clock behavior and white noise – taken into account. Unfortunately, the excellent results could be confirmed only partially. The $\Delta UT1$ repeatabilities, that serve as assessment criteria, reveal a great improvement for INT1 sessions. In particular, the scheduling method using the general impact factors improves the $\Delta UT1$ repeatability by about 20 % and the scheduling method using the $\Delta UT1$ impact factors improves the $\Delta UT1$ repeatability by impressive 30 %. The case is very different for the other Intensive setups, as both scheduling methods using impact factors neither increase nor decrease the $\Delta UT1$ repeatability for INT2 sessions. The same applies to INT3 sessions with respect to the scheduling method using the general impact factors, while the method based on the $\Delta UT1$ impact factors shows a worsening of the $\Delta UT1$ repeatability by about 30 %. Among others, this indicates that the scheduling method using the $\Delta UT1$ impact factors is less suitable to handle multi station setups, as standard INT3 sessions, contrary to the other Intensives, consist of a three station network. Excluding this one case, the developed scheduling method is on a par with the current IVS scheduling method and shows promise for further improvements. At present, the scheduling method is tested on real INT3 observations.

The principal purpose of developing a new scheduling method has been the usage of the new twin radio telescopes for Intensive sessions. One aim of this thesis has been to find out the advantage of such twin telescope setups for daily $\Delta UT1$ observations and how to create observing plans with an optimal utilization

of special twin telescope features. For this reason, the scheduling method contains the possibility to schedule multi station setups from the very beginning. The spatial neighborhood of twin radio telescopes has a positive effect on the parametrization of such a design with respect to the number of parameters to be estimated. The assumption of further twin radio telescopes at important VLBI Intensive sites offers the opportunity to replace the current single telescopes by twin radio telescopes. As the scheduling method using the general impact factors has proven itself for all Intensive types and, more importantly also for multi station sessions, this method has been used to create observing plans for twin telescope setups. The method produces observing plans for twin telescopes in such a way, that pairs of radio telescopes will be built which observe two different radio sources simultaneously. In fact, this has been considered to make the most sense before. In this way, the very short session duration for VLBI experiments of only one hour will best be populated with observations. The MCS reveals enormous improvements of the $\Delta UT1$ repeatability compared to standard single telescope observing sessions. In particular, for INT2 this improvement amounts to about outstanding 60 % and 50 % for INT1 and INT3 sessions, although at the latter, twin telescopes have just been assumed for two of the three participating stations. Even an alternative setup, including just one twin radio telescope at Wettzell, connecting both single telescopes in Tsukuba and Kokee Park and, thus, being a mixture of INT1 and INT2 setups, improves the $\Delta UT1$ repeatability by about 40 % compared to both standard INT1 and INT2 sessions. This is a great success, as this setup can already become operational in the near future. Hence, it can be concluded that twin radio telescopes help to overcome the problem of the lesser precision of Intensives which is 2 – 3 times worse compared to regular 24h-VLBI measurements with networks of 5 – 10 radio telescopes.

The results achieved with the new scheduling method appear very promising. Because of a foresightful programming, the scheduling program is also useful to schedule VLBI sessions for other applications. Owing to the variable minor options, appropriate observing plans can be created for many different telescope scenarios. For example, observing plans including observations to a satellite that transmits a quasar-like signal have been generated successively for investigation purposes. It is conceivable to extend the minor options of the scheduling procedure in many ways. Thus, more flexible observing plans, adapted to special requirements, could be created in the future.

References

Alef, W. (1989) Scheduling, Correlating, and Postprocessing of VLBI Observations. Felli, M. and R. E. Spencer (Eds.), *Very Long Baseline Interferometry*, Volume 283 of the series NATO ASI Series, Springer Netherlands, 97 – 139.

Altamimi, Z., X. Collilieux, J. Legrand, B. Garayt and C. Boucher (2007) ITRF2005: A new release of the International Terrestrial Reference Frame based on time series of station positions and Earth Orientation Parameters. *Journal of Geophysical Research*, 112:B09401, doi:10.1029/2007JB004949.

Altamimi, Z., X. Collilieux and L. Métivier (2011) ITRF2008: an improved solution of the International Terrestrial Reference Frame. *Journal of Geodesy*, 85(8):457 – 473, doi:10.1007/s00190-011-0444-4.

Aoki, S., H. Kinoshita, B. Guinot, G. H. Kaplan, D. D. McCarthy and P. K. Seidelmann (1982) The new definition of universal time. *Astronomy & Astrophysics*, 105(2):359 – 361.

Arias, E. F., P. Charlot, M. Feissel and J.-F. Lestrade (1995) The extragalactic reference system of the International Earth Rotation Service, ICRS. *Astronomy and Astrophysics*, 303:604 – 608.

Artz, T., L. Bernhard, A. Nothnagel, P. Steigenberger and S. Tesmer (2012) Methodology for the combination of sub-daily Earth rotation from GPS and VLBI observations. *Journal of Geodesy*, 86(3):221 – 239, doi:10.1007/s00190-011-0512-9.

Baver, K. (2013) , Mark-5 VLBI Analysis Software Calc/Solve. Web document `http://gemini.gsfc.nasa.gov/solve/`, December 2013. (last update of website: 2012/10/23).

Baver, K. and J. Gipson (2010) Strategies for Improving the IVS-INT01 UT1 Estimates. In: Behrend, D. and K.D. Baver (Eds.), *IVS 2010 General Meeting Proceedings*. NASA/CP, 256 – 260.

Baver, K. and J. Gipson (2013) Refining the Uniform Sky Strategy for IVS-INT01 Scheduling. In: Zubko, N. and M Poutanen (Eds.), *Proceedings of the 21th European VLBI for Geodesy and Astrometry Working Meeting,* 29 – 30 March 2013, Espoo. Reports of the Finnish Geodetic Institute, ISBN: 978-951-711-296-3, 205 – 209. available electronically at `http://evga.fgi.fi/sites/default/files/u3/Proceedings_EVGA2013.pdf`.

Baver, K., D. MacMillan, L. Petrov and D. Gordon (2004) Analysis of the VLBI Intensive Sessions. In: Vandenberg, Nancy R. and Karen D. Baver (Eds.), *IVS General Meeting Proceedings,* 9 – 11 February 2004, Ottawa, Canada. NASA/CP-2004-212255, 394 – 398. available electronically at `http://ivscc.gsfc.nasa.gov/publications/gm2004/baver.pdf`.

Baver, K., J. Gipson, M. S. Carter and K. Kingham (2012) Assessment of the First Use of the Uniform Sky Strategy in Scheduling the Operational IVS-INT01 Sessions. In: Behrend, D. and K.D. Baver (Eds.), *IVS 2012 General Meeting Proceedings*. NASA/CP, 251 – 255.

Böhm, J. (2004) *Troposphärische Laufzeitverzögerungen in der VLBI*. Dissertation, Technische Universität Wien. Geowissenschaftliche Mitteilungen, Heft Nr. 68, ISSN 1811-8380.

Böhm, J. and H. Schuh (2004) Vienna mapping functions in VLBI analyses. *Geophysical Research Letters*, 31(1), doi:10.1029/2003GL018984.

Böhm, J., A. Niell, P. Tregoning and H. Schuh (2006a) Global Mapping Function (GMF): A new empirical mapping function based on numerical weather model data. *Geophysical Research Letters*, 33(7), doi:10.1029/2005GL025546.

Böhm, J., B. Werl and H. Schuh (2006b) Troposphere mapping functions for GPS and very long baseline interferometry from European Centre for Medium-Range Weather Forecasts operational analysis data. *Journal of Geophysical Research: Solid Earth*, 111(B2), doi:10.1029/2005JB003629.

Böhm, J., S. Böhm, T. Nilsson, A. Pany, L. Plank, H. Spicakova, K. Teke and H. Schuh (2012) The new Vienna VLBI Software VieVS. In: Kenyon, S., M. C. Pacino and U. Marti (Eds.), *Proceedings of IAG Scientific Assembly 2009*, Volume 136 of the series International Association of Geodesy Symposia Series, 1007 – 1011.

Böhm, Johannes, T. Hobiger, R. Ichikawa, T. Kondo, Y. Koyama, A. Pany, H. Schuh and K. Teke (2010) Asymmetric tropospheric delays from numerical weather models for UT1 determination from VLBI Intensive sessions on the baseline Wettzell–Tsukuba. *Journal Of Geodesy*, 84(5):319 – 325, doi:10.1007/s00190-010-0370-x.

Bureau International des Poids et Mesures (2006) *The International System of Units (SI)*. Organisation Intergouvernementale de la Convention du Mètre, 8. Edition.

Campbell, J. (1987) Very long baseline interferometry. Turner, S. (Eds.), *Applied Geodesy*, Volume 12 of the series Lecture Notes in Earth Sciences, Springer Berlin / Heidelberg, 67 – 87.

Campbell, J. and B. Witte (1978) Grundlage und geodätische Anwendung der Very Long Baseline Interferometry (VLBI). *Zeitschrift für Vermessungswesen*, 103:10 – 20.

Capitaine, N., P. T. Wallace and D. D. McCarthy (2003) Expressions to implement the IAU 2000 definition of UT1. *Astronomy & Astrophysics*, 406(3):1135 – 1149, doi:10.1051/0004-6361:20030817.

Chao, C. C. (1972) A Model for Tropospheric Calibration from Daily Surface and Radiosonde Balloon Measurement. Technical Memorandum, Propulsion Laboratory, Pasadena, California.

Charlot, P. (1990) Radio-source structure in astrometric and geodetic very long baseline interferometry. *Astronomical Journal*, 99(4):1309 – 1326, doi:10.1086/115419.

Davis, J. L., T. A. Herring, I. I. Shapiro, A. E. E. Rogers and G. Elgered (1985) Geodesy by radio interferometry - Effects of atmospheric modeling errors on estimates of baseline length. *Radio Science*, 20(6):1593 – 1607, doi:10.1029/RS020i006p01593.

de Berg, M., O. Cheong, M. van Kreveld and M. Overmars (2008) *Computational Geometry: Algorithms and Applications*. Springer, third. Edition.

Delaunay, B. (1934) Sur la sphère vide. A la mémoire de Georges Voronoï. *Bulletin de l'Académie des Sciences de l'URSS. Classe des sciences mathématiques et naturelles*, 6:793 – 800.

Deller, A. T., S. J. Tingay, M. Bailes and C. West (2007) DiFX: A software correlator for very long baseline interferometry using multi-processor computing environments. *Publications of the Astronomical Society of the Pacific*, 119(853):318 – 336, doi:10.1086/513572.

Dodge, Y. and A. S. Hadi (1999) Simple graphs and bounds for the elements of the hat matrix. *Journal of Applied Statistics*, 26(7):817 – 823, doi:10.1080/02664769922052.

Du, D. and F. Hwang (1992) *Computing in Euclidean Geometry*, Volume 1 of the series Lecture notes series on computing. World Scientific.

Duda, R. O., P. E. Hart and D. G. Stork (2000) *Pattern Classification*. John Wiley & Sons Inc., New York, 2. Edition. ISBN: 978-0-471-05669-0.

Engelhardt, G. and V. Thorandt (2006) First Steps to Investigate Long-Term Stability of Radio Sources in VLBI Analysis. In: D., Behrend and K. Baver (Eds.), *IVS 2006 General Meeting Proceedings,* 9 – 11 January 2006, Concepción. NASA/CP-2006-214140, Greenbelt MD, 281 – 285. (available electronically at `ftp://ivscc.gsfc.nasa.gov/pub/general-meeting/2006/pdf/engelhardt.pdf`).

Feissel-Vernier, M. (2003) Selecting stable extragalactic compact radio sources from the permanent astro-geodetic VLBI program. *Astronomy & Astrophysics*, 403(1):105 – 110, doi:10.1051/0004-6361:20030348.

Fischer, D., A. Nothnagel, R. Kilger, W. Schlüter, S. Kurihara and K. Takashima (2003) The K4 Intensive Project 2002 for UT1 Determination. In: Schwegmann, W. and Thorandt V. (Eds.), *Proceedings of the 16th Working Meeting on European VLBI for Geodesy and Astrometry,* 9 – 10 May 2003, Leipzig. Bundesamt für Kartographie und Geodäsie, Frankfurt/Leipzig, 165 – 170. available electronically at `http://www.evga.org/files/2003EVGA-proc_Leipzig.pdf`.

Förstner, W. (1987) Reliability analysis of parameter estimation in linear models with applications to mensuration problems in computer vision. *Computer Vision, Graphics, and Image Processing*, 40 (3):273 – 310.

Giordano, V., S. Crop, P. Y Bourgeois, Y. Kersale, E. Rubiola, M. Mrad, C. Langham, M. Oxborrow and W. Schafer (2011) Cryogenic sapphire microwave oscillators for space, metrology and scientific applications. In: *General Assembly and Scientific Symposium, 2011 XXXth URSI*, 1 – 4.

Gipson, J. (2012) *Sked. VLBI Scheduling Software*. NASA Goddard Spaceflight Center, May 2012. available electronically at `http://lupus.gsfc.nasa.gov/files_user_manuals/sked/sked.pdf`.

Gipson, J. M. (2006) Correlation Due to Station Dependent Noise in VLBI. In: Behrend, D. and K. Baver (Eds.), *IVS 2006 General Meeting Proceedings,* 9 – 11 January 2006, Concepción. NASA/CP-2006-214140, Greenbelt MD, 286 – 290. (available electronically at `ftp://ivscc.gsfc.nasa.gov/pub/general-meeting/2006/pdf/gipson.pdf`).

Gipson, J. M. (2007) Incorporating Correlated Station Dependent Noise Improves VLBI Estimates. In: Böhm, J., A. Pany and H. Schuh (Eds.), *Proceedings of the 18th Workshop Meeting on European VLBI for Geodesy and Astrometry*, Volume 79. TU Wien, Geowissenschaftliche Mitteilungen, Schriftenreihe Vermessung und Geoinformation der TU Wien, 129 – 134.

Gipson, J. M., D. MacMillan and L. Petrov (2008) Improved Estimation in VLBI through Better Modeling and Analysis. In: Finkelstein, A. and D. Behrend (Eds.), *The 5th IVS General Meeting Proceedings*. Nauka, St. Petersburg, 157 – 162.

Golub, G. and W. Kahan (1965) Calculating the singular values and pseudo-inverse of a matrix. *SIAM Journal on Numerical Analysis*, 2(2):205 – 224.

Gray, J. B. and R. F. Ling (1984) K-Clustering as a detection tool for influential subsets in regression. *Technometrics*, 26(4):305 – 318.

Gross, R., G. Beutler and H.-P. Plag (2009) Integrated scientific and societal user requirements and functional specifications for the GGOS. Plag, H.-P. and M. Pearlman (Eds.), *The Global Geodetic Observing System: Meeting the Requirements of a Global Society on a Changing Planet in 2020*, Springer, Dordrecht Heidelberg London New York, 209 – 224. ISBN 978-3-642-02686-7, doi: 10.1007/978-3-642-02687-4_7.

Hase, H. (1999) *Theorie und Praxis globaler Bezugssysteme*. Dissertation, Technische Universität München. Mitteilungen des Bundesamtes für Kartographie und Geodäsie, Frankfurt am Main, Vol. 13, ISBN 3-88648-097-6.

Hase, H., R. Dassing, G. Kronschnabl, W. Schlüter, W. Schwarz, R. Kilger, P. Lauber, A. Neidhardt, K. Pausch and W. Göldi (2008) Twin Telescope Wettzell – a VLBI2010 Radio Telescope Project. In: Finkelstein, A. and D. Behrend (Eds.), *Proceedings of the Fifth IVS General Meeting "Measuring the Future",* 3 – 6 March 2008, St. Petersburg. Nauka, 109 – 113. (available electronically at `ftp://ivscc.gsfc.nasa.gov/pub/general-meeting/2008/pdf/hase.pdf`).

Hase, H., R. Dassing, G. Kronschnabl, T. Klügel, C. Plötz, A. Neidhardt, P. Lauber and R. Kilger (2009) Status of the Twin Telescope Wettzell Project. In: Bourda, G., P. Charlot and A. Collioud (Eds.), *Proceedings of the 19th European VLBI for Geodesy and Astrometry Working Meeting, 24-25 March 2009, Bordeaux, France*. Université Bordeaux 1 - CNRS, 127 – 132.

Herring, T. A. (1992) Modelling atmospheric delays in the analysis of space geodetic data. In: de Munck, J. C. and T. A. T. Spoelstra (Eds.), *Proceedings of the Symposium on Refraction of Transatmospheric Signals in Geodesy,* 19 – 22 May 1992, The Hague, Netherlands, number 36 in Publications on Geodesy, N.S. Netherlands Geodetic Commission, 157 – 164.

Hjelle, Ø. and M. Dæhlen (2006) *Triangulations and Applications.* Mathematics and visualization. Springer.

Hoaglin, D. C. and R. E. Welsch (1978) The Hat Matrix in Regression and ANOVA. *The American Statistician*, 32(1):pp. 17–22.

Kalman, D. (1996) A Singularly Valuable Decomposition: The SVD of a Matrix. *The College Mathematics Journal*, 27(1):2 – 23, doi:10.2307/2687269.

Kasdin, N. and T. Walter (1992) Discrete simulation of power law noise. In: *Proceedings of the 1992 IEEE Frequency Control Symposium,* 27 – 29 May 1992, Hershey, 274,- 283.

Kasdin, N. J. (1995) Descrete Simulation of Colored Noise and Stochastic Processes and $1/f^{\alpha}$ Power Law Noise Generation. In: *Proceedings of the IEEE*, Volume 83, 802 – 826.

Koch, K.-R. (1999) *Parameter Estimation and Hypothesis Testing in Linear Models.* Springer, Berlin, Heidelberg, New York. ISBN 3-540-18840-1.

Kolmogorov, A. N. (1941a) Energy dissipation in locally isotropic turbulence. In: *Doklady AN SSSR*, Volume 32, 19 – 21.

Kolmogorov, A. N. (1941b) The Local Structure of Turbulence in Incompressible Viscous Fluid for Very Large Reynolds' Numbers. In: *Dokl. Akad. Nauk SSSR*, Volume 30, 301 – 305.

Lay, D. C. (2003) *Linear algebra and its applications.* Addison-Wesley. ISBN 0-201-70970-8.

Lohmar, F. (1985) Zur Berechnung ionosphärischer Refraktionskorrekturen für VLBI-Beobachtungen aus simultanen Doppelmessungen aus Satelliten. In: *Mitteilungen aus den Geodätischen Instituten der Rheinischen Friedrich-Wilhelms-Universität Bonn*, number 67.

Luzum, B. and A. Nothnagel (2010) Improved UT1 predictions through low-latency VLBI observations. *Journal of Geodesy*, 84(6):399 – 402, doi:10.1007/s00190-010-0372-8.

Ma, C. (1978) *Very Long Baseline Interferometry Applied to Polar Motion, Relativity and Geodesy.* Nasa technical memorandum 79582, Maryland University, Maryland.

Ma, C. and D. S. MacMillan (2000) VLBI observations of Earth orientation. In: Dick, S., D. McCarthy and B. Luzum (Eds.), *Polar motion: historical and scientific problems*, Volume 208 of the series Proc IAU colloquium 178, astronomical society of the pacific conference series, 251 – 259.

Ma, C., J. M. Sauber, T. A. Clark, J. W. Ryan, L. J. Bell, D. Gordon and W. E. Himwich (1990) Measurement of horizontal motions in Alaska using very long baseline interferometry. *Journal of Geophysical Research*, 95(B13):21991–22011, doi:10.1029/JB095iB13p21991.

Ma, C., E. F. Arias, T. M. Eubanks, A. L. Fey, A.-M. Gontier, C. S. Jacobs, O. J. Sovers, B. A. Archinal and P. Charlot (1998) The International Celestial Reference Frame as Realized by Very Long Baseline Interferometry. *The Astronomical Journal*, 116(1):516 – 546, doi:doi:10.1086/300408.

Marini, John W. (1972) Correction of Satellite Tracking Data for an Arbitrary Tropospheric Profile. *Radio Science*, 7(2):223 – 231, doi:10.1029/RS007i002p00223.

Menke, W. (1984) *Geophysical data analysis: discrete inverse theory.* Academic Press.

Metropolis, N. and S. Ulam (1949) The Monte Carlo Method. *Journal of the American Statistical Association*, 44(247):335 – 341.

Michelson, A. A. (1890) On the application of interference methods to astronomical measurements. *Philosophical Magazine and Journal of Science, 5th Series*, 30(182):1 – 21.

Nafisi, V., M. Madzak, J. Böhm, A. A. Ardalan and H. Schuh (2012) Ray-traced tropospheric delays in VLBI analysis. *Radio Science*, 47:1 – 17, doi:10.1029/2011RS004918.

Niell, A., A. Whitney, W. Petrachenko, W. Schlüter, N. Vandenberg, H. Hase, Y. Koyama, C. Ma, H. Schuh and G. Tuccari. (2005) , VLBI2010: Current and Future Requirements for Geodetic VLBI Systems, 2005. IVS WG3 Report, (available electronically at `http://ivscc.gsfc.nasa.gov/about/wg/wg3`).

Niell, A. E. (1996) Global mapping functions for the atmosphere delay at radio wavelengths. *Journal of Geophysical Research*, 101:3227 – 3246, doi:10.1029/95JB03048.

Niemeier, W. (2002) *Ausgleichungsrechnung*. de Gruyter, Berlin New York.

Nilsson, T. and R. Haas (2008) Modeling tropospheric delays with atmospheric turbulence models. In: Finkelstein, A. and D. Behrend (Eds.), *The 5th IVS General Meeting Proceedings*. Nauka, St. Petersburg, 361 – 370.

Nilsson, T. and R. Haas (2010) Impact of atmospheric turbulence on geodetic very long baseline interferometry. *Journal of Geophysical Research*, 115:B03407, doi:10.1029/2009JB006579.

Nilsson, T., L. Gradinarsky and G. Elgered (2005) Correlations between slant wet delays measured by microwave radiometry. *IEEE T. Geoscience and Remote Sensing*, 43(5):1028 – 1035.

Nilsson, T., R. Haas and G. Elgered (2007) Simulations of atmospheric path delays using turbulence models. In: Boehm, J., A. Pany and H. Schuh (Eds.), *Proceedings of the 18th European VLBI for Geodesy and Astrometry Working Meeting,* 12-13 April 2007, Vienna. Geowissenschaftliche Mitteilungen, Heft Nr. 79, Schriftenreihe des Studienrichtung Vermessung und Geoinformation, Technische Universität Wien, ISSN 1811-8380, 175 – 180. (available electronically at `http://mars.hg.tuwien.ac.at/~evga/proceedings/S64_Nilsson.pdf`).

Nilsson, T., J. L. Davis and E. M. Hill (2009) Using ground-based GPS to characterize atmospheric turbulence. *Geophysical Research Letters*, 36, doi:10.1029/2009GL040090.

Nothnagel, A. (2000) *Der Einfluss des Wasserdampfes auf die modernen raumgestützten Messverfahren*. Mitteilungen des Bundesamtes für Kartographie und Geodäsie, Frankfurt am Main. Verlag des Bundesamtes für Kartographie und Geodäsie, Band 16, ISBN 3-88648-100-X.

Nothnagel, A. and J. Campbell (1991) Polar Motion Observed by Daily VLBI Measurements. In: *Proceedings of the AGU Chapman Conference on Geodetic VLBI: Monitoring Global Change, NOAA Technical Report NOS 137 NGS 49*. Washington D.C., 345 – 354.

Petit, G. and B. Luzum (2010) IERS Conventions 2010. IERS Technical Note 36, Verlag des Bundesamtes für Kartographie und Geodäsie, Frankfurt am Main. ISSN: 1019-4568 (available electronically at `http://www.iers.org/IERS/EN/Publications/TechnicalNotes/tn36.html`).

Petrachenko, B., J. Böhm, D. MacMillan, A. Niell, A. Pany, A. Searle and J. Wresnik (2008) VLBI2010 Antenna Slew Rate Study. In: Finkelstein, A. and D. Behrend (Eds.), *Proceedings of the Fifth IVS General Meeting "Measuring the Future"*, 3 – 6 March 2008, St. Petersburg. Nauka, 410 – 415. (available electronically at `ftp://ivscc.gsfc.nasa.gov/pub/general-meeting/2008/pdf/petrachenko.pdf`).

Robertson, D. S., W. E. Carter, J. Campbell and H. Schuh (1985) Daily Earth rotation determinations from IRIS very long baseline interferometry. *Nature*, 316(6027):424 – 427, doi:10.1038/316424a0.

Rogers, A. E. E. (1970) Very Long Baseline Interferometry with Large Effective Bandwidth for Phase-Delay Measurements. *Radio Science*, 5(10):1239 – 1247, doi:10.1029/RS005i010p01239.

Romesburg, H. C. (2004) *Cluster Analysis For Researchers*. Lulu Press, North Carolina.

Rutman, J. (1978) Characterization of Phase and Frequency Instabilities in Precision Frequency Sources: Fifteen Years of Progress. In: *Proceedings of the IEEE*, Volume 66, 1048 – 1075.

Saastamoinen, J. (1972) Contributions to the theory of atmospheric refraction. *Bulletin Geodesique*, 46(1):279 – 298, doi:10.1007/BF02521844.

Scales, J., M. Smith and S. Treitel (2001) *Introductory geophysical inverse theory*. Samizdat Press Golden.

Schlüter, W. and D. Behrend (2007) The International VLBI Service for Geodesy and Astrometry (IVS): current capabilities and future prospects. *Journal of Geodesy*, 81(6):379 – 387.

Schnell, D. (2006) *Quality aspects of short duration VLBI observations for UT1 determinations*. Dissertation, Rheinische Friedrich-Wilhelms-Universität Bonn, Bonn.

Schuh, H. (1987) *Die Radiointerferometrie auf langen Basen zur Bestimmung von Punktverschiebungen und Erdrotationsparametern.* Dissertation, Rheinische Friedrich-Wilhelms-Universität Bonn. Deutsche Geodätische Kommission Bayer. Akad. Wiss. München, Reihe C, Vol. 328, ISBN 3-7696-9378-7.

Schuh, H. and J. Campbell (1994) VLBI in Geodynamical Investigations. *Acta Geodaetica et Geophysica Hungarica*, 29:397 – 420.

Schuh, H. and V. Tesmer (2001) Considering A Priori Correlations in VLBI Data Analysis. In: Vandenberg, N. R. and K. D. Baver (Eds.), *IVS 2000 General Meeting Proceedings*. NASA/CP-2000-209893, 237- 242.

Schuh, H. and A. Wilkin (1989) Determination of Correlation Coefficients between VLBI-Observables. In: Rius, A. (Eds.), *Proceedings of the 7th Working Meeting on European VLBI*. CSIC, 79 – 91.

Schuh, H., R. Dill, H. Greiner-Mai, H. Kutterer, J. Müller, A. Nothnagel, B. Richter, M. Rothacher, U. Schreiber and M. Soffel (2003) *Erdrotation und globale dynamische Prozesse*. Mitteilungen des Bundesamtes für Kartographie und Geodäsie (ISSN 1436-3445), Band 32, erarbeitet innerhalb des DFG-Forschungsvorhabens "Rotation der Erde" von H. Schuh, R. Dill, H. Greiner-Mai, H. Kutterer, J. Müller, A. Nothnagel, B. Richter, M. Rothacher, U. Schreiber, M. Soffel. Frankfurt am Main (Germany): Bundesamtes für Kartographie und Geodäsie. ISBN 3-89888-883-5, 2003, IV + 118 pp.

Schwegmann, W. (2004) *Ein eingebettetes Expertensystem zur Automatisierung der VLBI-Auswertung*. Mitteilungen des Bundesamtes für Kartographie und Geodäsie, Rheinische Friedrich-Wilhelms-Universität Bonn, Frankfurt am Main. Verlag des Bundesamtes für Kartographie und Geodäsie, Band 30, ISBN 3-89888-880-0.

Shapiro, I. I., D. S. Robertson, C. A. Knight, C. C. Counselman III, A. E. E. Rogers, H. F. Hinteregger, S. Lippincott, A. R. Whitney, T. A. Clark, A. E. Niell and D. J. Spitzmesser (1974) Transcontinental Baselines and the Rotation of the Earth Measured by Radio Interferometry. *Science*, 186:920 – 922, doi:10.1126/science.186.4167.920.

Sovers, O. J., J. L. Fanselow and C. S. Jacobs (1998) Astrometry and geodesy with radio interferometry: experiments, models, results. *Rev. Mod. Phys.*, 70:1393 – 1454, doi:10.1103/RevModPhys.70.1393. (available electronically at `http://arxiv.org/abs/astro-ph/9712238`).

Steufmehl, H.-J. (1994) *Optimierung von Beobachtungsplänen in der Langbasisinterferometrie (VLBI).* Dissertation, Rheinische Friedrich-Wilhelms-Universität Bonn, Frankfurt am Main. Deutsche Geodätische Kommission Bayer. Akad. Wiss., Reihe C, Vol. 406, ISSN 0071-9196.

Strang, G. (2003) *Lineare Algebra*. Springer, Berlin. ISBN 3-54043949-8.

Sun, J. (2013) *VLBI scheduling strategies with respect to VLBI2010.* Dissertation, Department of Geodesy and Geoinformation, Vienna University of Technology, Vienna. Geowissenschaftliche Mitteilungen, Heft Nr. 92, ISSN 1811-8380.

Sun, J., J. Böhm, T. Nilsson, H. Krásná, S. Böhm and H. Schuh (2014) New VLBI2010 scheduling strategies and implications on the terrestrial reference frames. *Journal of Geodesy*, 88(5):449 – 461, doi:10.1007/s00190-014-0697-9.

Takahashi, F., T. Kondo, Y. Takahashi and Y. Koyama (2000) *Very Long Baseline Interferometer.* Wave Summit Course. Ohmsha, Ltd. / IOS Press.

Takahashi, Y. (1994) Estimation of Errors in VLBI Data and Position Determination Error. *Journal of the Geodetic Society of Japan*, 40(4):309 – 331.

Tesmer, V. (2003) Refinement of the Stochastic VLBI Model: First Results. In: Schwegmann, W. and Thorandt V. (Eds.), *Proceedings of the 16th Working Meeting on European VLBI for Geodesy and Astrometry,* 9 – 10 May 2003, Leipzig. Bundesamt für Kartographie und Geodäsie, Frankfurt/Leipzig, 207 – 218. available electronically at `http://www.evga.org/files/2003EVGA-proc_Leipzig.pdf`.

Tesmer, V. (2004) *Das stochastische Modell bei der VLBI-Auswertung.* Dissertation, Technische Universität München. Deutsche Geodätische Kommission Bayer. Akad. Wiss. München, Reihe C, Vol. 573, ISBN 3 7696 5012 3.

Tesmer, V. and H. Kutterer (2005) An Advanced Stochastic Model for VLBI Observations and its Application to VLBI Data Analysis. In: Vandenberg, N. R. and K. D. Baver (Eds.), *IVS 2004 General Meeting Proceedings,* 9 – 11 February 2004, Ottawa, Canada, 296 – 300.

Tesmer, V., J. Böhm, R. Heinkelmann and H. Schuh (2007) Effect of different tropospheric mapping functions on the TRF, CRF and position time-series estimated from VLBI. *Journal of Geodesy*, 81(6 – 8):409 – 421, doi:10.1007/s00190-006-0126-9.

Teunissen, P.J.G. (2000) *Adjustment Theory: An Introduction.* Series on Mathematical Geodesy and Positioning. Delft University of Technology.

Thomas, J. B. (1972) An Analysis of Long Baseline Interferometry. DSN Progress Report, JPL Technical Report 32-1526 8, Jet Propulsion Laboratory, Pasadena, California.

Thompson, A. R., J. M. Moran and G. W. Swenson (1986) *Interferometry and synthesis in radio astronomy.* A Wiley-Interscience publication. Wiley, New York.

Titov, O., V. Tesmer and J. Boehm (2004) OCCAM v.6.0 Software for VLBI Data Analysis. In: Vandenberg, Nancy R. and Karen D. Baver (Eds.), *IVS General Meeting Proceedings,* 9 – 11 February 2004, Ottawa, Canada. NASA/CP-2004-212255, 267 – 271. (available electronically at `ftp://ivscc.gsfc.nasa.gov/pub/general-meeting/2004/pdf/titov1.pdf`).

Trefethen, L. N. and D. Bau (1997) *Numerical Linear Algebra.* Society for Industrial and Applied Mathematics (SIAM), Philadelphia. ISBN 0-89871-3617.

Treuhaft, R. N. and G. E. Lanyi (1987) The effect of the dynamic wet troposphere on radio interferometric measurements. *Radio Science*, 22(2):251 – 265, doi:10.1029/RS022i002p00251.

Uunila, M. (2013) *Improving geodetic VLBI: UT1 accuracy, latency of results, and data quality monitoring.* Dissertation, School of Electrical Engineering, Helsinki. Aalto University publication series DOCTORAL DISSERTATIONS, 88/2013, ISBN 978-952-60-5179-6.

Uunila, M., A. Nothnagel and J. Leek (2012) Inflence of Source Constellations on UT1 Derived from IVS INT1 Sessions. In: Behrend, D. and K.D. Baver (Eds.), *IVS 2012 General Meeting Proceedings.* NASA/CP, 395 – 399.

Vandenberg, N. (1999) *Interactive/Automatic Scheduling Program. Program Reference Manual.* NASA/Goddard Space Flight Center, NVI, Inc., 1999.

Vanier, J. (1982) The Active Hydrogen Maser: State of the Art and Forecast. *Metrologia*, 18(4):173 – 186, doi:10.1088/0026-1394/18/4/001.

Vennebusch, M. (2008) *Singular Value Decomposition and Cluster Analysis as Regression Diagnostics Tools in Geodetic VLBI.* Dissertation, Rheinische Friedrich-Wilhelms-Universität Bonn, Bonn. Schriftenreihe des Instituts für Geodäsie und Geoinformation der Universität Bonn, Heft Nr. 3, ISSN 1864-1113.

Vennebusch, M., A. Nothnagel and H. Kutterer (2009) Singular value decomposition and cluster analysis as regression diagnostics tools for geodetic applications. *Journal of Geodesy*, 83:877 – 891, doi: 10.1007/s00190-009-0306-5.

Wheelon, A. D. (2001) *Electromagnetic Scintillation: 1. Geometrical Optics.* Cambridge University Press, Cambridge. ISBN 0-521-80198-2.

Whitney, Alan R. (2000) How Do VLBI Correlators Work? In: Vandenberg, N. R. and K. D. Baver (Eds.), *IVS 2000 General Meeting Proceedings,* 21 – 24 February, Kötzting. NASA/CP-2000-209893, Greenbelt MD, 187 – 205. (available electronically at `ftp://ivscc.gsfc.nasa.gov/pub/general-meeting/2000/pdf/whitney2.pdf`).

Wresnik, J. (2009) *Simulationen für die neue Generation von VLBI-Systemen.* Dissertation, Vienna University of Technology, Vienna. Geowissenschaftliche Mitteilungen, Heft Nr. 85, ISSN 1811-8380.

Wresnik, J., J. Boehm, A. Pany and H. Schuh (2009) VLBI2010 simulations at IGG Vienna. In: Bourda, G., P. Charlot and A. Collioud (Eds.), *Proceedings of the 19th European VLBI for Geodesy and Astrometry Working Meeting,* 24 – 25 March 2009, Bordeaux. Université Bordeuax 1 - CNRS - Laboratoire d'Astrophysique de Bordeaux, 147 – 150. (available electronically at `http://www.u-bordeaux1.fr/vlbi2009/proceedgs/33_Wresnik.pdf`).

Zeppenfeld, G. (1993) *Einflüsse der Quellenstruktur in der Praxis der geodätischen VLBI.* Dissertation, Rheinische Friedrich-Wilhelms-Universität Bonn, Bonn. Mitteilungen aus den geodätischen Instituten der Rheinischen Friedrich-Wilhelms-Universität Bonn, Heft Nr. 80, ISSN 07234325.

Abbreviations

ASD	Allan standard deviation
BIPM	Bureau international des Poids et Mesures
BKG	Federal Agency for Cartography and Geodesy (Bundesamt für Karthographie und Geodäsie)
CA	Cluster Analysis
CRF	Celestial Reference Frame
DORIS	Doppler Orbitography and Radiopositioning Integrated by Satellite
EOP	Earth Orientation Parameter
ERP	Earth Rotation Parameter
FSW	Fundamental Station Wettzell
GGOS	Global Geodetic Observing System
GMF	Global Mapping Function
GNSS	Global Navigation Satellite System
GPS	Global Positioning System
GSFC	Goddard Space Flight Center
GSI	Geospatial Information Authority of Japan
IAG	International Association of Geodesy
IAU	International Astronomical Union
ICRF	International Celestial Reference Frame
IERS	International Earth Rotation and Reference Systems Service
IGG	Institute of Geodesy and Geoinformation (University of Bonn)
INT	VLBI Intensive sessions
ITRF	International Terrestrial Reference Frame
IVS	International VLBI Service for Geodesy and Astrometry
LOD	Length Of Day
M	Mean value
MCS	Monte Carlo simulation
MED	Median
MS	Mean of Squares
NMF	Niell Mapping Function
NRC	National Research Canada
RMS	Root Mean Square
SEFD	System Equivalent Flux Density
SLR	Satellite Laser Ranging
SM	Scaled Mean
SMED	Scaled Median
SMS	Scaled Mean of Squares
SNR	Signal to Noise Ratio

SRMS	Scaled Root Mean Square
SUMS	sum of squares
SVD	Singular Value Decomposition
SSUM	Scaled Sum
SSUMS	Scaled Sum of Squares
TAI	International Atomic Time
TRF	Terrestrial Reference Frame
TTW	Twin Telescope Wettzell
UPGMA	unweighted pair-group method using arithmetic averages
USNO	United States Naval Observatory
UT1	Universal Time
UTC	Coordinated Universal Time
VLBI	Very Long Baseline Interferometry
VMF	Vienna Mapping Function

List of Symbols

Mathematical constants, variables and functions

τ_{geom}	geometric delay
τ_{obs}	observed time delay
τ_{j-aber}	annual aberration because of the motion of the Earth around the Solar System barycenter
τ_{t-aber}	diurnal aberration because of the rotation of the Earth
τ_{rel}	relativistic corrections to the geometric delay
τ_{load}	deformation of the Earth's surface because of loading effects
τ_{tid}	deformation of the Earth because of tides and changes of the angular momentum due to ocean tides
τ_{instr}	propagation delays through on-site cable runs and other instruments
τ_{clock}	mis-synchronization of the reference clocks at each observing site
τ_{tropo}	propagation delays through the non-ionized portions of the Earth's atmosphere
τ_{ionos}	propagation delays through the ionized portions of the Earth's atmosphere
t_i	observing time
c	velocity of light
α	right ascension
δ	declination
ε	elevation
$\Delta UT1$	Earth rotation parameter
cl_i	clock polynomial coefficient
at_i	atmospheric parameter
$n(\mathbf{r}(z), t)$	index of refraction
S	signal path
zhd	zenith hydrostatic delay
zwd	zenith wet delay
$m(\varepsilon)$	mapping function
$m_h(\varepsilon)$	hydrostatic mapping function
$m_w(\varepsilon)$	wet mapping function
A, B, C	observing sites
Ω	conversion factor from universal time to sidereal time
b_i	baseline component
$h\,(t)$	Greenwich hour angle
B_e	effective bandwidth of the receiving system
n	number of channels
f_i	channel frequencies
f_m	mean channel frequency
SNR	signal-to-noise ratio

η	quality of the digitization and filtering of the signals
F	luminosity of the radio source
k	Boltzmann's-constant
A_i	effective antenna areas of the telescopes
T_{S_i}	noise temperatures of receiving systems
T	coherent observing or integration time at the correlation process
r	rank of a matrix
σ_i	singular values
h_i	impact factors
h_{ij}	impact co-factors
r_i	redundancy numbers
n_{st}	number of stations
n_{bl}	number of baselines
n_{obs}	number of observations
n_{scan}	number of scans
u_{cl}	number of clock parameters per station
u_{at}	number of atmospheric parameters per station
$u_{\Delta UT1}$	number of Earth rotation parameters
$\tau_{X/S}$	group delay of the X/S-band
$f_{X/S}$	frequency of the X/S-band
$\Delta\tau_{ion,X}$	ionospheric refraction effect
$\sigma_{\tau_{X/S}}$	standard deviation of a group delay (X/S-band)
$\sigma_{\Delta\tau_{ion,X}}$	standard deviation of the ionospheric refraction effect
$\sigma_{\tau_{atm,i}}$	station dependent atmospheric noise term
a_{at}	noise coefficient
σ_τ	standard deviation of the observed delay
ρ_{ij}	correlation coefficient
$\sigma_{\Delta UT1}$	formal error of $\Delta UT1$
σ_{cl_i}	formal error of a clock parameter
σ_{at_i}	formal error of an atmospheric parameter
wn_{bl}	baseline dependent white noise
C_n^2	refractive index structure constant
$s_{\Delta UT1}$	repeatability of $\Delta UT1$

Vectors and Matrices

$\mathbf{b}$	baseline vector
$\mathbf{k}$	unit vector in the direction of the radio source
$\mathbf{r}_i$	geocentric position vectors of an observing site
$\mathbf{W}(t)$	transformation matrices arising from polar motion
$\mathbf{R}(t)$	transformation matrices arising from the rotation of the Earth around the axis associated with the pole

$\mathbf{Q}(t)$	transformation matrices arising from the motion of the celestial pole in the celestial reference system
$\mathbf{\Delta x}$	vector of parameters
$\mathbf{y}$	vector of observed delays
$\mathbf{y_0}$	vector of theoretical delays
$\mathbf{v}$	vector of residuals
$\mathbf{A}$	Jacobian matrix
$\mathbf{N}$	normal matrix
$\mathbf{\Sigma_{yy}}$	variance-covariance matrix of the observations
$\mathbf{\Sigma_{xx}}$	variance-covariance matrix of the parameters
$\mathbf{\Sigma_{vv}}$	variance-covariance matrix of the residuals
$\mathbf{S}$	rectangular diagonal matrix containing the singular values
$\mathbf{U}$	orthogonal matrix containing the left singular vectors
$\mathbf{V}$	orthogonal matrix containing the right singular vectors
$\mathbf{u}_i$	left singular vectors
$\mathbf{v}_i$	right singular vectors
$R(\mathbf{A})$	column space of the matrix $\mathbf{A}$
$R(\mathbf{A}^T)$	row space of the matrix $\mathbf{A}$
$\mathbf{U}_r$	first r columns of $\mathbf{U}$
$\mathbf{V}_r$	first r columns of $\mathbf{V}$
$\mathbf{H}$	data resolution matrix
$\mathbf{h}$	vector of impact factors
$\mathbf{I}$	identity matrix
$\mathbf{P}_{\mathbf{A}}^{\perp}$	orthogonal projector

Appendix

A. Comparison of different sized sub-nets

A major challenge of this work was the comparison of impact factors that belong to different sized sub-nets. This comparison is part of the main scheduling concept, which is described in Sec. 4.2.1. As a consequence of sub-netting, a scan could contain observations of just a sub-net of all participating radio telescopes instead of all. Furthermore, if two or more sub-nets will be built (depending on the station network size) two or more different sources can be observed simultaneously, resulting in various parallel scans. Additionally, it has to be pointed out that the more observations are carried out the lower the values of the impact factors because the total redundancy increases. Thus, a method for comparing different sized groups of impact factors have to be found.

For testing purposes, a four station network with the radio telescopes in Wettzell (Germany), Onsala (Sweden), Westford (USA) and St. Croix (U.S. Virgin Islands) is used to create various schedules with different methods for comparing the impact factors of the observations. The stations of the network are arranged in such a way that two stations are in relative vicinity or have at least a similar longitude, and both pairs of radio telescopes are divided by the North Atlantic Ocean, thus, building a great east-west extended network (see Fig. A.1). This network geometry is faintly reminiscent of an Intensive network using twin instead of single radio telescopes, but with greater distances between the pairs of radio telescopes. The expectation or aspiration towards the scheduling program is that observations of a sources with all participating radio telescopes as well as sub-nets of radio telescopes that observe different sources simultaneously occur. The network geometry has been chosen in a way that it opens the chance for both observing cases.

For this network, Intensive-like observing plans which last one hour have been created using several different methods for computing reference values of the different groups of impact factors. The first half of the examined methods, which are listed in Tab. A.1, are usual or simple practices to compute feature sizes of groups or vectors of values. The other half is comprised of the same methods as the first half with the only change that these methods are scaled by the root of the number of impact factors respectively for a better consideration of different total redundancies. Although the methods seem to be very similar they produces different results which will be analyzed by means of chosen groups of impact factors, that have to be compared to each other. For a better visualization of the different cases, the used methods will be abbreviated as it is listed in Tab. A.1.

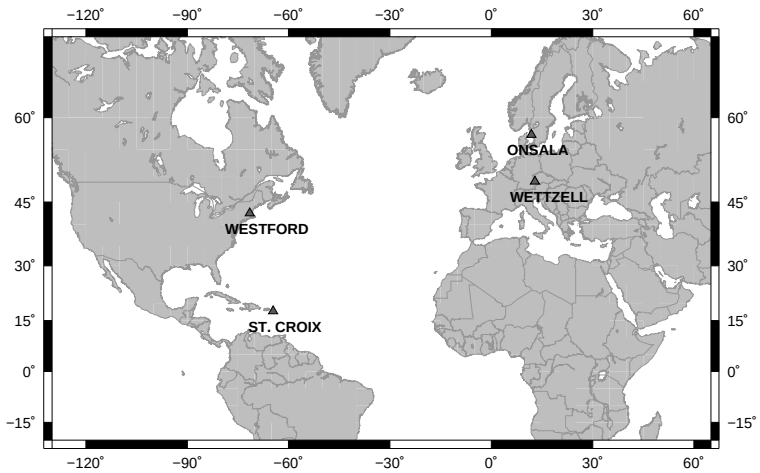

Figure A.1: Station network for the test schedules.

notation	abbreviation	formula
mean	M	$\frac{1}{n}\sum_{i=1}^{n} h_i$
mean of squares	MS	$\frac{1}{n}\sum_{i=1}^{n} h_i^2$
root mean square	RMS	$\sqrt{\frac{1}{n}\sum_{i=1}^{n} h_i^2}$
median	MED	$\begin{cases} h_{\frac{n+1}{2}} & \text{if } n \text{ odd} \\ \frac{1}{2}\left(h_{\frac{n}{2}} + h_{\frac{n}{2}+1}\right) & \text{if } n \text{ even} \end{cases}$ (**h** ordered)
sum	SUM	$\sum_{i=1}^{n} h_i$
sum of squares	SUMS	$\sum_{i=1}^{n} h_i^2$
scaled mean	SM	$\frac{1}{\sqrt{n}}\sum_{i=1}^{n} h_i$
scaled mean of squares	SMS	$\sqrt{n}\cdot\frac{1}{n}\sum_{i=1}^{n} h_i^2$
scaled root mean square	SRMS	$\sqrt{\sum_{i=1}^{n} h_i^2}$
scaled median	SMED	$\begin{cases} \sqrt{n}\cdot h_{\frac{n+1}{2}} & \text{if } n \text{ odd} \\ \sqrt{n}\cdot\frac{1}{2}\left(h_{\frac{n}{2}} + h_{\frac{n}{2}+1}\right) & \text{if } n \text{ even} \end{cases}$ (**h** ordered)
scaled sum	SSUM	$\sqrt{n}\cdot\sum_{i=1}^{n} h_i$
scaled sum of squares	SSUMS	$\sqrt{n}\cdot\sum_{i=1}^{n} h_i^2$

Table A.1: Used methods with its abbreviations and formulas where h_i is a single impact factor of a vector of impact factors **h** with length n.

A.1 Comparing groups of impact factors: Case 1

In the first case four different groups of impact factors are taken by chance for an arbitrary epoch (Tab. A.2). The first one (if_1) is a single impact factor that belongs to a single baseline observation and being the greatest value that occurs in case 1. The second group (if_2) consists of two impact factors with comparably great values that are just slightly lower as the one of if_1. Such a group results from pairwise observations of two different radio sources at an instant of time, thus, building two sub-nets. A group of three impact factors as it is the case for the third group (if_3) originate from an observation of a three station network. Thus, one of the four radio telescopes of the current network would be idle in the respective scan. The three values of this group are again lower than those of if_2 and, subjectively spoken, would also contribute less for improving the geometry. If all four radio telescopes observe the same radio source simultaneously, a scan of six observations

occurs as it is the case of the last group of impact factors (if_4). This group exhibits very low values that are the lowest values of the current case indeed. On the one hand, this matches the fact that the more observations will be performed the lower the values of the respective impact factors. On the other hand, the whole station network may only observe radio sources which do not improve the observing geometry much. Subjectively, the last group belongs to the most insignificant observations.

All methods of Tab. A.1 have been used to compute the reference values for the different groups of impact factors. The result is depicted in a bar chart in Fig. A.2. It can be seen that the first four methods – the mean value (M), the mean of squares (MS), the root mean square (RMS) and the median (MED) – weight the different groups of impact factors in sequence. Thus, the smallest group with the greatest value (if_1) is most highly weighted followed by the group with two relatively high but slightly lower values (if_2), afterwards the group consisting of three again lower values (if_3) and finally the biggest group with the smallest impact factors (if_4). Since these methods are counted among the unscaled ones, the different sizes of the observing vector and the related total redundancy will be neglected. Therefore, the first four methods seem to be insufficient. A similar situation, but in reverse order, happens for the methods sum (SUM), scaled sum (SSUM) and scaled sum of squares (SSUMS). Here, the groups of impact factors will be weighted by means of their quantities which does not make sense in the current case. The remaining methods are more interesting, as they weigh the groups of impact factors in other ways. The resulting order for the methods sum of squares (SUMS), scaled mean (SM), scaled root mean square (SRMS) and the scaled median (SMED) is group if_2, which seems to be the best group subjectively, followed by the group if_3, then group if_4 and finally group

notation	if_1	if_2	if_3	if_4
impact factors	0.85	0.82	0.63	0.46
		0.73	0.62	0.44
			0.55	0.39
				0.35
				0.33
				0.29

Table A.2: Different groups of impact factors that belongs to different sized sub-nets (case 1).

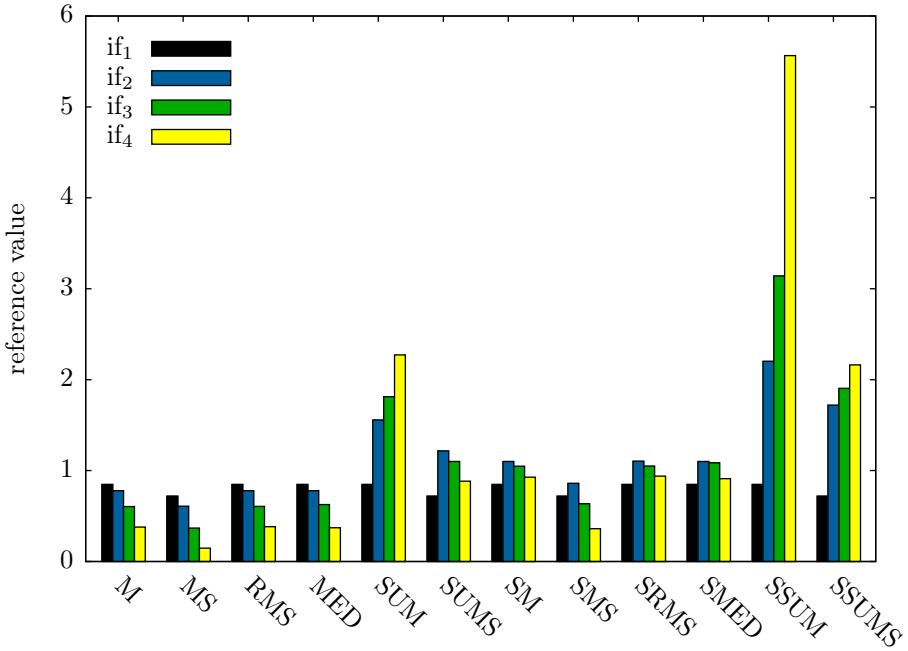

Figure A.2: Comparison of the reference values of the different groups of impact factors (case 1).

if_1. Just the method scaled mean of squares (SMS) orders the groups totally differently, as the first group (if_1) is weighted higher than the groups if_3 and if_4. But here also the group if_2 is rated best. In subjective terms, it is not easy to decide which of the orders is better, those of the scaled mean of squares or those of the prior to that mentioned methods. Thus, a second case will be regarded.

A.2 Comparing groups of impact factors: Case 2

Here, also four different groups of impact factors, which occurs in a second arbitrary epoch, have to be compared (Tab. A.3). Again, the first group (if_1) contains a single impact factor, the second group (if_2) consists of two impact factors, the third (if_3) of three impact factors and the forth (if_4) of six impact factors. As in case 1 the values of the impact factors decrease the greater the numbers of impact factors in a group. The difference to case 1 is that the groups of impact factors contains very high values as well as very low values (except for if_1 certainly). Subjectively, it is hard to decide which group would contribute the most useful information to an observing plan, presumably if_2 or if_3. The corresponding bar chart with the calculated reference values are shown in Fig. A.3. The first four methods (M, MS, RMS and MED) most highly weigh if_2, closely followed by if_1. Since the single impact factor of group if_1 (0.73) is lower than one of the impact factors of if_3 (0.79), the order of the first four methods does not seem appropriate. Similar to case 1, the

notation	if_1	if_2	if_3	if_4
impact factors	0.73	0.89	0.79	0.53
		0.58	0.31	0.51
			0.24	0.38
				0.22
				0.19
				0.15

Table A.3: Comparison of the reference values of the different groups of impact factors (case 2).

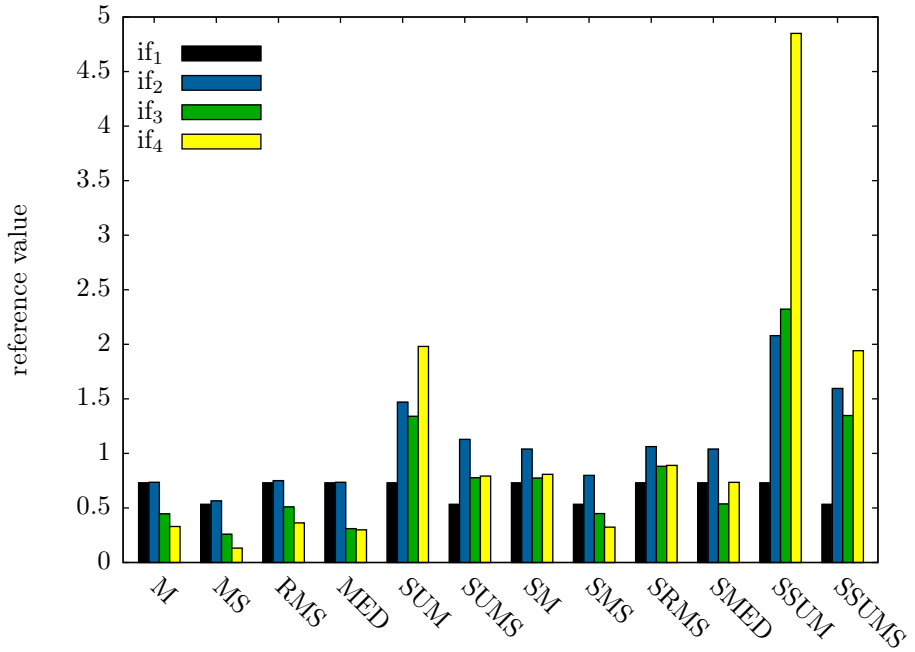

Figure A.3: Comparison of the reference values of the different groups of impact factors (case 2).

methods SUM, SSUM and SSUMS seem to be insusceptible towards small groups that contains very great impact factors, as they all most highly weigh the biggest group if_4. Groups that weigh the second group (if_2) mostly and, thus, are most interesting, are the same as in case 1, namely SUMS, SM, SMS, SRMS and SMED.

A.3 Observing plans

The two considered cases could only help to identify several methods that seem to be inappropriate for comparing the impact factors of different sized sub-nets. But, to come to a decision which method of the remaining ones should be used, is not possible on the basis of the presented consideration. For this reason, a closer look into the observing plans created with the different methods has been taken. In order to assure reliable results, several observing plans have been scheduled for the test network, more specifically, a time span of one year with observing sessions at two days a week have been used, resulting in 104 observing plans for each method. For the purposes of illustration, the average number of scans and observations as well as the ratio between both values are listed in Tab. A.4.

The ratio (obs./scans) is a very useful parameter to see quickly whether sub-netting occurs in a observing plan or not. If no sub-netting will be done, all participating radio telescopes observe in every scan. A scan of a station network of four radio telescopes consists of six observations, because six baselines will be built between four stations. Thus, a ratio of 6 indicates that no sub-netting has been done in an observing plan. Table A.4 reveals that this is true for the methods SUM, SMED and SSUM and nearly for SSUMS. This is not surprising for the methods containing the sum of the impact factors, as also the examined cases 1 and 2 (Sec. A.1 and A.2) have indicated that these methods most highly weigh the greatest group of impact factors, thus, scans with as many observations as possible. But, this has not been expected for the SMED method, as the order of weighting the groups of impact factors seem to be decent in the examined cases.

Another important value for the ratio is 1, as this indicates that as many observations as scans occur. This could only be the case if every scan contains a single observation only, meaning just two of the four telescopes participate. Regarding Tab. A.4, this concerns the methods M, MS, RMS and MED. That could have been foreseen for the first four methods, since they do not take into account the increasing redundancy with more observations. Furthermore, if a group of impact factors contains a very high but also a very low value, the group will be weighted worse than a single impact factor that might not be as high as the highest one of the others group, because the low value pulls down the reference value. This negative influence of a single low value in a group of impact factors is not constructive for a suitable selection process.

method	**scans**	**obs.**	**obs./scans**
M	26	26	1.0
MS	26	26	1.0
RMS	26	26	1.0
MED	29	29	1.0
SUM	24	143	6.0
SUMS	27	124	4.6
SM	27	124	4.6
SMS	42	51	1.2
SRMS	27	124	4.6
SMED	26	157	6.0
SSUM	24	143	6.0
SSUMS	24	142	5.9

Table A.4: Average numbers of scans, observations and theirs ratio of the test sessions.

Not as extreme but similar is the method SMS with a ratio of 1.2. A look at the bar charts of the examined cases (Fig. A.2 and A.3) reveals that the order of this method is similar to that of the other methods with a ratio of one. Therefore, scans with just two radio telescopes will be carried out mainly and only one to two scans contain three or four radio telescopes per session.

Consulting Tab. A.4, the most qualified methods seem to be SUMS, SM and SRMS with a ratio of 4.6. Here, scans of sub-nets and scans with all radio telescopes occur in a well-balanced mixture. An examination of the observing plans of the SUMS and SRMS methods reveals that they coincide exactly, because the SRMS equals the square root of the SUMS and, thus, producing the same orders for different groups of impact factors with just another magnitude. The observing plans scheduled with the SM method differs only slightly from the others, but seem to be a little bit more diversified.

A.4 Decision

Several of the examined methods for comparing the impact factors of different sized sub-nets could be discarded by regarding the reference values of different groups of impact factors in the two presented examples. The discarded methods on the one hand are those which are unscaled and, thus, ignore the change of the total redundancy, namely M, MS, RMS and MED. On the other hand, methods that are dominated by the total sum of the impact factors, in particular SUM, SSUM and SSUMS, have been disqualified.

Further investigations of the observing plans revealed the inappropriateness of two more methods – SMS and SMED – because of their smaller ratio of number of observations to number of scans. Furthermore, it has become clear that two of the remaining three methods equal each other, SUMS and SRMS. Eventually, two methods remain that produces very similar results, the SM and SUMS method.

In order to come to a decision, a final examination of the achieved $\Delta UT1$ formal errors with both methods have been done. The $\Delta UT1$ formal errors are compared in Fig. A.4. These on average amount to 7.60 µs for the SM method and 7.72 µs for the SUMS method. The difference between the $\Delta UT1$ formal errors is not significant and, thus, can hardly contribute to come to a decision. Due to the fact that the observing plans scheduled with the SM method are slightly more diversified than those that are scheduled with the SUMS method, it has been decided to use the SM method within the scheduling procedure for comparing the impact factors of different sized sub-nets.

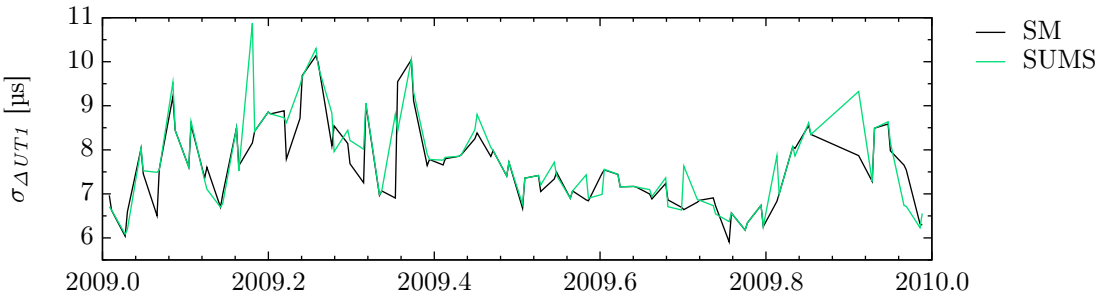

Figure A.4: $\Delta UT1$ formal errors for the test sessions scheduled with SM and SUMS.